

1 **Early Jurassic climate and atmospheric CO<sub>2</sub> concentration in the**  
2 **Sichuan paleobasin, Southwest China**

3  
4 Xianghui Li<sup>1</sup>, Jingyu Wang<sup>1</sup>, Troy Rasbury<sup>2</sup>, Min Zhou<sup>1</sup>, Zhen Wei<sup>1</sup>, Chaokai Zhang<sup>1</sup>

5 <sup>1</sup>State Key Laboratory for Mineral Deposits Research, School of Earth Sciences and Engineering, Nanjing University,  
6 Nanjing 210023 China.

7 <sup>2</sup>Department of Geosciences, Stony Brook University, Stony Brook, NY 11794-2100, USA

8 *Correpondence to:* Xiangui Li ([leeschhui@126.com](mailto:leeschhui@126.com))

9

10 **Abstract:** Climatic oscillations had been developed through the (Early) Jurassic from marine sedimentary archives, but  
11 remain unclear from terrestrial records. This work presents investigation of climate-sensitive sediments and carbon and  
12 oxygen isotope analyses of lacustrine and pedogenic carbonates for the Early Jurassic Ziliujing Formation from the grand  
13 Sichuan paleobasin (GSB), Southwest China. Sedimentary and stable isotope proxies manifest that an overall secular (semi-)  
14 arid climate dominated the GSB during the Early Jurassic except for the Hettangian. This climate pattern is similar to the  
15 arid climate in the Colorado Plateau region, western North America, but distinct from the relatively warm-humid climate in  
16 North China and high latitude in Southern Hemisphere. The estimated atmospheric CO<sub>2</sub> concentration (*p*CO<sub>2</sub>) from carbon  
17 isotopes of pedogenic carbonates shows a range of 980-2610 ppmV (~ 3.5-10 times the pre-industrial value) with a mean of  
18 1660 ppmV. Three phases of *p*CO<sub>2</sub> (the Sinemurian 1500-2000 ppmV, the Pliensbachian 1000-1500 ppmV, and the early  
19 Toarcian 1094-2610 ppmV) and two events of rapid falling *p*CO<sub>2</sub> by ~1000-1300 ppmV are observed, illustrating the *p*CO<sub>2</sub>  
20 perturbation in the Early Jurassic. The perturbation of *p*CO<sub>2</sub> is compatible with seawater temperature and carbon cycle from  
21 the coeval marine sediments, suggesting a positive feedback of climate to *p*CO<sub>2</sub> through the Early Jurassic.

22

## 23 1. Introduction

24 Global paleotemperatures were possibly 5-10°C higher than present during the Jurassic period based on climate modelling  
25 results (e.g., Rees et al., 1999; Sellwood and Valdes, 2008). However, seawater temperature fluctuated by -5 °C to +5 °C, or  
26 even much higher magnitude (e.g., Suan et al., 2008; Littler et al., 2010), based on estimates from the oxygen isotopes of the  
27 belemnite and bivalve fossils (Dera et al., 2011, and references therein). In the Sinemurian–Pliensbachian age, the mean sea  
28 surface temperatures of the North Atlantic were in excess of 28°C (TEX<sub>86</sub>), comparable with similar palaeolatitudes during  
29 the Cretaceous and Early Cenozoic (Robinson et al., 2017); whereas in the late Pliensbachian age, the northern West Tethys  
30 Ocean (e.g., Paris basin, northern Spain basin) was ~12.7°C (e.g., Gómez et al., 2008; Gómez and Goy, 2011; Arabas et al.,  
31 2017), leading to a polar icesheet hypothesis (e.g., Sellwood and Valdes, 2008; Suan et al., 2010; Dera et al., 2011; Gómez et  
32 al., 2015). At ~183 Ma of the early Toarcian oceanic anoxia event (T-OAE), the surface seawater temperature was high to  
33 ~35°C (e.g., Bailey et al., 2003; Korte et al., 2015), and a high temperature (plateau) even continued in the whole Toarcian  
34 (Dera et al., 2011). Examples of seawater temperature transitions between cold and hot show the climate oscillation through  
35 the Early Jurassic.

36 Data from the terrestrial realm also provide important details of environmental and climatic change (e.g., Hesselbo et al.,  
37 2000; Suan et al., 2010; Jenkyns, 2010; Philippe et al., 2017), from which the oscillated climate could be observed and  
38 revealed too. Terrestrial proxies, such as flora (e.g., Riding et al., 2013; Deng et al., 2017; Philippe et al., 2017), vegetation  
39 (Pole, 2009), and geochemistry (e.g., Riding et al., 2013; Kenny, 2015; Tramoy et al., 2016) as well as the *p*CO<sub>2</sub> record (e.g.,  
40 Retallack, 2001a; Beerling and Royer, 2002; McElwain et al., 2005; Berner, 2006; Steinthorsdottir and Vajda, 2015) provide  
41 an emerging record of the Early Jurassic terrestrial climate and environment changes. Correspondingly, the proxy application  
42 of terrestrial sedimentary archives could play a key role in the global Early Jurassic correlation of the marine and terrestrial  
43 climate.

44 Proxies for *p*CO<sub>2</sub> are the important linkage between the marine and terrestrial climatic condition. Studies of the terrestrial  
45 *p*CO<sub>2</sub> record have focused on the Triassic-Jurassic boundary (e.g., Tanner et al., 2001; Cleveland et al., 2008; Schaller et al.,  
46 2011; Steinthorsdottir and Vajda, 2015) and the Toarcian oceanic anoxic event (McElwain et al., 2005), where *p*CO<sub>2</sub>  
47 estimates range 1000 ppm to 4000 ppmV (e.g., Tanner et al., 2001; Cleveland et al., 2008; Schaller et al., 2011). Few  
48 relatively continuous *p*CO<sub>2</sub> records and coupled terrestrial climate changes have been documented for the Early Jurassic.

49 There are several large Triassic-Jurassic terrestrial basins in West China, in which the Sichuan Basin has a relatively  
50 complete and continuous continental sedimentary sequence of the Upper Triassic-Paleogene (e.g., SBGM, 1991, 1997;  
51 Wang et al., 2010). During the Early Jurassic, the Sichuan Basin was in a Boreotropical climate zone based on  
52 climate-sensitive sediments (Fig. 1a. Boucot et al., 2013), or a warm temperate climate is suggested based on clay mineralogy  
53 and phytogeography (e.g., Dera et al., 2009). In this work, we present a field investigation, including lithofacies and paleosol

54 interpretation, and carbon and oxygen isotope analyses of both lacustrine and pedogenic carbonates in Sichuan Basin. New  
55 results allow us to reconstruct the paleoclimate and relatively consecutive  $p\text{CO}_2$  record through the Early Jurassic, for which  
56 we compare to stable isotopes of marine sediments and estimated sea water temperature.

## 57 **2. Geological setting and stratigraphy**

58 Southwest China, including the provinces of Yunnan, Sichuan, Chongqing, and Guizhou, had been the main part of the  
59 upper Yangtze Plate since the Proterozoic, possibly since the Neoproterozoic. With the amalgamation of the Cathaysia and  
60 Yangtze plates, it became the western South China plate or cratonic basin since the Neoproterozoic (Sinian), and continued to  
61 the late Middle Triassic. By the Indosinian orogeny, new foreland basins were formed since the Late Triassic (e.g., He and  
62 Liao, 1985; Li et al., 2003), recording the Mesozoic and Cenozoic evolution of tectonics, environment, and climate in  
63 Southwest China.

64 The Mesozoic Sichuan paleobasin was confined by the Longmenshan thrust belt in the northwest, the Micangshan-Dabashan  
65 arcuate thrust belt in the northeast (Fig. 1b), and the northern hilly topography boundary of the Yunnan-Guizhou plateau in  
66 the south and east. It was mainly developed during the Late Triassic-Jurassic and includes provincial areas of eastern  
67 Sichuan, entire Chongqing, northern Guizhou, western Hubei, and northwestern Hunan. This Triassic-Jurassic Sichuan  
68 foreland basin was much larger than the present Sichuan Basin in the eastern Sichuan province. We estimate the size of  
69 Sichuan paleobasin is roughly 480,000 km<sup>2</sup> based on lithofacies paleogeography (Fig. 1b. Ma et al., 2009; Li and He, 2014),  
70 and suggest naming this the grand Sichuan paleobasin (GSB).

71 The Mesozoic terrestrial sediments accumulated up to ~9 km (Guo et al., 1996) in the GSB; and the Jurassic part can be as  
72 much as 3-3.5 km thick (SBGM, 1991). Two types of Lower Jurassic deposits have been distinguished (Table 1): the  
73 Baitianba Formation (Fm) in the north (~10%) and the Ziliujing Fm (e.g., SBGM, 1991; Wang et al., 2010) in the south  
74 (over 90% of the basin).

75 The Baitianba Fm was deposited unconformably on the Upper Triassic Xujiache Fm and is overlain conformably by the  
76 Middle Jurassic Xintiangou Fm / Qianfuyan Fm (Table 1). It is mainly composed of grayish shales and sandstones with coal  
77 layers and massive conglomerates. Abundant plant fossils, sporopollens, conchostracans, bivalves, and gastropods indicate it  
78 is of the Early Jurassic (SBGM, 1991, 1997). Sporopollen assemblages of the Hettangian-Sinemurian age were found in the  
79 lower part (Zhang and Meng, 1987) and the Pliensbachian-Toarcian assemblages were reported in the upper part (Wang et  
80 al., 2010).

81 The Ziliujing Fm is composed of variegated and reddish mudrocks (some shales) intercalated with sandstones, siltstones, and  
82 bioclastic limestones as well as dolomitic marlstones / limy dolomites, conformably or unconformably overlying the Xujiache  
83 Fm or Luqiao Fm and conformably underlying the Xintiangou Fm (SBGM, 1997. Table 1). It has been dated as the Early

84 Jurassic by fossil assemblages of bivalves, ostracods, conchostracans, and plants. Dinosaur fauna can be well correlated to  
85 the Lufeng Fauna in central Yunnan (e.g., Dong, 1984; SBGM, 1991, 1997; Peng, 2009). This formation is subdivided into  
86 five parts in an ascending order: the Qijiang, Zhenzhuchong, Dongyuemiao, Ma'anshan, and Da'anzhai members (SBGM,  
87 1997. Table 1). Of these, the former two are sometimes combined as the Zhenzhuchong Fm (e.g., SBGM, 1991; Wang et al.,  
88 2010).

89 The Da'anzhai Member is characterized by dark gray to black shales and bioclastic limestones with a southward increase of  
90 reddish mudrocks (SBGM, 1991, 1997; Wang et al., 2010), and is regarded the sediment in a grand Sichuan paleolake (e.g.,  
91 Ma et al., 2009; Li and He, 2014). Ostracod assemblages indicate it is the late Early Jurassic (e.g., Wei, 1982; Wang et al.,  
92 2010). A Re–Os isochron age of  $180.3 \pm 3.2$  Ma associated with an organic carbon isotope excursion indicates that the lower  
93 Da'anzhai Member corresponds to the T-OAE (Xu et al., 2017).

94 The Ma'anshan Member is comprised of violet-red mudrocks with a few greyish, greenish thin-bedded fine sandstones and  
95 siltstones, in which floral fossils are common (Li and Meng, 2003). The Dongyuemiao Member consists of greenish and  
96 reddish mudrocks and siltstones with greyish bioclastic limestone and marlstone, of which abundant bivalve and plant fossils  
97 were reported from eastern Sichuan and Chongqing (Li and Meng, 2003; Meng et al., 2003; Wang et al., 2010). The  
98 Zhenzhuchong Member is dominated by violet red mudrocks/shales intercalated with thin-bedded sandstones and / or  
99 siltstones and numerous plant fossils of the Early Jurassic affinity (e.g., Duan and Chen, 1982; Ye et al., 1986). Taken  
100 together, fossil associations suggest that the three members were deposited in the middle-late Early Jurassic. The age  
101 limitation of the overlying Da'anzhai Member and the correlation to the Lufeng dinosaur fauna places these members in the  
102 Sinemurian – Pliensbachian, and the Zhenzhuchong and Dongyuemiao Fms are suggested to be the Sinemurian (Table 1).

103 The Qijiang Member is composed of quartz arenite interbedded/intercalated with dark shales. Coal seams are often seen in  
104 the middle of the Qijiang Member. This member mainly occurs in the central part of the GSB. It is likely the earliest Jurassic,  
105 possibly Hettangian age, but plant fossils cannot precisely indicate the age (Wang et al., 2010).

### 106 **3. Materials and methods**

107 We have measured sections and made detailed observations and descriptions of sedimentary characteristics for lithofacies  
108 analysis at six outcrop sections (Locations A1 to A4, A6 and A7, Fig. 1). Published descriptions for other sections  
109 (Locations A5, A8, and A9, Fig. 1) are integrated into our observations. Details of microscopic examination of sedimentary  
110 rocks and analysis of sedimentary facies underpinning the climate analysis are attached as the supplementary data Note S1.  
111 Below we state climate-sensitive sediment observation, carbon and oxygen isotope analyses, and estimate of  $p\text{CO}_2$ .

#### 112 **3.1. Observation of climate-sensitive sediments**

113 Climate-sensitive sediments are mainly dolomites, gypsum, and paleosols, which are used to analyze the climate in this work

114 (Table S1).

115 Dolomites and gypsum are relatively easy to recognize in both field and under microscope. We distinguish dolomites from  
116 limestones following Tucker (2011) and Flügel (2004). As Flügel (2004) stated, field distinctions of limestone and dolomite  
117 can also be made although detailed differentiation of carbonate rocks is best performed in the laboratory. In field, we  
118 recognize gypsum by particular structures such as chicken-wire cage, gypsum pseudomorph, and cluster of (0.5-1 cm) pore.  
119 There are multiple classifications of paleosols (e.g., Wright, 1992; Mack et al., 1993; Retallack, 2001b; Imbellone, 2011),  
120 mostly based on the US Soil Taxonomy. We recognized paleosols in the field based on color, structures, horizonation, root  
121 traces, and textures, and followed the general classification paleosols by Mack et al. (1993) and Retallack (2001b). In this  
122 paper, paleosols are described following the procedures of the Soil Survey Manual and classified according to Soil Survey  
123 Staff (1998).

124 Within the measured and observed sections, paleosol profiles were mainly identified from the two main locations/sections  
125 A4 and A6 (Figs. S1 and S2, and Table S2). Horizonation, BK horizon thickness, boundaries, structures, trace fossils,  
126 rootlets, carbonate accumulations (calcretes), etc. were recorded (Table S2). Paleosols interpreted in other cited sections (Fig.  
127 1) rely on the description of lithology, structure, and calcrete in the original references. Based upon a modification of the  
128 Retallack (1998) categorization of paleosol maturity, the relative paleosol development (maturity) was assigned.

### 129 **3.2. Analyses of carbon and oxygen isotopes**

130 Ten lacustrine carbonate samples were analysed for carbon and oxygen isotopes from the Da'anzhai Member at the Shaping  
131 section, Ya'an (Location A4, Fig. S1 and Table S3). 26 pedogenic carbonate samples were analyzed for carbon and oxygen  
132 isotopes from 32 paleosols of the Ziliujing Fm at the same section (Fig. S1 and Table S4). Two or three microdrilling  
133 powder samples (columns 7 and 8 in Table S4) were taken from the same individual calcrete for stable isotope analysis, and  
134 then a mean value for each calcrete sample was calculated (columns 9 and 10 in Table S4).

135 At the field scale, calcretes are ginger-like and sporadically spaced within the soil horizon. We observed no linear and planar  
136 calcretes that would indicate precipitation at or below the water table. Before drilling, thin-sections were petrographically  
137 studied using polarized light microscopy and cathodoluminescence imaging. Micritic calcite is predominant in both  
138 lacustrine and pedogenic carbonate samples, with no evidence for carbonate detritus in calcretes (Fig. 2a and 2b). The  
139 micritic calcites used for stable isotope analyses are chiefly null- to non-luminescent, with <10% light orange and brownish  
140 luminescence, indicating genesis primarily in the vadose zone. While luminescent calcretes indicate a high possibility of  
141 hydrological influence (e.g., Mintz, et al., 2016), we sampled to avoid this. Based on petrography and CL imaging together  
142 with the field observations, the dense micritic zones sampled for the stable isotope composition should give pristine  $\delta^{13}\text{C}$   
143 values that can be used to estimate  $p\text{CO}_2$ .

144 Microsampling of lacustrine and pedogenic carbonates focused on only micrites, avoiding diagenetic spar from cracks, veins,

145 and vug spaces. Powder samples were obtained using a dental drill (aiguille diameter  $\phi=1-2$  mm).  
146 Isotopic analyses were conducted on 0.3 ~ 0.5 mg powder samples. Powder samples were dried in an oven at 60°C for 10  
147 hours before being moved to the instrument. Carbon dioxide for isotopic analysis was released using orthophosphoric acid at  
148 70°C and analysed on-line in a DELTA-Plus xp (CF-IRMS) mass spectrometer at the State Key Laboratory for Mineral  
149 Deposits Research, Nanjing University. The precision of the measurements was regularly checked with a Chinese national  
150 carbonate standard (GBW04405) and the international standard (NBS19) and the standard deviation of  $\delta^{13}\text{C}$  was  $\pm 0.1\%$  over  
151 the period of analysis. Calibration to the international PeeDee Belemnite (PDB) scale was performed using NBS19 and  
152 NBS18 standards.

### 153 3.3. Calculation of atmospheric CO<sub>2</sub> concentration

154 The Cerling (1991, 1999) equation was used to calculate the  $p\text{CO}_2$  using the carbon isotope of pedogenic carbonates as  
155 below:

$$156 C_a = S_{(z)}(\delta^{13}\text{C}_s - 1.0044\delta^{13}\text{C}_r - 4.4)/(\delta^{13}\text{C}_a - \delta^{13}\text{C}_s)$$

157 where  $C_a$  is  $p\text{CO}_2$ ;  $\delta^{13}\text{C}_s$ ,  $\delta^{13}\text{C}_r$ ,  $\delta^{13}\text{C}_a$  are the isotopic compositions (‰) of soil CO<sub>2</sub>, soil-respired CO<sub>2</sub>, and atmospheric CO<sub>2</sub>,  
158 respectively; and  $S_{(z)}$  is the CO<sub>2</sub> contributed by soil respiration (ppmV).

159  $\delta^{13}\text{C}_s$  is often calibrated by fractionation factor  $-8.98\%$  with the formula  $-8.98\% + \delta^{13}\text{C}_c$  (Ekart et al., 1999), with which  $\delta^{13}\text{C}_c$   
160 is the measured result of pedogenic calcrite. Alternatively,  $\delta^{13}\text{C}_s$  can be replaced by  $\delta^{13}\text{C}_{sc}$ , which is calibrated by carbon  
161 isotope ratio of pedogenic carbonate at 25°C based on latitude–temperature correlations (Besse and Courtillot, 1988; Ekart et  
162 al., 1999) following the equation  $\delta^{13}\text{C}_{sc} = (\delta^{13}\text{C}_c + 1000)/((11.98 - 0.12 * T)/1000 + 1) - 1000$  (Romanek et al., 1992). We used  
163 both  $\delta^{13}\text{C}_s$  and  $\delta^{13}\text{C}_{sc}$  to calculate the  $p\text{CO}_2$  (Table S4).

164  $\delta^{13}\text{C}_r$  represents carbon isotope ratio of average bulk C3 vascular tissue (Arens et al., 2000), reflecting atmospheric  $\delta^{13}\text{C}$   
165 (Jahren et al., 2008). The  $\delta^{13}\text{C}_{om}$  of organic matter within paleosols based on the range of modern C3 ecosystem  
166 fractionations (Buchmann, et al., 1998; Ekart et al., 1999), is commonly used for  $\delta^{13}\text{C}_r$ . However, the  $\delta^{13}\text{C}_r$  could be could be  
167 compromised in fossil soils due to oxidation and metabolism of organic matter after burial (Nadelhofer and Fry, 1988). In  
168 this paper, we use the  $\delta^{13}\text{C}_{om}$  from the Paris Basin (Bougeault et al., 2017; Peti et al., 2017) for the Sinemurian-Pliensbachian  
169  $\delta^{13}\text{C}_r$  and from Cardigan Bay, UK (Xu et al., 2018) for the Toarcian.

170  $\delta^{13}\text{C}_a$ , the carbon isotopic composition of the atmosphere, was about  $-8\%$  in the 1980s, being depleted relative to the  
171 pre-industrial atmosphere which was around  $-6.5\%$  (Friedli et al., 1986). The average value of  $-6.5\%$  has been chosen as the  
172  $\delta^{13}\text{C}_a$  for acquiring  $\delta^{13}\text{C}_r$  and  $S_{(z)}$  (e.g., Ekart et al., 1999; Robinson et al., 2002), and the  $\delta^{13}\text{C}_a$  was generally calibrated as  
173  $\delta^{13}\text{C}_{ac}$  from  $\delta^{13}\text{C}_r$  using the formula  $(\delta^{13}\text{C}_r + 18.67)/1.1$  (Arens et al., 2000). Herein we used both calibrations to calculate the  
174  $\delta^{13}\text{C}_a$  (Table S4).

175  $S_{(z)}$  is the largest source of uncertainty in  $p\text{CO}_2$  estimates (Breecker, 2013) and the uncertainty arises primarily from their  
176 sensitivity to soil-respired  $\text{CO}_2$  ( $S_{(z)}$ ) (Montañez, 2013). It is a function of depth and effectively constant below 50 cm (e.g.,  
177 Cerling, 1991).  $S_{(z)}=2500$  ppmV is suggested for the sub-humid temperate and tropical climates (Breecker et al., 2010),  
178 2500-5000 ppmV for higher moisture and productivity soil (Montañez, 2013), 2000 ppmV for semi-arid areas (Breecker et  
179 al., 2009), 1500-2000 ppmV for aridisols and alfisols (calcisol-argillisol) and  $2000\pm 1000$  for paleo-vertisol (Montañez,  
180 2013), and 1000 ppmV in desert areas (Breecker et al., 2010) or  $400 \pm 200$  ppmV for immature soil (Montañez, 2013). In  
181 this context, we chose the  $S_{(z)}=2000$  ppmV for calculating  $p\text{CO}_2$  at  $25^\circ\text{C}$  as the calcisols are reddish-brownish aridisols, and  
182 we also compared the results with that by  $S_{(z)}=2500$  ppmV (Table S4). Additionally, we took samples at the middle and  
183 lower Bk horizon (often  $> \sim 20\text{-}30$  cm to the BK top). That means the depth of calcrete samples in the examined palaeosols  
184 was generally deeper than 50 cm below the paleosol surface, meeting the requirement for a constant value of  $S_{(z)}$ .

## 185 **4. Results**

186 Based on the investigation of cross-sections (locations A1-A4, and A6-A7. Fig. 1), we have classified six sedimentary facies  
187 units in the Ziliujing Fm. They are alluvial fan, fluvial river, flood plain, lake, lake-delta, and swamp facies. Details of  
188 description and interpretation are in the supplementary data Note S1. Below are results of climate-sensitive sediment  
189 observation, stable isotope analyses, and  $p\text{CO}_2$  calculation.

### 190 **4.1. Climate-sensitive sediments**

191 Field observation combined with published calcrete materials shows that paleosols widely occur in the Lower Jurassic  
192 Ziliujing Fm of the GSB (Figs. 1, 3, and 4). A total of 32 paleosols were observed and described at the Shaping section,  
193 Ya'an, and five paleosols were found at the Tanba section, Hechuan (Table S2).

194 Most of paleosols are reddish (GSA Munsell Rock-Color 5R 2/2, 5R 3/4, 5R 4/2) and brownish (10R 3/4, 10R 5/4) (Fig. 3  
195 and Table S2). Peds of paleosols are mainly angular and subangular, and a few are prismatic and platy. Slickensides are  
196 common. Mottles (Fig. 3a), rootlets /rhizoliths (Fig. 3c), and burrows sometimes occur with strong leaching structures (Fig.  
197 3a). Occasionally mudcracks are associated with the aforementioned structures (Fig. 3d).

198 All paleosols are calcic with more or less calcretes in Bk horizons. The thickness of Bk horizons mainly changes from 30 cm  
199 and 100 cm, and partly up to 170 cm (Table S2). Calcretes are generally ginger-like, ellipsoid, subglobular, and irregular in  
200 shape (Fig. 3b and 3e) and nodules are 1-3 cm even up to 8-15 cm (paleosols J1z-10-01 and J1z-12-01) in size (Fig. 3e).  
201 Calcrete is often less than 0.5-1% in an individual paleosol, but a few can be up to 3-5% (paleosol J1z-3-01. Fig. 3b) even 10%  
202 (paleosols J1z-5-02 and 18HC-10).

203 All above paleosols are defined as relatively mature calcisols (Mack et al., 1993), a kind of aridisol (Soil Survey Staff, 1998;  
204 Retallack, 2001b). The original lithofacies were chiefly argillaceous and silty (split-fan) overbank, interchannel, and flood



205 plain deposits (Figs. S1 and S2). Some formed landward the paleo-lakeshore.  
206 Dolomites were found at seven loactions in central and southern GSB (Figs. 1, 4, and Table S1). The dolomites chiefly occur  
207 in the Toracian Da'anzhai Member and a few in the Sinemurian-Plienbachian Dongyuemiao and Ma'anshan members (Fig.  
208 4). They are often massive whitish (Figs. 3f and S3e) and micritic (Figs. S4b and S4d), likely indicating an authigenic origin.  
209 Gypsum is recorded in two loactions (Figs. 1, 4, and Table S1). One is located at Zigong (Location A5. SBG, 1980a). The  
210 other lies at Hechuan (Location A6), which can be identified by chicken-wire cage structure and is associated with micriditic  
211 dolomites (Fig. 3f).

## 212 4.2. Carbon and oxygen isotope values

213  $\delta^{13}\text{C}$  values of lacustrine carbonate samples range from -2.02‰ to -4.07‰ and  $\delta^{18}\text{O}$  values range from -9.91‰ to -12.28‰  
214 (Table S3 and Fig. 5). An increasing trend of both carbon and oxygen isotope ratios is observed from lower to upper  
215 horizons across a 45 m stratal interval of the lower Da'anzhai Member (Fig. 6).

216 Pedogenic carbonate samples have  $\delta^{13}\text{C}$  values from -3.52‰ to -8.10‰, which fall in the typical stable isotope range for  
217 pedogenic carbonates. Values of -6‰ to -8.0‰ characterize the sequence of the Zhenzhuchong Member and main  
218 Ma'anshan Member, with an abrupt increase to -5.5‰ to -3.5‰ at the top of Ma'anshan Member (samples J1z-16-01 and  
219 J1z-18-01. Fig. 6).  $\delta^{18}\text{O}$  values are mainly from -11.3‰ to -13.10‰ in the interval of the Zhenzhuchong Member and  
220 Ma'anshan Member.  $\delta^{18}\text{O}$  follows  $\delta^{13}\text{C}$  with a sudden increase to -5.5‰ at the top of the Ma'anshan Member (Fig. 6). Large  
221 and frequent variations of both carbon and oxygen isotope ratios can be observed in the lower Da'anzhai Member (Fig. 6 and  
222 Table S4).

## 223 4.3. CO<sub>2</sub> concentrations

224  $p\text{CO}_2$  values based on paleobarometer modelling of paleosol calcite (Cerling, 1999) vary depending on the parameters used  
225 for the calculation.

226 If  $S_{(z)}=2500$  ppmV and  $\delta^{13}\text{C}_a=-6.5\text{‰}$  (constant pre-industrial atmosphere),  $p\text{CO}_2$  values range between ~1140 ppmV and  
227 ~3460 ppmV with a mean of 1870 ppmV (column 15 in Table S4); and when  $S_{(z)}=2500$  ppmV and  $\delta^{13}\text{C}_a=(\delta^{13}\text{C}_r+18.67)/1.1$ ,  
228  $p\text{CO}_2$  values change between ~1230 ppmV and ~3260 ppmV with a mean of 2070 ppmV (column 16 in Table S4).

229 When  $S_{(z)}=2000$  ppmV and  $\delta^{13}\text{C}_s=-8.98+\delta^{13}\text{C}_c$  are used,  $p\text{CO}_2$  values are ~ 940-2530 ppmV with the mean 1600 ppmV  
230 (column 17 in Table S4); and if  $S_{(z)}=2000$  ppmV and  $\delta^{13}\text{C}_s = (\delta^{13}\text{C}_c+1000) / ((11.98-0.12*25) / 1000+1) -1000$  are adopted,  
231  $p\text{CO}_2$  values become ~980 ppmV to ~2610 ppmV with the mean 1660 ppmV (column 18 in Table S4). Details of the  
232 different parameters and  $p\text{CO}_2$  results can be seen in Table S4.

233 Results further show that  $p\text{CO}_2$  values at  $S_{(z)}=2500$  ppmV are larger than at  $S_{(z)}=2000$  ppmV. The highest difference is ~  
234 1000 (3640-2610) ppmV, while the lowest is ~300 (1230-930) ppmV and the mean is ~ 370 (2070-1600) ppmV. In addition,

235 when  $S_{(z)}$  is the same, the  $p\text{CO}_2$  values are close even if other parameters are different (comp. between columns 15 and 16,  
236 17 and 18 in Table S4, and Fig. 6).

237 Whatever parameters used, the trend of  $p\text{CO}_2$  over the epoch is quite similar (Fig. 6). We chose  $S_{(z)}=2000$  ppmV (column 18  
238 in Table S4) to illustrate the nature of the Early Jurassic  $p\text{CO}_2$  in the GSB.

239  $p\text{CO}_2$  values mostly range between 980 ppmV and 2610 ppmV, and the mean 1660 ppmV is  $\sim 6$  times the pre-industrial 275  
240 ppmV. Most of the  $p\text{CO}_2$  values are 1000-2000 ppmV with the mean 1580 ppmV in the Zhenzhuchong and Ma'anshan  
241 members,  $\sim 3.5$ - $7.5$  times the pre-industrial  $p\text{CO}_2$  value.

242 It is noted that the errors of  $p\text{CO}_2$  range from 384 ppmV to 1017 ppmV with a mean 647 ppmV (Table S5), leading to a large  
243 uncertainty of the mean  $\sim 39\%$ . The largest source of the uncertainty is the standard error (766 ppmV) of modern soil carbonate  
244 (Breecker and Retallack, 2014). The  $p\text{CO}_2$  uncertainty decreases by  $\sim 20\%$  if half (383 ppmv) of the standard error of soil  
245 carbonate is selected, and decreases to  $\sim 12\%$  if  $1/4$  ( $\sim 191$  ppmV) standard error is used. The second largest source of error in  
246 the  $p\text{CO}_2$  is the  $S_{(z)}$  estimate. The uncertainty of  $p\text{CO}_2$  becomes much smaller when the  $S_{(z)}$  is larger, e.g., it will fall from  $\sim 39\%$   
247 to  $\sim 17\%$  if  $S_{(z)}=5000$  ppmV instead of 2000 ppmV. Other parameters such as temperature,  $\delta^{13}\text{C}_r$ ,  $\delta^{13}\text{C}_a$ ,  $\delta^{13}\text{C}_s$ , contribute very  
248 little to the calculated  $p\text{CO}_2$  uncertainty.

## 249 **5. Discussion**

250 The Jurassic marine record shows climatic and environmental oscillations (e.g., van de Schootbrugge et al., 2005; Dera et al.,  
251 2011; Gómez et al., 2015; Arabas et al., 2017), including sea water temperature fluctuation and carbon cycle reorganization  
252 recorded in both carbonate and organic matter. The climate changes and events recorded in the the marine realm have been  
253 mainly attributed to Karoo-Ferrar volcanism (e.g., Hesselbo et al., 2000; Caruthers et a., 2013), sea-level change (e.g.,  
254 Hesselbo and Jenkyns, 1998; Hallam and Wignall, 1999), orbital forcing (e.g., Kemp et al., 2005; Huang and Hesselbo, 2014,  
255 Storm et al., 2020), and / or the opening of the Hispanic corridor (e.g., van de Schootbrugge et al., 2005; Arias, 2009).  
256 Eruption of the Karoo-Ferrar and Central Atlantic mgama is thought to have released large amounts of  $\text{CO}_2$  into the  
257 atmosphere in a short amount of time, resulting in rising temperatures of both marine and continental realms. The nearly  
258 continuous record of Jurassic strata in the GSB provides an excellent test of this hypothesis in the terrestrial realm. We  
259 compare the climate and  $p\text{CO}_2$  record from the GSB in relationship to the marine temperature records.

### 260 **5.1. Paleoclimate variation**

261 During the Late Triassic, Southwest China was warm-hot and humid and occupied a tropical and / or subtropical zone, as  
262 demonstrtd by palynoflora, coals, and perennial riverine and lacustrine lithofacies in the Xujiahe Fm (e.g., Huang, 1995; Li  
263 et al., 2016). However, the climate became dry through the Early Jurassic manifested by climate-sensive sediments and  
264 stable isotopes albeit there are two lithofacies packages reflecting two major lake stages (for details refer to supplementary

265 data Note S1) in the GSB.

### 266 **5.1.1 The Hettangian Age**

267 In the Hettangian, the climate was warm-humid like the Late Triassic in the GSB. The Qijiang Member is comprised of  
268 mainly mature quartz arenites and siltstones with coals (Fig. 7) as well as siderite concretions, indicating a stable tectonic  
269 setting and warm-humid climate in the eastern and southern GSB. Climate was similar across the whole region, because  
270 multiple coal layers occur in the lower Baitianba Fm. The alluvial fan system of the lower Baitianba Fm. (Figs. 7 and S6) is  
271 characterized by moderate-good roundness and sorting of gravels with sandy matrix (Fig. S3a. e.g., Liu et al., 2016; Qian et  
272 al., 2016; and this work). In the Newark basin of eastern North America, climate-sensitive sediments such as nodules of  
273 carbonate and gypsum (pseudomorph) as well as mudcrack in mudflat facies indicate an arid climate in the fifth cycle of the  
274 Hettangian (>199 Ma) Passaic Fm (Kent et al., 2017). More widespread, the eolian Navajo Sandstone, dated as  
275 Hettangian-Sinemurian (200-195 Ma. Parrish et al., 2019), indicates arid in Colorado Plateau (Fig. 1a. Boucot et al., 2013).

### 276 **5.1.2 The Sinemurian Age**

277 The early Sinemurian Zhenzhuchong Member is a combination of riverine flood plain and lacustrine facies (supplementary  
278 Note S1). The lithology is dominated by violet-red mudrocks with few thin greyish, greenish fine sandstones and siltstones.  
279 The reddish color of rocks may indicate a change of climate. Differences in the color appearance show that the reddish color  
280 started in the middle member in the central basin (Location A6. Fig. S2) but almost developed through the whole member in  
281 the western basin (Location A4. Fig. 6).

282 Within reddish mudrocks of the flood plain facies, multiple calcisols were observed at the Shaping section, Ya'an (Location  
283 A4. Figs. 1, 4, and 7), including a strongly leached calcisol horizon (Fig. S3c). We also interpret the reddish muddy  
284 sediments with abundant calcretes as the calcisol at sections of Dafang (Location A8. Zhang et al., 2016), Tianzhu (Location  
285 A9. Li and Chen, 2010), and Weiyuan (Location A10. SBG, 1980a). The calcisols indicate a (semi-) arid climate in the  
286 Sinemurian.

287 This climate change, interpreted from reddish mudrocks and paleosols, is consistent with the floral fossils (e.g., Huang, 2001;  
288 Wang et al., 2010), suggesting the decreasing humidity and increasing temperature from the Late Triassic epoch and the  
289 Hettangian age into the Sinemurian age in the southern GSB. However, in the northern GSB there are few proxies for  
290 climate change, and alluvial fan and lacustrine delta facies common in the middle Baitianba Fm (Fig. S6. e.g., Qian et al.,  
291 2016) do not give us information on climate.

292 The late Sinemurian Dongyuemiao Member also has reddish mudrocks and calcisols, similar to the Zhenzhuchong Member.  
293 Pedogenic calcretes were reported at Dafang (Location A8. Zhang et al., 2016), Tianzhu (Location A9. Li and Chen, 2010),  
294 and Yunyang (Location A15. Meng et al., 2005) and in the central and southern GSB (Figs 4 and 7 and Table S2), indicating

295 continued arid climate conditions at the time.

296 The interpreted Sinemurian (semi-) arid climate from reddish mudrocks and calcisols is supported by the flora (Li and Meng,  
297 2003) and the mudrock geochemistry (Guo et al., 2017). Few records of coeval terrestrial climate are known from other  
298 continents or regions in the literature. The Whitmore Point Member of the Moenave Fm deposited in dryland lakes (Tanner  
299 and Lucas, 2008) and the upper part of eolian Navajo Sandstone (Blakey et al., 1988) could represent the coevally similar  
300 climate in Colorado Plateau although relatively cool (~9 to 18 °C) continental climate was inferred from oxygen and  
301 hydrogen isotope composition of chert precipitated in interdune, freshwater lakes in the Navajo Sandstone (Kenny, 2015).  
302 With a difference, in eastern England, the co-occurrence of the acmes of thermophilic pollens *Classopollis classoides* and  
303 *Liasidium variabile* indicates the warm-humid climate in the late Sinemurian (Riding et al., 2013).

### 304 **5.1.3 The Pliensbachian Age**

305 The Ma'anshan Member of the Pliensbachian displays a prominent change in the distribution and extent of red color  
306 sediment and pedogenesis. The reddish sediments extend through the entire member (comp. Figs. 6 and S2) and can be  
307 observed across most of the GSB. Calcisols are documented in both the western and central GSB (Figs. 6, 7, S1, and S2).  
308 Ten calcisol horizons were recognized at the Shaping section, Ya'an (Figs. 6 and S1). Strongly leached pedogenic structures  
309 and mudcracks are seen in Bed H8 of the Tanba section, Hechuan (Fig. 3a and 3d). Abundant calcretes within terrestrial red  
310 mudrocks are widely described at Gaoxian of Dafang (Location A8. Zhang et al., 2016), Hulukou of Weiyuan (Location A10.  
311 SBG, 1980a), Geyaoguan of Gulin (Location A13. SBG, 1976), Taiyuan of Fengdu (Location A16. SBG, 1975), and Yaxi of  
312 Zunyi (Location A17. Yang, 2015). The widespread distribution of redbeds and calcisols (Figs. 4 and 7) denotes an  
313 intensification of the (semi-) arid climate.

314 Plant and sporopollen fossils also show a change to drier climate in the Pliensbachian. Compared to the Sinemurian members,  
315 more plant fossils are reported in this member (e.g., Meng and Chen, 1997; Wang et al, 2010). The Pliensbachian-Toarcian  
316 sporopollen assemblages are dominated by sporomorph genera assemblage *Dictyophyllidites-Cyathidites-Classopollis*, in  
317 which the dry-type gymnosperm spore *Classopollis* is more prevalent than in the Hettangian-Sinemurian (Zhang and Meng,  
318 1987).

319 Similar dry temperate / subtropical climate is interpreted for the upland coniferous forest in Qaidam Basin, Northwest China  
320 (Wang et al., 2005) and by interdune playa mudstones of the Kayenta Fm in Colorado Plateau (e.g., Bromley, 1992) albeit it  
321 was a cool-humid climate in South Kazakhstan, central Asia (Tramoy et al., 2016).

### 322 **5.1.4 The Toarcian Age**

323 In spite the fact that the Da'anzhai Member was deposited in the largest lacustrine transgression period (Fig. 7. details see  
324 supplementary data Note S1), abundant evidence for arid conditions, including backshore reddish mudrocks with calcisols,

325 lacustrine micritic dolomites and / or gypsum, and stable isotopic geochemistry of lacustrine carbonate, indicate that the  
326 Toarcian aridification could be the most intensive of the late Early Jurassic in the GSB.

327 Redbeds with abundant calcretes are well developed in this member (Figs. 4 and 7). Four calcisols in the Shaping section  
328 (Figs. 6 and S1) and the leaching/illuvial structure (Bed H13) in the Tanba section (Fig. 3c) were observed. Calcisols with  
329 calcretes also occur at sections of Dafang (Location A8. Zhang et al., 2016), Nanxi (Location A11. SBG 1980a), Gongxian  
330 (Location A12. Liang et al., 2006), and Yunyang (Location A15. Meng et al., 2005). The widespread occurrence of calcisols  
331 within the lacustrine facies reveals that subaerial exposure of sediments often interrupted the lake environment, illustrating  
332 dynamic lake level fluctuations and an arid climate.

333 Gypsum and micritic dolomites are reported in the western and southern GSB (SBG, 1980a; Mo and Yu, 1987; Peng, 2009;  
334 and this work) (Figs. 1, 4, and 7). Though there are a number of hypotheses on the dolomite formation in deep time, such as  
335 authigenic origin, diagenetic replacement, microbial mediation (e.g., Vasconcelos et al., 1995; Mckenzie et al., 2009; Petrash  
336 et al., 2017), a high abundance of dolomite was interpreted to form during greenhouse periods, characterized by warm  
337 climates, probably reflecting favourable conditions for evaporite deposition and dolomitization via hypersaline reflux  
338 (Warren, 2000). Dolomites are also thought the results of interplay of climate and sea-level / base-level change (e.g.,  
339 Newport et al., 2017) or are interacted with climatic regimes (Vandeginste et al., 2012). The widespread micritic dolomites  
340 in the Da'anzhai Member, which are associated with gypsum (Fig. 3f), likely indicate an arid climate in the central and  
341 western GSB (Fig. 1b). Gypsum occasionally occurs at Maliuping of Hechuan (Fig. 3f) and Wujiaba of Zigong (SBG,  
342 1980a), showing a possible evaporitic climate in the early Toarcian in the central GSB.

343 Carbon and oxygen isotopes of lacustrine carbonates further support the interpretation of an arid climate in the Toarcian age  
344 in the GSB. The mainly positive  $\delta^{13}\text{C}$  values 0 to 2 ‰ (Fig. 5) from Hechuan (Wang et al., 2006) indicate the lakes were  
345 brackish or even saline. The relatively heavy negative  $\delta^{13}\text{C}$  values -1‰ to -3.5 ‰ (Fig. 5) from Zigong (Wang et al. 2006)  
346 and Ya'an (this work) denote low depletions of  $^{13}\text{C}$  during calcite/aragonite precipitation and mean that the lakes were  
347 possibly brackish. Lightly negative  $\delta^{18}\text{O}$  values -5‰ to -12 ‰ (Fig. 5) of the lacustrine carbonates, suggest closed lacustrine,  
348 palustrine and pond systems formed in a regional arid-semiarid climate with evaporation exceeding precipitation.

349 The covariance of  $\delta^{13}\text{C}$  and  $\delta^{18}\text{O}$  is a criterion to distinguish closed or open lakes (e.g., Talbot, 1990; Li and Ku, 1997).  
350 Pronounced positive covariances ( $R^2=0.44-0.96$ ) between carbon and oxygen isotopes (Fig. 5) indicate a typical  
351 arid-semiarid pattern of lakes in the central and western GSB.

352 The Da'anzhai Member has the same palynofloral assemblage with the Ma'anshan Member, in which the dry-type  
353 gymnosperm spore *Classopollis* is more abundant than in underlying strata (e.g., Zhang and Meng, 1987; Wang et al., 2010),  
354 supporting the aridification indicated by climate-sensitive sediments and stable isotope ratios of lacustrine carbonates  
355 aforementioned.

356 Coastal Cheirolepidiacean (gymnosperm) forests indicate (temperate to subtropical) warm-humid climate punctuated by

357 locally dry and/or arid events in the Toarcian in Qaidam Basin, Northwest China (Wang et al., 2005). In Inner Mongolia of  
358 North China, the thermophilous plants such as the dipteridaceous fern *Hausmannia*, bennettitales *Ptilophyllum*, display  
359 similar warm and humid climate interrupted by hot and even arid conditions in a short intervals of the Toarcian (Deng et al.,  
360 2017). The warm-wet climate was also indicated by assemblages of sporomorph and vegetation in the late Early Jurassic in  
361 Jurong of Jiangsu, Lower Yangtze area (Huang et al., 2000). In South Kazakhstan, central Asia, paleoflora and  $\delta^2\text{H}$  values  
362 suggest slightly less humid and warmer conditions starting from the early Toarcian (Tramoy et al., 2016).

363 Climate-sensitive sediments, carbon and oxygen isotope values and covariance, and palynoflora, together indicate that an  
364 overall (semi-) arid climate dominated the GSB during the Early Jurassic, possibly accompanied by occasional evaporitic  
365 climate. Relatively abundant calcisols suggest that the GSB was in a subtropical arid zone based on the paleoclimatic  
366 zonation model of paleosols (Mack and James, 1994) during the middle-late Early Jurassic. Through the Early Jurassic, this  
367 (semi-) arid climate in GSB is thoroughly comparable with the simultaneous arid climate recorded in dryland lacustrine and  
368 eolian facies in Colorado Plateau (e.g., Blakey et al., 1988; Bromley, 1992; Tanner and Lucas, 2008; Parrish et al., 2017), but  
369 distinct from the relatively warm-humid climate indicated by sedimentological and floral characteristics in North China (e.g.,  
370 Wang et al., 2005, Deng et al., 2017) and in the relatively high latitudes of Southern Hemisphere (Pole, 2009).

371 In summary, the increasing aridity and warming in the GSB and arid climate in the Colorado Plateau could have been  
372 consecutive through the Early Jurassic, and seems not harmonized with the global fluctuated climate that could be  
373 imprinted by two large volcanic eruptions of the Central Atlantic magmatic province and Karro-Ferrar Large Igneous  
374 Province. The secular arid climate in the two areas might be more possibly constrained by paleotopography, where both were  
375 laid in the relatively low latitudes 15-30°N (Fig. 1a).

## 376 **5.2. $p\text{CO}_2$ perturbations and events**

377 Pedogenic carbonates found in various continental settings precipitate in direct contact with soil atmosphere and bed rock  
378 and hold a meaningful signature of past climate (Alonso-Zarza and Tanner, 2006). There are few high age resolution  $p\text{CO}_2$   
379 reconstructions for the Early Jurassic. The focus on  $p\text{CO}_2$  estimates has on the event horizons, such as the transition of the  
380 Triassic to Jurassic (e.g., Tanner et al., 2001; Schaller et al., 2011). Herein we present a  $p\text{CO}_2$  estimate based on data from  
381 the GSB at ~1.0 Myr age resolution for ~20 Myr (199-179 Ma) interval of the Early Jurassic (Figs. 6 and 8a).

### 382 **5.2.1. $p\text{CO}_2$ perturbation**

383 Results of model estimates show that the  $p\text{CO}_2$  values range 980-2610 ppmV with a mean 1660 ppmV in the Early Jurassic  
384 post the Hettangian and can be divided into three intervals (Figs. 6 and 8a): phase I, stable 1500-2000 (mean ~1700) ppmV  
385 in the Zhenzhuchong and Dongyuemiao members (Sinemurian age); phase II, main 1000-1500 (mean ~ 1300) ppmV in the  
386 Ma'anshan Member (Pliensbachian age); and phase III, great fluctuation 1094-2610 (mean ~1980) ppmV in the lower

387 Da'anzhai Member (early Toarcian age).

388 The evolution and level of  $p\text{CO}_2$  estimated by carbon isotope ratios of the pedogenic carbonates from the GSB compare  
389 favorably with the global composite based on the plant stomata method (data of the composite curve see Table S6), but show  
390 significant differences relative to the global composite  $p\text{CO}_2$  based on paleosols (Fig. 8a. Suchecki et al., 1988; Cerling,  
391 1991; Ekart et al., 1999), which may be attributed to the shortage (<4 samples) of global data and large age uncertainties (Fig.  
392 8a and Table S5 and S6).

393 The changes in  $p\text{CO}_2$  from the GSB, has a similar pattern to coeval seawater temperature estimates through the Early  
394 Jurassic although there are some discrepancies in pace and in detail (comp. Fig. 8a and 8b). That is, the relatively high  $p\text{CO}_2$   
395 1500-2000 ppmV approximately corresponds to the relatively high seawater mean temperature  $-2^\circ\text{C}$  to  $+2^\circ\text{C}$  in the  
396 Sinemurian, low  $p\text{CO}_2$  1000-1500 ppmV corresponds to low seawater mean temperature  $-5^\circ\text{C}$  to  $-2^\circ\text{C}$  in the Pliensbachian,  
397 and quick rising  $p\text{CO}_2$  of 1200 ppmV to  $\sim 2500$  ppmV corresponds to the rapidly increased seawater temperature of  $-4^\circ\text{C}$  to  
398  $+4^\circ\text{C}$  in the late Pliensbachian-early Toarcian.

399 The  $p\text{CO}_2$  record roughly trends with the carbon isotope records of marine carbonates and organic matter (comp. Fig. 8a to  
400 8d), suggesting a possible linkage of the  $p\text{CO}_2$  record in the GSB to the global carbon cycle (see section 5.2.2). Nevertheless,  
401 it is difficult for the proxies to compare in a higher detail, making it difficult to relate the record to orbital forcing of the  
402 global carbon cycle in the Sinemurian-Pliensbachian (Storm et al., 2020).

403 As a greenhouse gas, atmospheric  $\text{CO}_2$  has a strong control over global temperatures for much of the Phanerozoic (e.g.,  
404 Crowley and Berner, 2001; Royer, 2006; Price et al., 2013), but a decoupling of  $\text{CO}_2$  and temperature has also been  
405 suggested (e.g., Veizer et al., 2000; Dera et al., 2011; Schaller et al., 2011). The pattern of the Early Jurassic  $p\text{CO}_2$   
406 reconstructed from the carbon isotope of pedogenic carbonates in GSB, Southwest China, supports the coupled relationship  
407 of  $\text{CO}_2$ -temperature. Models of the coupling and decoupling of  $\text{CO}_2$ -temperature and  $\text{CO}_2$ -carbon cycle have to consider: 1),  
408 age order of  $\text{CO}_2$ -temperature/carbon cycle relevance, i.e. they should be related in the same age (long term or short term)  
409 hierarchy; 2) precise age constraints of individual  $\text{CO}_2$  and temperature data; 3) methods of  $\text{CO}_2$  and temperature estimates,  
410 depending on precondition, presumptions, parameters, uncertainty, sample diagenesis, etc.; 4) controls or influences of key  
411 factors such ice sheet, tectonic, paleogeography, cosmic ray flux, biota, volcanic eruption, and so on.

### 412 **5.2.2. Rapid $p\text{CO}_2$ falling events**

413 The GSB Early Jurassic  $p\text{CO}_2$  curve reveals two rapid falling events (Fig. 6 and 8a). The first event ( $1\text{E}_{\text{CO}_2}$ ) shows a quick  
414 drop from  $\sim 2370$  ppmV (sample J1z-08-01 at depth 84.7 m) to 1350 ppmV (sample J1z-10-02 at depth 94.4 m) near the  
415 boundary of the Dongyuemiao and Ma'anshan Members (Fig. 6), or to 1075 ppmV (sample J1z-11-02 at depth 111.7 m),  
416 which took place in the early Pliensbachian ( $\sim 190.4$ - $189.9/189.1$  Ma. Fig. 8c). The extent of the rapid falling  $p\text{CO}_2$  is  
417  $\sim 1000$ - $1300$  ppmV in 9.7-17.0 m. In other words,  $\sim 1000$  ppmV drop could be accomplished within  $\sim 0.5$ - $1.0$  Myr based on

418 the estimate of sedimentation rate (Table S4).

419 While the corresponding early Pliensbachian climatic and isotopic-shifting events are not observed in the smoothed curves of  
420 the Early Jurassic seawater temperature and carbon cycle (Dera et al. 2011), the rapid falling event 1E<sub>CO2</sub> is well correlated  
421 to the nearly coeval excursion events of carbon and oxygen isotopes recorded in western Tethys and North Atlantic (Fig. 8).  
422 The 1E<sub>CO2</sub> compares well to: 1) the rapid carbon isotope negative excursion of (oysters, belemnites, and brachiopods) shells  
423 from the Cleveland Basin, UK (Korte and Hesselbo, 2011) and northwest Algeria (Baghli et al., 2020), 2) that of organic  
424 matter and marine carbonates from southern Pairs Basin (Bougeault et al., 2017; Peti, et al., 2017) and Cardigan Bay Basin,  
425 UK (Storm et al., 2020), and 3) rapid oxygen isotope negative excursion (seawater warming) of belemnites from northern  
426 Spain (van de Schootbrugge et al., 2005). The rapid change of the stable isotope record had been called the  
427 Sinemurian-Pliensbachian boundary event (SPBE) and dated in the ammonite of the upper *Raricostatum* - lower *Jamesoni*  
428 zones (Bougeault et al., 2017).

429 The second event 2E<sub>CO2</sub> displays a large drop of 2574 ppmV (sample J1z-18-01 at depth 252.7 m) to 1094 ppmV (sample  
430 J1z-19-01 at depth 272.3 m), ~1500 ppmV decrease within 19.6 m (estimated age interval ~0.8 Myr. Table S4 and Fig. 8a).  
431 Following the second drop, *p*CO<sub>2</sub> rises rapidly by ~1300 ppmV of 1094 ppmV to 2386 ppmV (sample J1Z-20-01 at depth  
432 294.3 m) although only a few samples support the this cycle of *p*CO<sub>2</sub> falling-rising.

433 Strata in western Sichuan (Xu et al., 2017), may correlate to the time interval of the T-OAE, during which *p*CO<sub>2</sub> doubled  
434 over background values, from ~1000 ppmV to ~2000 ppmV (e.g., Beerling and Royer, 2002; McElwain et al., 2005; Berner,  
435 2006). Given that chronostratigraphical correlation is challenging, the *p*CO<sub>2</sub> falling-rising cycle might correspond to the  
436 quick shifting cycle of stable isotopes during the T-OAE (Fig. 8a and 8c-8d). In detail, the rapid falling-rising of *p*CO<sub>2</sub> is  
437 consistent with: 1) the quick negative-positive carbon isotope excursion of marine carbonates from Italy (Jenkyns and  
438 Clayton, 1986; Sabatino et al., 2009), England and Wales (Jenkyns and Clayton, 1997), north Spain (van de Schootbrugge et  
439 al., 2005), the Lusitanian Basin of Portugal (Hesselbo et al., 2007), Paris Basin (Hermoso et al., 2009), and Morocco (Bodin  
440 et al., 2016); 2) that of invertebrate calcareous shells from the Cleveland Basin of UK (Korte and Hesselbo, 2011) and  
441 northwest Algeria (Baghli et al., 2020); 3) that of marine organic matter from Morocco (Bodin et al., 2016), Yorkshire of  
442 England (Cohen et al., 2004; Kemp et al, 2005), Cardigan Bay Basin of UK (Xu et al., 2018), northern Germany (van de  
443 Schootbrugge et al., 2013), Alberta and British Columbia of Canada (Them II et al., 2017), northern Tibet of China (Fu et al.,  
444 2016), and Japan (Izumi et al., 2018); 4) that of terrestrial organic matter from Sichuan Basin, China (Xu et al., 2017); and 5)  
445 quick oxygen isotope negative-positive shifting (seawater warming) of brachiopods (Suan et al., 2008) and fossil wood  
446 (Hesselbo et al., 2007) from the Lusitanian Basin, Portugal.

447 Multiple hypotheses have been proposed to interpret the 5°–6 °C decrease of sea surface temperatures in the late  
448 Pliensbachian (Bailey et al., 2003; van de Schootbrugge et al., 2005; Suan et al., 2010) and warming ~8 °C in the early  
449 Toarcian (Bailey et al., 2003; Suan et al., 2010), such as the sea level falling and rising, methane release, Karoo–Ferrar



450 eruption, Hispanic corridor opening, etc. Perhaps, these hypotheses somewhat explain the rapid change of sea surface  
451 temperatures, but might not link to drastic falling of  $p\text{CO}_2$ . As we know, atmospheric  $\text{CO}_2$  is controlled by volcanism,  
452 weathering, vegetation on land and phytoplankton in ocean, and orbiting forcing. The Sr isotope curve shows a rapid change  
453 in the early Toarcian but does not in the early Pliensachian (e.g., Jones et al., 1999), indicating a distinct transfer of  
454 weathering took place on the land only at the T-OAE time. No robust evidence shows the rapid changes of terrestrial  
455 vegetation and marine primary productivity for the two intervals except for the floral change in western Tethys during the  
456 T-OAE (Slater et al. 2019). The Karoo–Ferrar eruption could be responsible for the rapid rising of  $p\text{CO}_2$  but not for the  
457 falling. Then the orbital forcing might be an alternative.

458 To sum up, the rapid falling events of the Early Jurassic  $p\text{CO}_2$  values in the GSB, are compatible with the response of stable  
459 isotopes (carbon cycle) and seawater temperature from coeval marine sediments in a total tendency and eventful change, but  
460 not harmonized at a high-resolution time scale. Whatever caused the rapid variations of sea surface temperatures, stable  
461 isotopes, and  $p\text{CO}_2$ , their near concordance suggests that it is a positive feedback of the sea surface temperature and carbon  
462 cycle to the  $p\text{CO}_2$  in trend and event through the Early Jurassic; whereas the higher frequency changes in the  
463 Sinemurian-Pliensbachian might may support other causal driving of the climate, such as orbital forcing (Storm et al., 2020).

## 464 **6. Conclusions**

465 Based on analyses of climate-sensitive sediments and stable isotopes and the reconstruction of paleoclimate and  $p\text{CO}_2$ , we  
466 conclude:

467 1) An overall warm-hot and (semi-) arid climate dominated the GSB during the Early Jurassic, possibly accompanied by  
468 occasional evaporitic climate in the Toarcian. This (semi-) arid climate in GSB is comparable with that in Colorado Plateau,  
469 western America, but distinct from the relatively warm-humid terrestrial climate recognized in other places of Chinese  
470 mainland (e.g., Qaidam, Inner Mongolia, and Lower Yangtze) and the high latitudes of Southern Hemisphere.

471 2) The Early Jurassic  $p\text{CO}_2$  values show that a range between 980 ppmV and 2610 ppmV is  $\sim 3.5$ -10 times the pre-industrial  
472 value 275 ppmV and the mean 1720 ppmV is  $\sim 6$  times the pre-industrial value. Three phases of  $p\text{CO}_2$  values were  
473 distinguished: 1500-2000 (mean  $\sim 1700$ ) ppmV in the Sinemurian age, 1000-1500 (mean  $\sim 1300$ ) ppmV in the Pliensbachian  
474 age, and 1094-2610 (mean  $\sim 1980$ ) ppmV in the early Toarcian. Two events of rapidly falling  $p\text{CO}_2$  were also recognized:  
475  $\sim 1000$ -1300 ppmV drop at the Sinemurian-Pliensbachian boundary and quick falling (-rising) by  $\sim 1500$  ppmV in the early  
476 Toarcian. The phases and events manifest the perturbation of  $p\text{CO}_2$  in the Early Jurassic.

477 3) The perturbation and rapid falling events of the Early Jurassic  $p\text{CO}_2$  from the GSB are compatible with the carbon cycle  
478 and seawater temperature from coeval marine sediments in the North Atlantic and western Tethys in a total tendency and  
479 eventful change. The compatibility suggests that it is a positive linkage of the sea surface temperature and carbon cycle to

480 the  $p\text{CO}_2$  through the Early Jurassic. On the contrary, differences at a high-resolution time scale implies additional climate  
481 drivers, such as orbital forcing are important in the Sinemurian-Pliensbachian record.

## 482 **Acknowledgements**

483 We thank Professors Helmut Weissert and Dan Breecker for careful scrutiny, constructive comments and suggestions. It is  
484 acknowledged this research was supported by Natural Science Foundation of China (NSFC) project 41672097.

485

## 486 **References**

- 487 Alonso-Zarza, A. M. and Tanner, L. H.: Preface. *Geol. Soc. Am. Spe. Pap.*, 416, v-vii, doi, 10.1130/0-8137-2416-3.v, 2006.
- 488 Arabas, A., Schlogl, J., and Meiste C.: Early Jurassic carbon and oxygen isotope records and seawater temperature variations:  
489 Insights from marine carbonate and belemnite rostra (Pieniny Klippen Belt, Carpathians), *Palaeogeogr. Palaeoclimatol.*  
490 *Palaeoecol.*, 485, 119–135, 2017
- 491 Arens, N. C., Jahren, A. H., and Amundson, R.: Can  $\text{C}_3$  plants faithfully record the carbon isotopic composition of  
492 atmospheric carbon dioxide, *Paleobiology*, 26, 137–164, 2000,
- 493 Arias, C.: Extinction pattern of marine Ostracoda across the Pliensbachian-Toarcian boundary in the Cordillera Ibérica, NE  
494 Spain: Causes and consequences, *Geobios*, 42, 1-15, 2009.
- 495 Baghli, H., Mattioli, E., Spangenberg, J. E., Bensalah, M., Arnaud-Godet, F., Pittet, B., and Suan, G.: Early Jurassic climatic  
496 trends in the south-Tethyan margin. *Gondwana. Res.*, 77, 67-81, doi, 10.1016/j.gr.2019.06.016, 2020.
- 497 Bailey, T. R., Rosenthal, Y., McArthur, J. M., van de Schootbrugge, B., and Thirlwall, M. F.: Paleoceanographic changes of  
498 the Late Pliensbachian-Early Toarcian interval: a possible link to the genesis of an Oceanic Anoxic Event, *Earth Planet.*  
499 *Sci. Lett.*, 212, 307-320, 2003.
- 500 Beerling, D. J. and Royer, D. L.: Reading a  $\text{CO}_2$  signal from fossil stomata, *The New Phytologist*, 153, 387-397, doi:0.  
501 1046/j. 0028-646X. 2001. 00335. x, 2002.
- 502 Berner, R. A.: GEOCARBSULF: A combined model for Phanerozoic atmospheric  $\text{O}_2$  and  $\text{CO}_2$ , *Geochi. Cosmochi. Ac.*,  
503 70(23 Spec. Iss. ), 5653-5664, 2006.
- 504 Besse, J., and Courtillot, V.: Paleogeographic maps of the continents bordering the Indian Ocean since the Early Jurassic: J.  
505 *Geophys. Res.*, 93, 11791–808, 1988.
- 506 Blakey, R. C., Peterson, F., and Kocurek, G.: Synthesis of late Paleozoic and Mesozoic eolian deposits of the Western  
507 Interior of the United States, *Sediment. Geol.*, 56, 3-125, doi, [https://doi.org/10.1016/0037-0738\(88\)90050-4](https://doi.org/10.1016/0037-0738(88)90050-4), 1988.
- 508 Bodin, S., Krencker, F. N., Kothe, T., Hoffmann, R., Mattioli, E., Heimhofer, U., and Kabiri, L.: Perturbation of the carbon

509 cycle during the late Pliensbachian – early Toarcian: New insight from high-resolution carbon isotope records in  
510 Morocco, *J. Afr. Earth Sci.*, 116, 89–104, doi, 10.1016/j.jafrearsci.2015.12.018, 2016.

511 Boucot, A. J., Chen, X., Scotese, C. R., and Morley, R. J.: Phanerozoic Paleoclimate: An Atlas of Lithologic Indicators of  
512 Climate, *SEPM Concepts in Sedimentology and Paleontology* 11. SEPM, Tulsa, 1-478, 2013.

513 Bougeault, C., Pellenard, P., Deconninck, J. F., Hesselbo, S. P., Dommergues, J. L., Bruenau, L., Cocquerez, T., Laffont, R.,  
514 Huret, E., and Thibault, N.: Climatic and palaeoceanographic changes during the Pliensbachian (Early Jurassic) inferred  
515 from clay mineralogy and stable isotope (C-O) geochemistry (NW Europe), *Global Planet. Change*, 149, 139-152,  
516 2017.

517 Breecker, D. O. and Retallack, G. J.: Refining the pedogenic carbonate atmospheric CO<sub>2</sub> proxy and application to Miocene  
518 CO<sub>2</sub>, *Palaeogeogr. Palaeoclimatol. Palaeoecol.*, 406, 1-8, 2014.

519 Breecker, D. O., Sharp, Z. D., and McFadden, L. D.: Atmospheric CO<sub>2</sub> concentrations during ancient greenhouse climates  
520 were similar to those predicted for A. D. 2100, *PNAS*, 107, 2, 576-580, 2009.

521 Breecker, D. O., Sharp, Z. D., and McFadden, L. D.: Seasonal bias in the formation and stable isotope composition of  
522 pedogenic carbonate in modern soil from central New Mexico, USA, *Geol. Soc. Am. Bull.*, 12, 630-640, 2010.

523 Breecker, D. O.: Quantifying and understanding the uncertainty of atmospheric CO<sub>2</sub> concentrations determined from calcic  
524 paleosols. *Geochem. Geophys. Geosyst.*, 14, 3210–3220, 2013.

525 Bromley, M.: Topographic inversion of early interdune deposits, Navajo Sandstone (Lower Jurassic), Colorado Plateau,  
526 USA, *Sediment. Geol.*, 80, 1-25, 1992.

527 Buchmann, N., Brooks, R. J., Flanagan, L. B., and Ehleringer, J. R.: Carbon isotope discrimination of terrestrial ecosystems.  
528 In Griffiths, H., ed. *Stable Isotopes: Integration of Biological, Ecological and Geochemical Processes*, BIOS Scientific  
529 Publications, Oxford, United Kingdom, 203–21, 1998.

530 Caruthers, A. H., Smith, P. L., Gröcke, D. R.: The Pliensbachian-Toarcian (Early Jurassic) extinction, a global multi-phased  
531 event, *Palaeogeogr. Palaeoclimatol. Palaeoecol.*, 386, 104-118, 2013.

532 Cerling, T. E.: Carbon dioxide in the atmosphere: evidence from Cenozoic and Mesozoic paleosols: *Am. J. Sci.*, 291,  
533 377-400, 1991.

534 Cerling, T. E.: Stable carbon isotopes in palaeosol carbonates, in: *Palaeoweathering, palaeosurfaces and related continental*  
535 *deposits*, edited by: Thiry, M. and Simm-Coinçon, R., *Spec. P. Intl. Asso. Sedi.*, 27, 43-60, 1999.

536 Cleveland, D. M., Nordt, L. C., Dworkin, S. I., and Atchley, S. C.: Pedogenic carbonate isotopes as evidence for extreme  
537 climatic events preceding the Triassic-Jurassic boundary: implications for the biotic crisis? *GSA Bull.*, 120, 1408-1415,  
538 2008.

539 Cohen, K. M., Finney, S. C., Gibbard, P. L., and Fan, J. X. The ICS International Chronostratigraphic Chart (2013 updated).  
540 *Episodes*, 36, 199-204, 2013.

541 Cohen, A. S., Coe, A. L., Harding, S. M., and Schwark, L.: Osmium isotope evidence for the regulation of atmospheric CO<sub>2</sub>  
542 by continental weathering, *Geology*, 32, 157–160, 2004.

543 Crowley, T. J. and Berner, R. A.: CO<sub>2</sub> and climate change, *Science*, 292, 870–872, 2001.

544 Deng, S. H., Zhao, Y., Lu, Y. Z., Shang, P., Fan, R., Li, X., Dong, S. X., and Liu, L.: Plant fossils from the Lower Jurassic  
545 coal-bearing formation of central InnerMongolia of China and their implications for palaeoclimate, *Palaeoworld*, 26:  
546 279-316, 2017.

547 Dera, G., Brigaud, B., Monna, F., Laffont, R., Pucéat, E., Deconinck, J. F., Pellenard P., Joachimski, M. M., and Durlet, C.:  
548 Climatic ups and downs in a disturbed Jurassic world, *Geology*, 39(3), 215-218, 2011.

549 Dera, G., Pellenard, P., Neige, P., Deconinck, J. F., Pucéat, E., and Dommergues, J. L.: Distribution of clay minerals in Early  
550 Jurassic Peritethyan seas: Palaeoclimatic significance inferred from multiproxy comparisons, *Palaeogeogr.*  
551 *Palaeoclimatol. Palaeoecol.*, 271(1-2), 39–51, doi, 10.1016/j.palaeo.2008.09.010, 2009.

552 Dong, Z. M.: A new prosauropod from Ziliujing Formation of Sichuan Basin, *Verte. Palasiatica*, 22(4), 310-313, 1984 (in  
553 Chinese with English abstract).

554 Duan, S. Y. and Chen, Y.: Mesozoic fossil plants and coal formation of eastern Sichuan Basin, in: *Continental Mesozoic*  
555 *Stratigraphy and Paleontology in Sichuan Basin of China: Part II*, Paleontological Professional Papers, People's Publ.  
556 House Sichuan, Chengdu, 491-519, 1982 (in Chinese).

557 Ekart, D. D., Cerling, T. E., Montñez, I. P., and Tabor, N. J.: A 400 million year carbon isotope record of pedogenic  
558 carbonate: implications for paleoatmospheric carbon dioxide, *Am. J. Sci.*, 299, 805-827, 1999.

559 Flügel, E.: *Microfacies of Carbonate Rocks: Analysis, Interpretation and Application*, Springer-Verlag, Berlin, Heidelberg,  
560 New York, 976 pp. 2004.

561 Friedli, H., Lotscher, H., Oeschger, H., Siegenthale, U., and Stauffer, B.: Ice core record of the <sup>13</sup>C/<sup>12</sup>C ratio of atmospheric  
562 CO<sub>2</sub> in the past two centuries, *Nature*, 324, 237–238, 1986.

563 Fu, X. G., Wang, J., Feng, X. L., Wang, D., Chen, W. B., Song, C. Y., and Zeng, S. Q.: Early Jurassic carbon-isotope  
564 excursion in the Qiangtang Basin (Tibet), the eastern Tethys: implications for the Toarcian Oceanic anoxic event, *Chem.*  
565 *Geol.*, 442, 67–72, 2016.

566 Gómez, J. J., and Goy, A.: Warming-driven mass extinction in the Early Toarcian (Early Jurassic) of northern Spain,  
567 Correlation with other time-equivalent European sections. *Palaeogeogr. Palaeoclimatol. Palaeoecol.*, 306, 176-195,  
568 2011.

569 Gómez, J. J., Comas-Rengifo, M. J., and Goy, A.: Palaeoclimatic oscillations in the Pliensbachian (Early Jurassic) of the  
570 Asturian Basin (Northern Spain), *Clim. Past*, 12, 1199-1214, 2015.

571 Gómez, J. J., Goy, A., and Canales, M. L.: Seawater temperature and carbon isotope variations 15 in belemnites linked to  
572 mass extinction during the Toarcian (Early Jurassic) in Central and Northern Spain. Comparison with other European

- 573 sections, *Palaeogeogr. Palaeoclimatol. Palaeoecol.*, 258, 28-58, 2008.
- 574 Guo, L. Y., Zhang, S. W., Xie, X. N., Li, Z. S., Huang, C. Y., and Chen, B. C.: Geochemical characteristics and organic  
575 matter enrichment of the Dongyuemiao Member mudstone of Lower Jurassic in the Western Hubei-Eastern Chongqing,  
576 *Ear. Sci.*, 42(7): 1235-1246, 2017 (in Chinese with English abstract).
- 577 Guo, Z. W., Deng, K. L., and Han, Y. H.: Formation and Evolution of the Sichuan Basin, Geo. Publ. House, Beijing, 200,  
578 1996.
- 579 Hallam, A., and Wignall, P. B.: Mass extinctions and sea-level changes, *Earth Sci. Rev.*, 48, 217-250, 1999.
- 580 He, T. H. and Liao, C. F.: Control of Upper Triassic division and correlation and Indosinian Movement on oil and gas  
581 accumulation in Sichuan Basin, *Acta Geol. Sichuan*, 00, 40-55, 1985 (in Chinese).
- 582 Hermoso, M., Le Callonnec, L., Minoletti, F., Renard, M., and Hesselbo, S. P.: Expression of the Early Toarcian negative  
583 carbon-isotope excursion in separated carbonate microfractions (Jurassic, Paris Basin), *Earth Planet. Sci. Lett.*, 277,  
584 194-203, 2009.
- 585 Hesselbo, S. P. and Jenkyns, H. C.: British Lower Jurassic sequence stratigraphy, in: *Mesozoic-Cenozoic Sequence*  
586 *Stratigraphy of European Basins*, edited by: de Graciansky, P. C., Hardenbol, J., Jacquin, Th., and Vail, P. R., SEPM  
587 *Spec. Pap.*, 60, 562-581, 1998.
- 588 Hesselbo, S. P., Gröcke, D. R., Jenkyns, H. C., Bjerrum, C. J., Farrimond, P., Morgans Bell, H. S., Green, O. R.: Massive  
589 dissociation of gas hydrate during a Jurassic oceanic anoxic event, *Nature*, 406, 392-395, doi:10. 1038/35019044.,  
590 2000.
- 591 Hesselbo, S. P., Jenkyns, H. C., Duarte, L. V., and Oliveira, L. C. V.: Carbon-isotope record of the Early Jurassic (Toarcian)  
592 Oceanic Anoxic Event from fossil wood and marine carbonate Lusitanian Basin, Portugal, *Earth Planet. Sci. Lett.*, 253,  
593 455-470, 2007.
- 594 Huang, P., Guan, Y. M., and Yang, X. Q.: Early Jurassic palynoflora from a drilling section of Jurong, Jiangsu, *Acta*  
595 *Micropalaeontol. Sin.*, 17(1), 85- 98, 2000.
- 596 Huang, C. J., and Hesselbo, S. P.: Pacing of the Toarcian Oceanic Anoxic Event (Early Jurassic) from astronomical  
597 correlation of marine sections. *Gondwana Res.*, 25, 1348-1356, doi, org/10.1016/j.gr.2013.06.023, 2014.
- 598 Huang, Q. S.: Paleoclimate and coal-forming characteristics of the Late Triassic Xujiahe stage in northern Sichuan, *Geol.*  
599 *Rev.*, 41(1): 92-99, 1995, (in Chinese with English abstract).
- 600 Huang, Q. S.: The flora and paleoenvironment of the Early Jurassic Zhenzhuchong Formation in Daxian-Kaixian region,  
601 northern margin of the Sichuan Basin, *Ear. Sci. J. China Uni. Geosci.*, 3, 221-229, 2001 (in Chinese with English  
602 abstract).
- 603 Imbellone, P. A.: Classification of Paleosols. São Paulo, UNESP, *Geociências*, 30(1), 5-13, 2011,
- 604 Izumi, K., Kemp, D., Itamiya, S., and Inui, M.: Sedimentary evidence for enhanced hydrological cycling in response to rapid

605 carbon release during the early Toarcian oceanic anoxic event, *Earth Planet. Sci. Lett.*, 481, 162–170, 2018.

606 Jahren, A. H., Arens, N. C., and Harbeson, S. A.: Prediction of atmospheric  $\delta^{13}\text{C}_{\text{CO}_2}$  using fossil plant tissues, *Rev. Geophys.*,  
607 46, RG1002, doi: 10.1029/2006RG000219, 2008.

608 Jenkyns, H. C. and Clayton, C. J.: Black shales and carbon isotopes in pelagic sediments from the Tethyan Lower Jurassic,  
609 *Sedimentology*, 33, 87-106, 1986.

610 Jenkyns, H. C., and Clayton, C. J., Lower Jurassic epicontinental carbonates and mudstones from England and Wales:  
611 chemostratigraphic signals and the early Toarcian anoxic event, *Sedimentology*, 44, 687-706, 1997.

612 Jenkyns, H. C., Jones, C. E., Gröcke, D. R., Hesselbo, S. P., and Parkinson, D. N.: Chemostratigraphy of the Jurassic System:  
613 Applications, limitations and implications for palaeoceanography, *J. Geol. Soc. London*, 159, 351-378, 2002.

614 Jenkyns, H. C.: Geochemistry of oceanic anoxic events, *Geochem. Geophys. Geosyst.*, 11, Q03004. doi:10.  
615 1029/2009GC002788, 2010.

616 Jones, C. E., Jenkyns, H. C., and Hesselbo, S. P.: Strontium isotopes in Early Jurassic seawater: *Geoch. Cosmoch. Acta*, 58,  
617 1285–1301, 1994.

618 Kemp, D. B., Coe, A. L., Cohen, A. S., and Schwark, L.: Astronomical pacing of methane release in the Early Jurassic  
619 period, *Nature*, 437, 396-399, doi, org/10.1038/nature04037, 2005.

620 Kenny, R.: A cool time in the Early Jurassic: first continental palaeoclimate estimates from oxygen and hydrogen isotope  
621 ratios in chert from Navajo Sandstone carbonate lenses, Utah (USA), *Carbonate Evaporite*, doi,  
622 10.1007/s13146-015-0276-z, 2015.

623 Kent, D. V., Olsen, P. E., and Muttoni, G.: Astrochronostratigraphic polarity time scale (APTS) for the Late Triassic and  
624 Early Jurassic from continental sediments and correlation with standard marine stages, *Earth-Sci. Rev.*, 166, 153-180,  
625 2017.

626 Korte, C., and Hesselbo, S. P.: Shallow marine carbon and oxygen isotope and elemental records indicate  
627 icehouse-greenhouse cycles during the Early Jurassic, *Paleoceanography*, 26, 1–18, 2011.

628 Korte, C., Hesselbo, S. P., Jenkyns, H. C., Rickaby, R. E. M., and Spötl, C.: Palaeoenvironmental significance of carbon-  
629 and oxygen-isotope stratigraphy of marine Triassic-Jurassic boundary sections in SW Britain, *J. Geol. Soc. London*,  
630 166(3), 431-445, 2009.

631 Korte, K., Hesselbo, S. P., Ullmann, C.V., Dietl, G., Ruhl, M., Schweigert, G., Thibault, N.: Jurassic climate mode governed  
632 by ocean gateway, *Nat. Commun.*, 6, 10015, doi, 10.1038/ncomms10015, 2015.

633 Li, H. C. and Ku, T. L.:  $\delta^{13}\text{C}$ - $\delta^{18}\text{O}$  covariance as a paleohydrological indicator for closed basin lakes, *Palaeogeogr.*  
634 *Palaeoclimatol. Palaeoecol.*, 133, 69-80, 1997.

635 Li, L. Q., Wang, Y. D., Liu, Z. S., Zhou, N., and Wang, Y.: Late Triassic palaeoclimate and palaeoecosystem variations  
636 inferred by palynological record in the northeastern Sichuan Basin, China, *Paläontol. Zeits.*, 309-324, DOI 10.

637 1007/s12542-016-0309-5, 2016.

638 Li, W. M. and Chen, J. S.: Discovery and significances of the Jurassic Ziliujing Formation in Tianzhu, Guizhou, China New  
639 Techn. Prod., 13, 134-135, 2010 (in Chinese).

640 Li, X. B. and Meng, F. S.: Discovery of fossil plants from the Ziliujing Formation in Hechuan of Chongqing. Geol. Min.  
641 Resour. South China, 3: 60-65, 2003 (in Chinese with English abstract).

642 Li, Y. Q. and He, D. F.: Evolution of tectonic-depositional environment and prototype basins of the Early Jurassic in Sichuan  
643 Basin and adjacent areas, Acta Petrol. Sin., 35(2), 219-232, 2014 (in Chinese with English abstract).

644 Li, Y., Allen, P. A., Densmore, A. L., and Xu, Q.: Evolution of the Longmen Shan Foreland Basin (Western Sichuan, China)  
645 during the Late Triassic Indosinian Orogeny. Basin Res., 15, 117-138, 2003.

646 Liang, B., Wang, Q. W., and Kan, Z. Z.: Geochemistry of Early Jurassic mudrocks from Ziliujing Formation and  
647 implications for source-area and weathering in dinosaur fossils site in Gongxian, Sichuan province, J. Min. Petr., 26(3),  
648 94-99, 2006 (in Chinese with English abstract).

649 Littler, K., Hesselbo, S. P., and Jenkyns, H. C.: A carbon-isotope perturbation at the Pliensbachian-Toarcian boundary:  
650 evidence from the Lias Group, NE England. Geol. Mag., 147, 181-192, 2010.

651 Liu, J. L., Ji, Y. L., Zhang, K. Y., Li, L. D., Wang, T. Y., Yang, Y., and Zhang, J.: Jurassic sedimentary system transition  
652 and evolution model in western Sichuan Foreland Basin, Acta Petrol. Sin., 37(6), 743-756, 2016 (in Chinese with  
653 English abstract).

654 Ma, Y. S., Chen, H. D., Wang, G. L., Guo, T. L., Tian, J. C., Liu, W. J., Xu, X. S., Zheng, R. C., Mou, C. L., and Hou, M. C.:  
655 Atlas of Lithofacies Paleogeography on the Sinian-Neogene Tectonic-Sequence in South China, Science Press, Beijing,  
656 162-165, 2009 (in Chinese).

657 Mack, G. H. and James, W. C.: Paleoclimate and the Global Distribution of Paleosols, J. Geol., 102, 360-366, 1994.

658 Mack, G. H., James, W. C., and Monger, H. C.: 1 Classification of paleosols, Geol. Soc. Am. Bull., 105, 129-136, 1993.

659 McElwain, J. C., Wade-Murphy, J., and Hesselbo, S. P.: Changes in carbon dioxide during an oceanic anoxic event linked to  
660 intrusion into Gondwana coals, Nature, 435, 479-482, doi:org/10.1038/nature03618, 2005.

661 McKenzie, J. A., and Vasconcelos C.: Dolomite Mountains and the origin of the dolomite rock of which they mainly consist:  
662 historical developments and new perspectives, Sedimentology, 56, 205 - 219, doi, 10.1111/j.1365-3091.2008.01027.x,  
663 2009.

664 Meng, F. S., Chen, H. M., and Li, X. B.: Study on Lower Middle Jurassic boundary in Chongqing region, Geol. Min. Resour.  
665 S China, 3, 64-71, 2005 (in Chinese with English abstract).

666 Meng, F. S., Li, X. B., and Chen, H. M.: Fossil plants from Dongyuemiao Member of the Ziliujing Formation and  
667 Lower-Middle Jurassic boundary in Sichuan basin, China, Acta Palaeontol. Sin., 42(4), 525-536, 2003. (in Chinese with  
668 English abstract).

669 Metodiev, L. and Koleva-Rekalova, E.: Stable isotope records ( $\delta^{18}\text{O}$  and  $\delta^{13}\text{C}$ ) of Lower - Middle Jurassic belemnites from  
670 the Western Balkan mountains (Bulgaria), Palaeoenvironmental application, *Appl. Geochem.*, 23, 2845–2856, 2008.

671 Mintz, J. S., Driese, S. G., Breecker, D. O., and Ludvigson, G. A.: Influence of changing hydrology on pedogenic calcite  
672 precipitation in Vertisols, Dance Bayou, Brazoria County, Texas, USA: implications for estimating paleoatmospheric  
673  $p\text{CO}_2$ , *J. Sedi. Res.*, 81(6), 394-400, 2011.

674 Mo, Y. Z. and Yu, H. Y.: The discovery and its geological significance of dolomite in Ziliujing Groups of Middle and Lower  
675 Jurassic Series in Ma'anshan Member, *Geol Guizhou*, 10(1), 110-113, 1987 (in Chinese with English abstract).

676 Montañez, I. P.: Modern soil system constraints on reconstructing deep-time atmospheric  $\text{CO}_2$ , *Geochim. Cosmochim. Acta*,  
677 101, 57–75, 2013.

678 Nadelhofer K. J., and Fry B.: Controls on natural nitrogen-15 and carbon-13 abundances in forest soil organic matter, *Soil*  
679 *Sci. Soc. Am. J.*, 52, 1633-1640, 1988.

680 Newport, R., Hollis, C., Bodin, S., and Redfern, J.: Examining the interplay of climate and low amplitude sea-level change  
681 on the distribution and volume of massive dolomitization: Zebbag Formation, Cretaceous, Southern Tunisia, *Deposit.*  
682 *Rec.*, 3(1), 38–59, doi,10.1002/dep2.25, 2017.

683 Parrish, J. T., Hasiotis, S. T., and Chan, M. A.: Carbonate deposits in the Lower Jurassic Navajo Sandstone, southern Utah  
684 and northern Arizona, *J. Sedi. Res.*, 87, 740-762, doi, <https://doi.org/10.2110/jsr.2017.42>, 2017.

685 Parrish, J. T., Rasbury, E. T., Chan, M. A., and Hasiotis, S. T.: Earliest Jurassic U-Pb ages from carbonate deposits in the  
686 Navajo Sandstone, southeastern Utah, USA, *Geology*, 47(11), 1015–1019, doi, 10.1130/g46338.1, 2019.

687 Peng, G. Z.: Assemblage characters of Jurassic dinosaurian fauna in Zigong of Sichuan, *J. Geosci.*, 33(2), 113-123, 2009 (in  
688 Chinese with English abstract).

689 Peti, L., Thibault, N., Clémence, M. E., Korte, C., Dommergues, J. L., Bougeault, C., Pellenard, P., Jelby, M. E., and  
690 Ullmann, C. V.: Sinemurian-Pliensbachian Calcareous Nannofossil Biostratigraphy and Organic Carbon Isotope  
691 Stratigraphy in the Paris Basin: Calibration to the Ammonite Biozonation of NW Europe, *Palaeogeogr. Palaeoclimatol.*  
692 *Palaeoecol.*, 468, 142–161, 2017.

693 Petrash, D. A., Bialik, O. M., Bontognali, T. R. R., Vasconcelos, C., Roberts, J. A., McKenzie, J. A., and Konhauser, K. O.:  
694 Microbially catalyzed dolomite formation: From near-surface to burial, *Earth Sci. Rev.*, 171, 558–582, doi,  
695 10.1016/j.earscirev.2017.06.015, 2017.

696 Philippe M., Puijalon S., Suan G., Mousset S., Thévenard F., and Mattioli E.: The palaeolatitudinal distribution of fossil  
697 wood genera as a proxy for European Jurassic terrestrial climate, *Palaeogeogr. Palaeoclimatol. Palaeoecol.*, 466, 373–  
698 381, 2017.

699 Pole, M.: Vegetation and climate of the New Zealand Jurassic, *GFF*, 131:1-2, 105-111, DOI: 10. 1080/11035890902808948,  
700 2009.



701 Price, G. D., Twitchett, R. J., Wheeley, J. R., and Buono, G.: Isotopic evidence for long term warmth in the Mesozoic, *Sci.*  
702 *Rep.*, 3, 1438, doi, 10.1038/srep01438, 2013.

703 Qian, T., Liu, S. F., Wang, Z. X., Li, W. P., and Chen, X. L.: Characteristics of the Baitianba Formation conglomerate of  
704 Lower Jurassic in the northern Sichuan basin and its constraint to the uplift of the south Dabashan, China *Sci. Paper*,  
705 11(21), 2402-2408, 2016 (in Chinese with English abstract).

706 Rees, P. A., Zeigler, A. M., and Valdes, P. J.: Jurassic phytogeography and climates: new data and model comparisons, in:  
707 *Warm Climates in Earth History*, edited by: Huber, B., MacLeod, K., and Wing, S., Cambridge University Press, 297–  
708 318, 1999.

709 Retallack, G. J.: A 300-million-year record of atmospheric carbon dioxide from fossil plant cuticles, *Nature*, 411, 287-290,  
710 2001a.

711 Retallack, G. J.: Adapting soil taxonomy for use with paleosols. *Quatern. Int.*, 51/52: 55-57, doi,  
712 10.1016/S1040-6182(98)00039-1, 1998.

713 Retallack, G. J.: *Soils of the Past--An Introduction to Paleopedology*, Blackwell Science Ltd, Oxford, 333, 2001b.

714 Riding, J. B., Leng, M. J., Kender, S., Hesselbo, S. P., and Feist-Burkhardt, S.: Isotopic and palynological evidence for a new  
715 Early Jurassic environmental perturbation, *Palaeogeogr. Palaeoclimatol. Palaeoecol.*, 374: 16–27, 2013.

716 Robinson, S. A., Andrews, J. E., Hesselbo, S. P., Radley, J. D., Dennis, P. F., Harding, I. C., and Allen, P.: Atmospheric  
717  $p\text{CO}_2$  and depositional environment from stable-isotope geochemistry of calcrite nodules (Barremian, Lower  
718 Cretaceous, Wealden Beds, England), *J. Geol. Soc., London*, 159, 215–24, 2002.

719 Robinson, S. A., Ruhl, M., Astley, D. L., Naafs, B. D. A., Farnsworth, A. J., Bown, P. R., Jenkyns, H. C., Lunt D. J.,  
720 O'Brien, C., Pancost, R. D., and Markwick, P. J.: Early Jurassic North Atlantic sea-surface temperatures from TEX86  
721 palaeothermometry. *Sedimentology*, 64(1), 215–230, doi, 10.1111/sed.12321, 2017.

722 Romanek, C., Grossman, E. and Morse, J.: Carbon isotopic fractionation in synthetic aragonite and calcite: effects of  
723 temperature and precipitation rate, *Geochim. Cosmochim. Ac.*, 56, 419-430, 1992.

724 Rosales, I., Quesada, S., and Robles, S.: Primary and diagenetic isotopic signals in fossils and hemipelagic carbonates: the  
725 Lower Jurassic of northern Spain, *Sedimentology*, 48, 1149–1169, 2001.

726 Royer, D. L.: CO<sub>2</sub>-forced climate thresholds during the Phanerozoic: *Geochim. Cosmochim. Ac.*, 70, 56, 65–75, doi: 10.  
727 1016/j.gca.2005.11.031, 2006.

728 Sabatino, N., Neri, R., Bellanca, A., Jenkyns, H., Baudin, F., Parisi, G., and Masetti, D.: Carbon isotope records of the Early  
729 Jurassic (Toarcian) oceanic anoxic event from the Valdorbia (Umbria-Marche Apennines) and Monte Mangart (Julian  
730 Alps) sections: palaeogeographic and stratigraphic implications, *Sedimentology*, 56, 1307-1328, 2009.

731 SBG (Sichuan Bureau of Geology): Reports of 1:200,000 Regional Geology Investigations (Profile Qianjiang), 48, 1975 (in  
732 Chinese).

733 SBG (Sichuan Bureau of Geology): Reports of 1:200,000 Regional Geology Investigations (Profile Xuyong), 55, 1976 (in  
734 Chinese).

735 SBG (Sichuan Bureau of Geology): Reports of 1:200,000 Regional Geology Investigations (Profiles Suining, Zigong,  
736 Neijiang, Yibin, and Luzhou), 43-50, 1980a (in Chinese).

737 SBG (Sichuan Bureau of Geology): Reports of 1:200,000 Regional Geology Investigations (Profiles Yilong, Tongjiang,  
738 Nanchong, Guang'an, and Chongqing), 100-101, 1980b (in Chinese).

739 SBGM (Sichuan Bureau of Geology and Mineral Resources): Geology of Sichuan Province, Geol. Publ. House, Beijing, 730,  
740 1991 (in Chinese with English summary).

741 SBGM: Lithostratigraphy of Sichuan Province, China Uni. Geosci. Press, Wuhan, 388, 1997 (in Chinese).

742 Schaller, M. F., Wright, J. D., and Kent, D. V.: Atmospheric  $p\text{CO}_2$  perturbations associated with the Central Atlantic  
743 Magmatic Province, *Science*, 331, 1404-1409, doi, 10.1126/science.1199011, 2011.

744 Sellwood, B. W., and Valdes, P. J.: Jurassic climates, *P. Geologist Assoc.*, 119, 5-17, 2008.

745 Scotese, C. R.: Atlas of Jurassic Paleogeographic Maps, PALEOMAP Atlas for ArcGIS, volume 4, The Jurassic and Triassic,  
746 Maps 32-42, Mollweide Projection, PALEOMAP Project, Evanston, IL, 2014.

747 Slater, S. M., Twitchett, R. J., Danise, S., and Vajda, V.: Substantial vegetation response to Early Jurassic global warming  
748 with impacts on oceanic anoxia, *Nature Geo.*, doi, 10.1038/s41561-019-0349-z, 2019.

749 Soil survey Staff: Keys to Soil Taxonomy, Pocahontas Press, Blacksburg, VA, 1998.

750 Steinhorsdottir, M. and Vajda, V.: Early Jurassic (late Pliensbachian)  $\text{CO}_2$  concentrations based 5 on stomatal analysis of  
751 fossil conifer leaves from eastern Australia, *Gondwana Res.* 27, 829-897, 2015.

752 Storm, M. S., Hesselbo, S. P., Jenkyns, H. C., Ruhl, M., Ullmann, C. V., Xu, W., Leng, M. J., Riding, J. B., Gorbanenko, O.:  
753 Orbital pacing and secular evolution of the Early Jurassic carbon cycle. *PNAS*, 117(8), 3974-3982, doi,  
754 10.1073/pnas.1912094117, 2020.

755 Suan, G., Mattioli, E., Pittet, B., Lécuyer, C., Suchéras-Marx, B., Duarte, L. V., Philippe, M., Reggiani, L., and Martineau, F.:  
756 Secular environmental precursors to Early Toarcian (Jurassic) extreme climate changes, *Earth Planet. Sci. Letts.*, 290,  
757 448-458, doi, org/10. 016/j.epsl.2009.12.047, 2010.

758 Suan, G., Mattioli, E., Pittet, B., Mailliot, S., and Lécuyer, C.: Evidence for major environmental perturbation prior to and  
759 during the Toarcian (Early Jurassic) oceanic anoxic event from the Lusitanian Basin, Portugal, *Paleoceanography*, 23,  
760 PA1202, doi, org/10. 1029/2007PA001459, 2008.

761 Talbot, M. R.: A review of the palaeohydrological interpretation of carbon and oxygen isotopic ratios in primary lacustrine  
762 carbonates. *Chem. Geol. (Isotope Geoscience Section)*, 80, 261-2791, 1990.

763 Tanner, L. H., and Lucas, S. The Whitmore Point Member of the Moenave Formation: Early Jurassic Dryland Lakes on the  
764 Colorado Plateau, Southwestern USA, *Volum. Jur.*, 6(6), 11-21, 2008.

765 Tanner, L. H., Hubert, J. F., Coffey, B. P., and McInerney, D. P.: Stability of atmospheric CO<sub>2</sub> levels across the  
766 Triassic/Jurassic boundary, *Nature*, 411, 675-677, 2001.

767 Them, TR, II, Gill, B. C., Caruthers, A. H., Gröcke, D. R., Tulsy, E. T., Martindale, R. C., Poulton, T. P., and Smit, P. L.:  
768 High-resolution carbon isotope records of the Toarcian oceanic anoxic event (Early Jurassic) from North America and  
769 implications for the global drivers of the Toarcian carbon cycle, *Earth Planet. Sci. Lett.*, 459, 118–126, 2017.

770 Tramoy, R., Schnyder, J., Nguyen, Tu T. T., Yans, J., Jacob, J., Sebilö, M., Derenne, S., Philippe, M., Huguet, A., Pons, D.,  
771 and Baudin, F.: The Pliensbachian-Toarcian paleoclimate transition: New insights from organic geochemistry and C, H,  
772 N isotopes in a continental section from Central Asia, *Palaeogeogr. Palaeoclimatol. Palaeoecol.*, 461, 310–327, 2016.

773 Tucker, M. E.: *Sedimentary rocks in the field - a practical guide* (4th ed.), Wiley-Blackwell, Chichester, England, 276 pp,  
774 2011.

775 Vandeginste, V., and John, C. M.: Influence of climate and dolomite composition on dedolomitization: insights from a  
776 multi-proxy study in the central Oman Mountains, *J. Sediment. Res.*, 82(3), 177-195, doi, 10.2110/jsr.2012.19, 2012.

777 van de Schootbrugge, B., Bachan, A., Suan, G., Richoz, S., Payne, J. L.: Microbes, mud, and methane: Cause and  
778 consequence of recurrent Early Jurassic anoxia following the end-Triassic mass-extinction, *Palaeont.*, 56, 685-709,  
779 2013.

780 van de Schootbrugge, B., Bailey, T. R., Katz, M. E., Wright, J. D., Rosenthal, Y., Feist-Burkhardt, S., and Falkowski, P. G.:  
781 Early Jurassic climate change and the radiation of organic walled phytoplankton in the Tethys Sea, *Paleobiology*, 31,  
782 73–97, 2005.

783 Vasconcelos, C., McKenzie, J. A., Bernasconi, S., Grujic, D., and Tien, A. J.: Microbial mediation as a possible mechanism  
784 for natural dolomite formation at low temperatures, *Nature*, 377, 220–222, 1995.

785 Veizer, J., Godderis, Y., and François, L. M.: Evidence for decoupling of atmospheric CO<sub>2</sub> and global climate during the  
786 Phanerozoic eon, *Nature*, 408, 698-701, 2000.

787 Wang, Q. W., Liang, B., Kan, Z. Z.: Carbon and oxygen isotopic compositions of lacustrine carbonates of the Early Jurassic  
788 Ziliujing Formation in the Sichuan Basin and their paleolimnological significance, *J. Min. Petr.*, 26(2), 87-91, 2006 (in  
789 Chinese with English abstract).

790 Wang, Y. D., Fu, B. H., Xie, X. P., Huang, Q. S., Li, K., Liu, Z. S., Yu, J. X., Pan, Y. H., Tian, N., and Jiang, Z. K.: The  
791 Terrestrial Triassic and Jurassic Systems in the Sichuan Basin, China, in: *Contributions to the 8<sup>th</sup> International Congress  
792 odd the Jurassic System*, edited by: Sha, J. G., Shi, X. Y., Zhou, Z. H., Wang, Y. D., Uni. Sci. Techn., China Press,  
793 Hefei, Anhui, 1-136, 2010 (in Chinese).

794 Wang, Y. D., Mosbrugger, V., and Zhang, H.: Early to Middle Jurassic vegetation and climatic events in the Qaidam Basin,  
795 Northwest China, *Palaeogeogr. Palaeoclimatol. Palaeoecol.*, 224, 200–216,  
796 <http://dx.doi.org/10.1016/j.palaeo.2005.03.035>, 2005.

797 Warren, J.: Dolomite: occurrence, evolution and economically important associations, *Earth Sci. Rev.*, 52, 1–81, 2000.

798 Wei, M.: *Continental Mesozoic Stratigraphy and Paleontology in the Sichuan Basin*, People's Publ. House of Sichuan,  
799 Chengdu, 346-363, 1982 (in Chinese with English summary).

800 Wen, W. and Zhao, B.: Stratigraphic character and sedimentary facies of the Ziliujing Formation in the Pujiang-Ya'An area,  
801 Sichuan province, *J. Stratigr.*, 34(2), 219-224, 2010 (in Chinese with English abstract).

802 Wright, V. P.: Paleosol Recognition: A guide to early diagenesis in terrestrial settings (Chapter 12), in: *Developments in*  
803 *Sedimentology*, edited by: Wolf K, H. and Chilingarian, G. V., 47, 591-619, 1992.

804 Xu, W. M., Ruhl, M., Jenkyns, H. C., Leng, M. J., Huggett, J. M., Minisini, D., Ullmann, C. V., Riding, J. B., Weijers, J. W.  
805 H., Storm, M. S., Percival, L. M. E., Tosca, N. J., Idiz, E. F., Tegelaar, E. W., Hesselbo, S. P.: Evolution of the Toarcian  
806 (Early Jurassic) carbon-cycle and global climatic controls on local sedimentary processes (Cardigan Bay Basin, UK),  
807 *Earth Planet. Sci. Lett.*, 484, 396-411, 2018.

808 Xu, W. M., Ruhl, M., Jenkyns, H. C., Hesselbo, S. P., Riding, J. B., Selby, D., Naafs, B. D. A., Weijers, J. W. H., Pancost, R.  
809 D., Tegelaar, E. W., and Idiz, E. F.: Carbon sequestration in an expanded lake system during the Toarcian oceanic  
810 anoxic event, *Nat. Geosci.*, 129-135, doi, 10. 1038/NGEO2871, 2017.

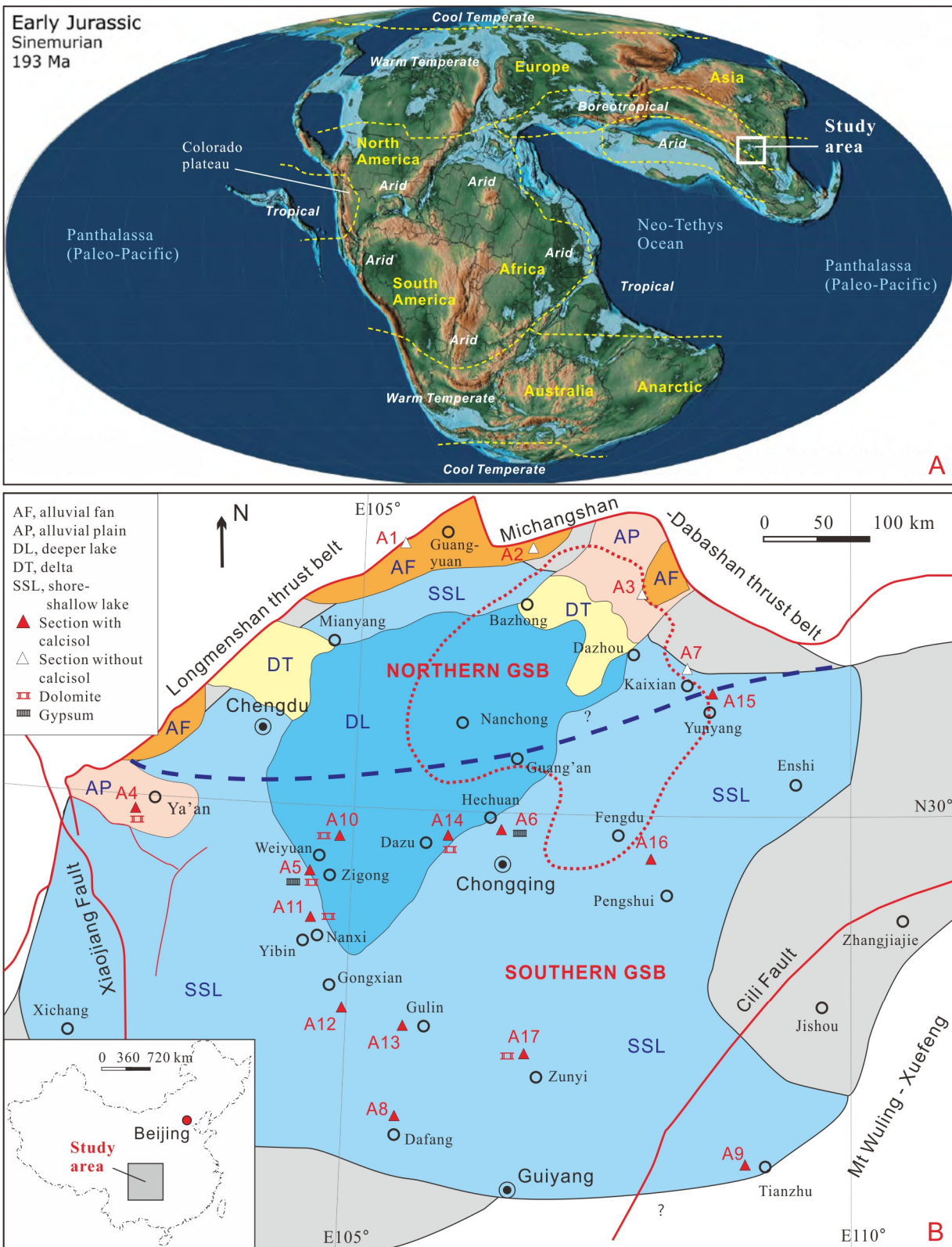
811 Yang, G. L.: Heavy mineral stratigraphy of Mesozoic continental clastic facies in Yaxi area, northern Guizhou, *J. Stratigr.*,  
812 39(1), 89-96 , 2015 (in Chinese with English abstract).

813 Ye, M. N., Liu, X. Y., and Huang, G. Q.: Late Triassic and Early-Middle Jurassic fossil plants from northeastern Sichuan,  
814 *Sci. Techn. Press. Hefei, Anhui*, 1986 (in Chinese with English summary).

815 Zhang, X. S., Zhao, B., Tan, M., Zhou, B. Y., Sun, J.: Stratigraphic Characteristics of Ziliujing Formation, Jurassic Series  
816 and Discovery of Dinosaur Footprints in Dafang, Guizhou, *Geol. Guizhou*, 33(1), 50-70, 2016 (in Chinese with English  
817 abstract).

818 Zhang, Z. L. and Meng, F. S.: Chapter 2, the Jurassic. In Zhang Zhenlai and Meng Fansong eds. *The Triassic-Jurassic*  
819 *Biostratigraphy in Yangtze Gorges* (4), Geol. Publ. House, Beijing, 408, 1987 (in Chinese with English summary).

820



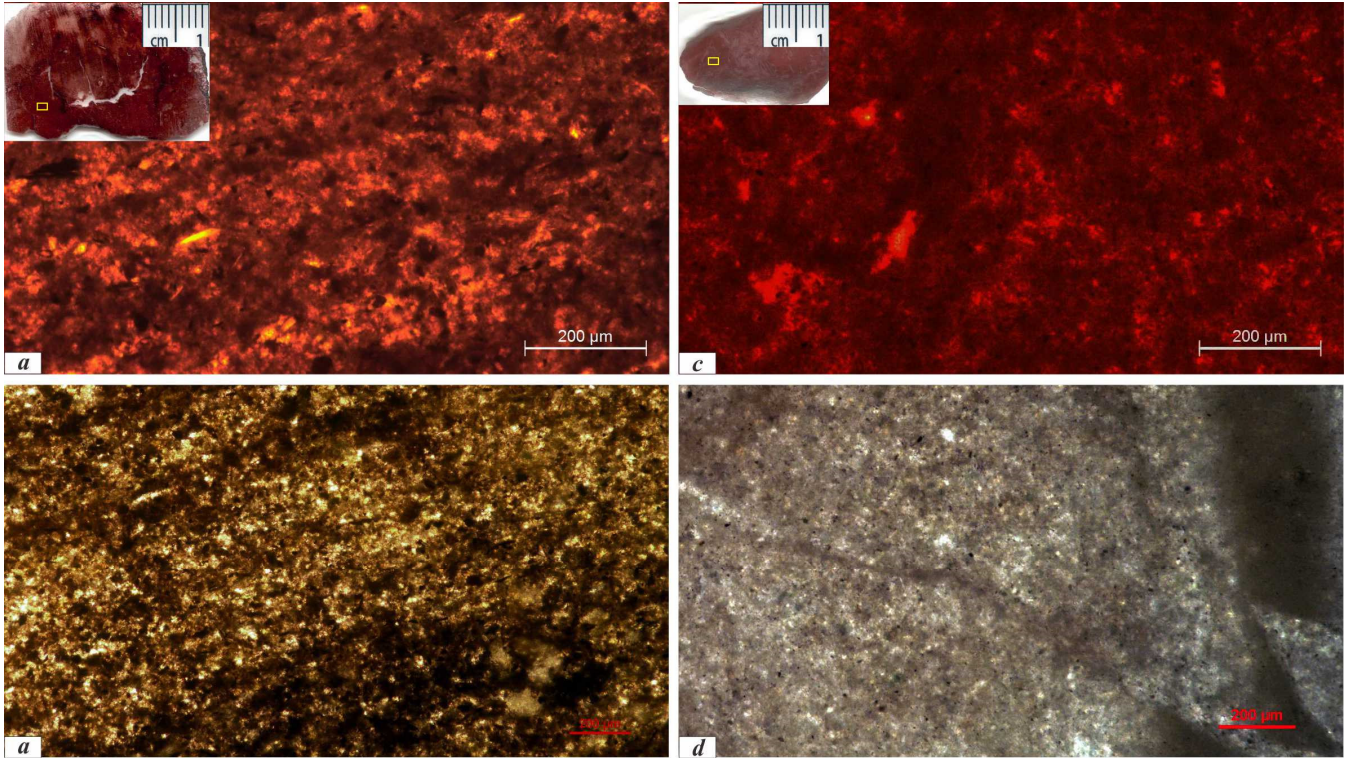
822

823 **Figure 1** A, Global Early-Middle Jurassic climate zones (Boucot et al., 2013) laid on the Early Jurassic (~193 Ma, Sinemurian)  
 824 paleogeographic map (Scotese, 2014). B, Lithofacies paleogeographic sketch of the grand Sichuan paleobasin (GSB) in the early  
 825 Early Jurassic (Zhenzhuchong and Dongyuemiao members) showing locations of the observed and analysed sections and  
 826 climate-sensitive sediments. Lithofacies paleogeographic map was composed and modified from Ma et al. (2009) and Li and He  
 827 (2014). Blue area is the extent of paleolake, estimated as ~380,000 km<sup>2</sup>; blue + gray region is the basin shape, estimated ~480,000  
 828 km<sup>2</sup>. Dot red line confines the deeper lake area in the late Early Jurassic (Ma'anshan and Da'anzhai members). Bold dashed line is

829 the northern edge of calcisol occurrence, which may separate the climate of the GSB as the northern and southern types. Triangles  
830 with numbers are locations of observed and analysed sections: A1, Xiasi section, Jian'ge; A2, Puji section, Wangcang; A3,  
831 Shiguansi section, Wanyuan; A4, Shaping section, Ya'an (bed and thickness from Wen and Zhao, 2010); A6, Tanba and Maliping  
832 section, Hechuan (bed and thickness from Wang et al., 2010); A7, Wenquan section, Kaixian (thickness from Wang et al., 2010).  
833 Location and source data of sections A5 and A8-A17 (climate-sensitive sediments) refer to supplementary data Table S1.

834

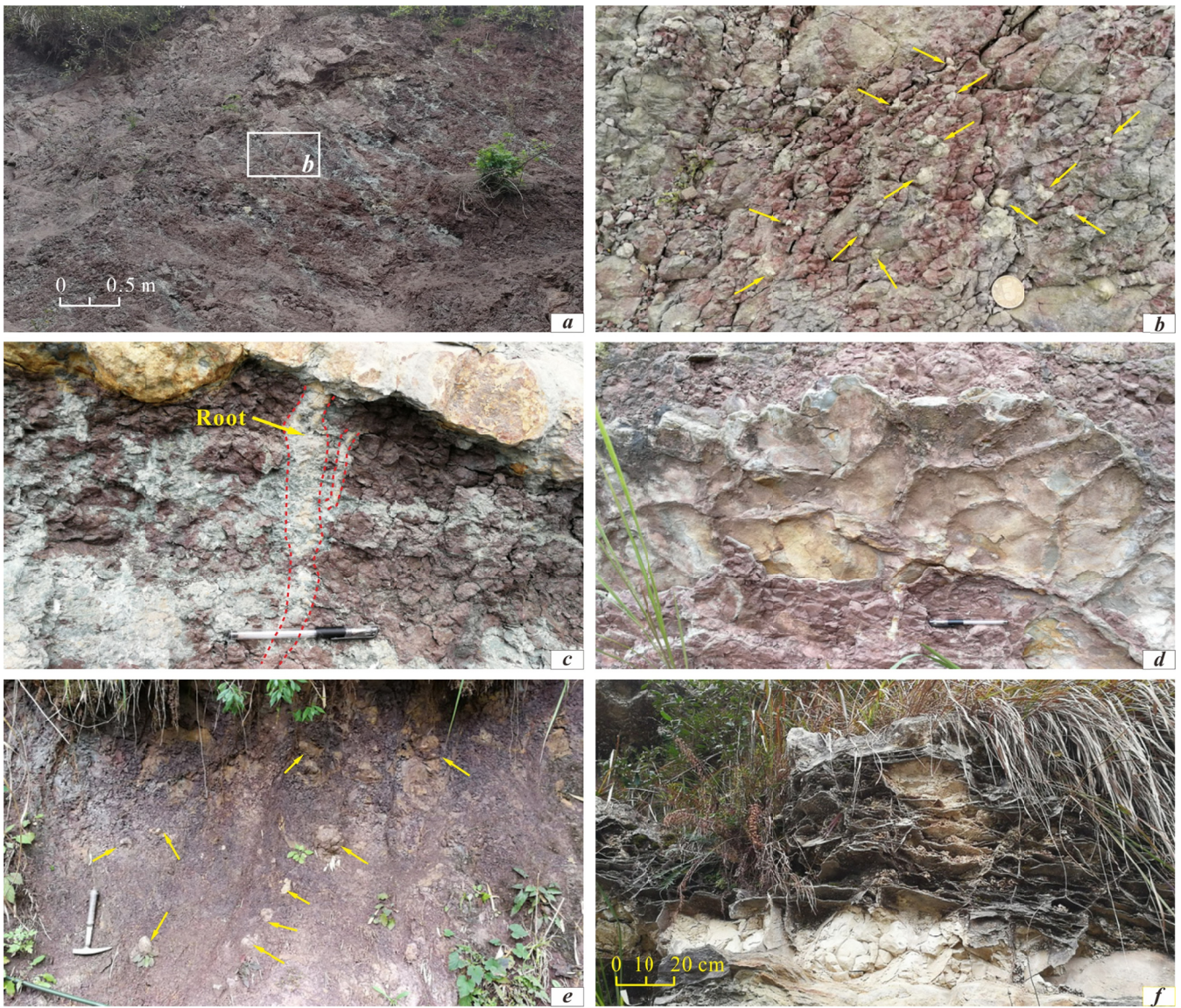
835



836

837 **Figure 2** Microscopic cathodoluminescence photos of representative calcrete samples from the Ziliujing Fm at the Shaping  
838 section, Ya'an. *a*, Sample J<sub>1z</sub>-12-01, Bed B12, Ma'anshan Member; *b*, Sample J<sub>1z</sub>-22-01, Bed B22, Da'anzhai Member. Pedogenic  
839 calcites are mainly null to non-luminescent, minor are orange/red luminescence. Inserts are the scanned photos of thin-section, and  
840 rectangles are the area under cathodoluminescence and drilling.

841



842 **Figure 3** Field photographs of climate-sensitive sediments from the Lower Jurassic Ziliujing Fm in the GSB. *a*, Reddish purple  
 843 calcisol with strong leaching structure. Lower Bed H8 of the upper Ma'anshan Member at Tanba, Hechuan. *b*, Reddish purple  
 844 calcisol showing the density and size of calcretes. The horizon and location same as *a*. Arrows point to calcretes. Coin 2.0 cm  
 845 in diameter. *c*, Reddish purple calcisol with strong leaching structure and rhizoliths. Bed H13 of the top Ma'anshan Member at  
 846 Maliuping, Hechuan. Pen 15 cm long. *d*, Mudcracks. Lower Bed H8 of the upper Ma'anshan Member at Maliuping, Hechuan. Pen  
 847 15 cm long. *e*, Brownish red calcisol with big calcretes (calcareous concretions). Arrows point to big calcretes. Calcisol horizon  
 848 J<sub>1z</sub>-10-01, Bed B10 of Ma'anshan Member at Shaping, Ya'an. Hammer 34 cm long. *f*, Chicken-wire structure. Bed H12 of the  
 849 Da'anzhai Member at Maliuping, Hechuan.

850

851

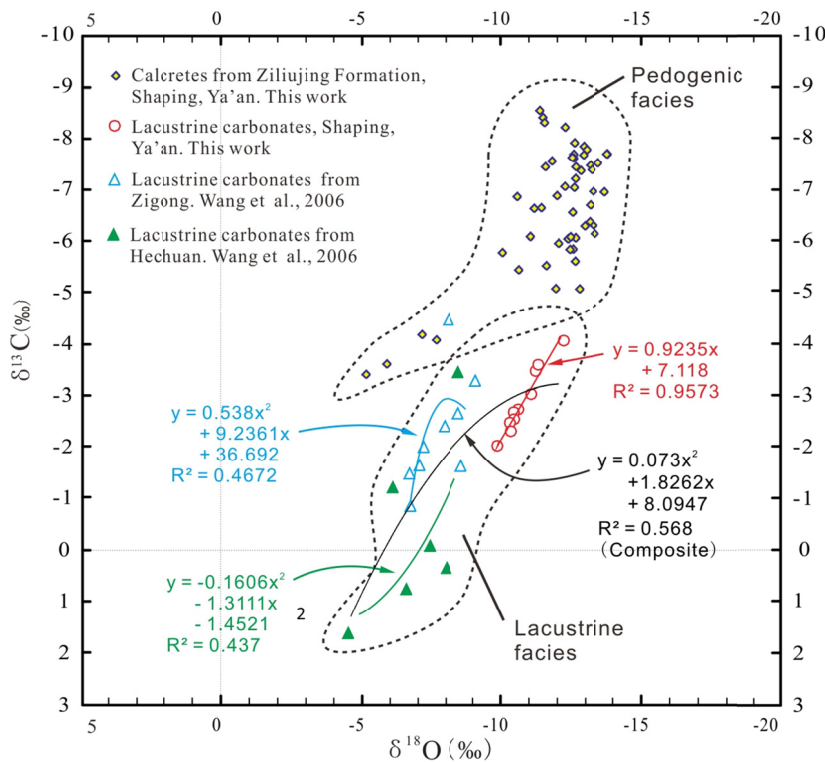
Series	Stage	Fm	Mem	A4	A10	A14	A6	A16	A15	A5	A11	A12	A13	A17	A8	A9	
174																	
(Ma)																	
176	Toa	Ziliujing?	Da'anzhai	West						East							
178																	
180																	
182.7	Pli	Ziliujing?	Ma'anshan														
190.8																	
194	Sin	Ziliujing?	Dongyue-mao														
196																	
198																	
199.3	Het	Ziliujing?	Zhengzhu-chong														
201.3																	
				Qijiang		Qijiang					Qijiang						

▭▭▭▭ Hiatus ▲ Calcisol □ Dolomitic sediment ▨ Gypsum?

852 **Figure 4** Diagram showing the temporal and spatial variation of climate-sensitive sediments in GSB. Section loactions and data  
853 sources refer to Table S1.

854

855



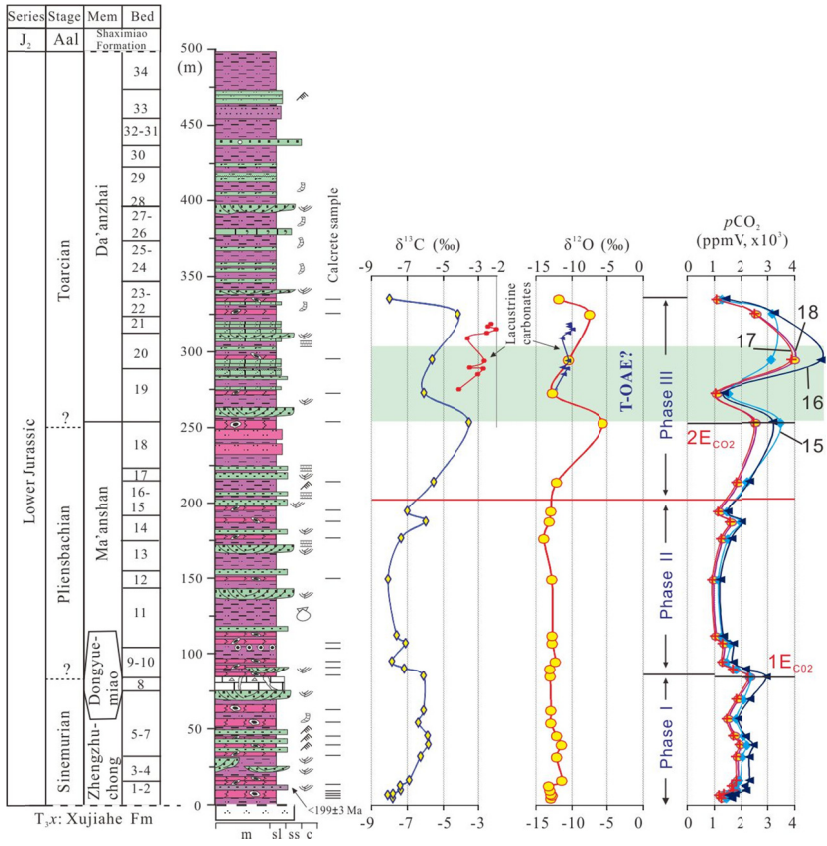
856 **Figure 5** Cross-plot and covariance of carbon and oxygen isotopic values of the Lower Jurassic pedogenic and lacustrine  
857 carbonates from the GSB. Note, the pronounced covariance ( $R^2=0.957$ ) between  $\delta^{13}\text{C}$  and  $\delta^{18}\text{O}$  from Shaping section, Ya'an,  
858 indicating a compositional arid-evaporate and closed pattern lake; the moderate covariance ( $R^2=0.47$  and  $0.44$ ) between  $\delta^{13}\text{C}$  and  
859  $\delta^{18}\text{O}$  from Zigong and Hechuan, indicating a (semi-) arid and semi-closed pattern lake.

860

861

862





863

864

865

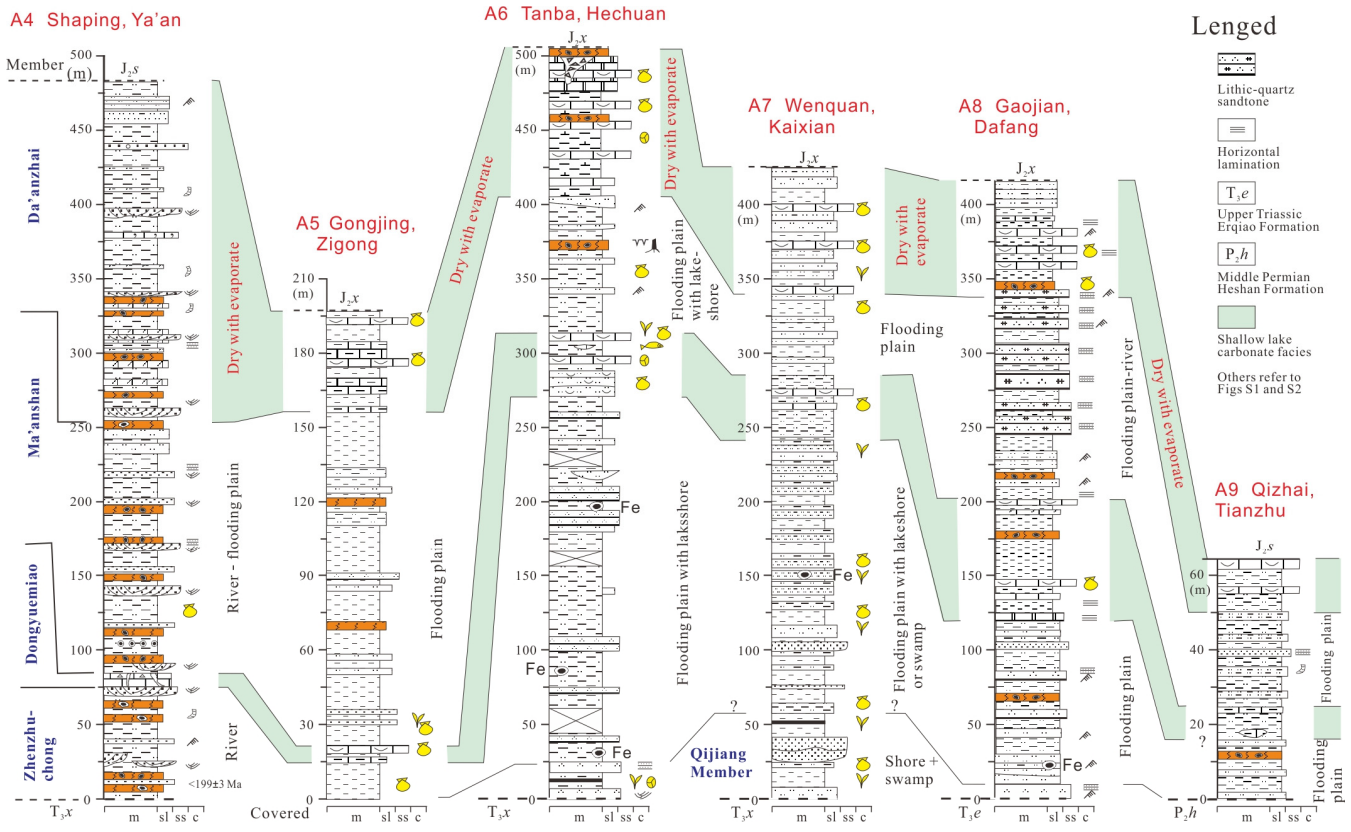
866

867

868

869

**Figure 6** Diagram of the Lower Jurassic strata and lithological log at the Shaping section, Ya'an with carbon and oxygen isotope values of pedogenic and lacustrine carbonates and  $p\text{CO}_2$  curve. Three phases and two events can be observed for both stable isotope values of pedogenic carbonates and  $p\text{CO}_2$  estimate. Legend of lithology in log refers to supplementary Figs. S1 and S2. T-OAE, Toarcian oceanic anoxic event. 1E $\text{CO}_2$  and 2E $\text{CO}_2$ , rapid falling event of  $p\text{CO}_2$ . Numbers 15 to 18 are the curves of  $p\text{CO}_2$  in different parameters, and details refer to supplementary Table S4.



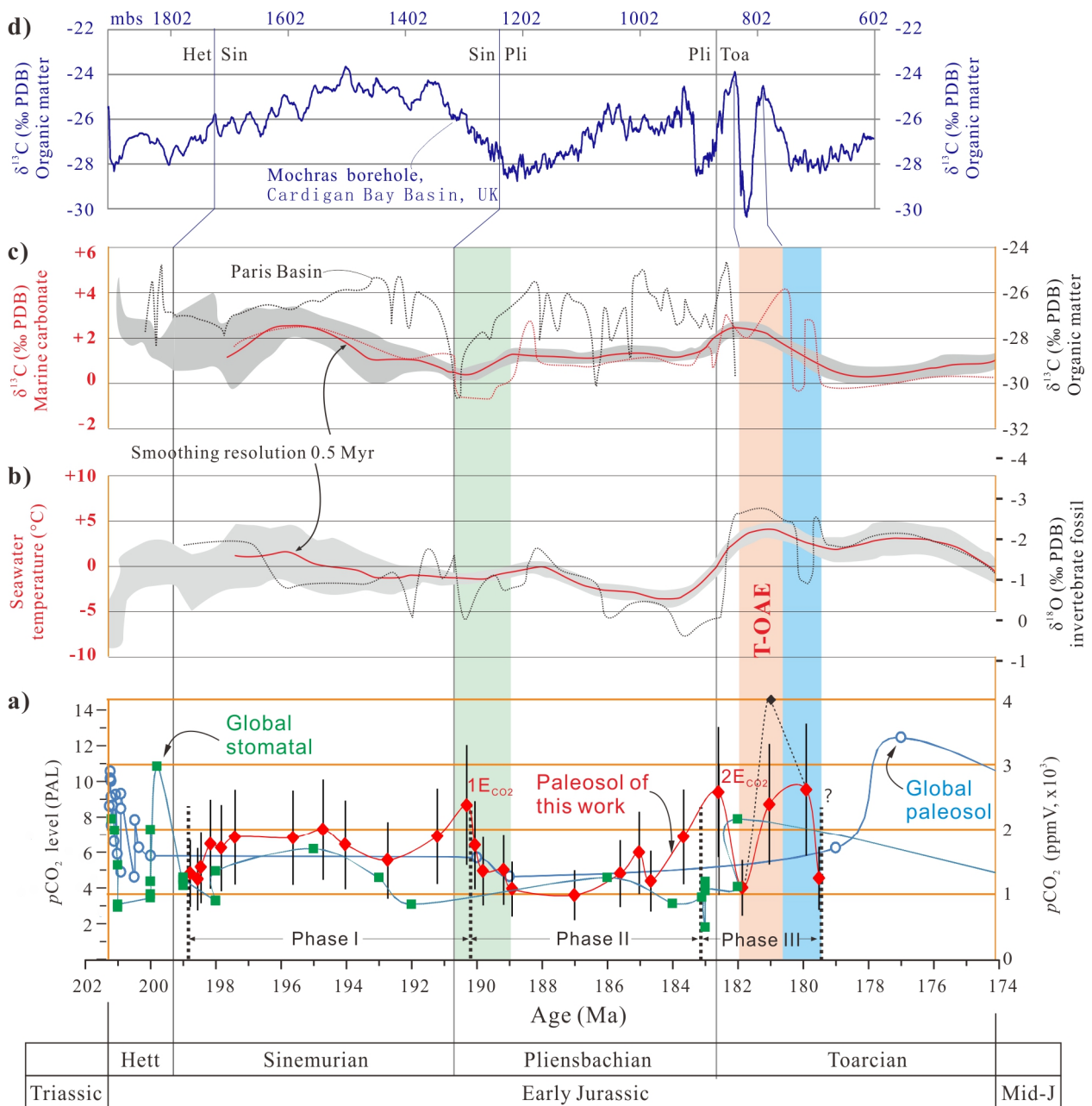
870

871

**Figure 7 Stratigraphic correlation and depositional environment interpretation of the Lower Jurassic in the GSB. Data of**

872

873



874 **Figure 8** Comparison among the Early Jurassic  $p\text{CO}_2$ ,  $\delta^{13}\text{C}$  of marine carbonates and organic matters,  $\delta^{18}\text{O}$  of invertebrate  
875 fossils, and seawater temperature. Age model is from Cohen et al. (2013). a),  $p\text{CO}_2$  values of this work and the composite  $p\text{CO}_2$  by  
876 paleosol and stomatal index (supplementary Table S6 and S7). Vertical bars are errors ( $1\sigma$ ) of  $p\text{CO}_2$  (Table S5). Errors are  
877 propagated using the Gaussian approach (Breecker and Retallack, 2014). Note: 1)  $p\text{CO}_2 = 4027$  ppmV (black solid diamond,  
878 sample J1z-20-01) if the  $\delta^{13}\text{C}_r = -29.0$  ‰ at 181 Ma from Xu et al. (2018) in case of other constant parameters; 2) the early  
879 published  $p\text{CO}_2$  values from both carbon isotope of pedogenic carbonates and stomatal index of fossil plants (data refer to Table  
880 S6 and S7) were awfully rough dated with the average age of a lithostratigraphic formation or group, with which the uncertainty  
881 can be upto 10 Myr, leading to the difficulty of precise and accurate  $p\text{CO}_2$  correlation in pace, frequency, and event. b),  $\delta^{18}\text{O}$  and  
882 seawater temperature (black dot line) of marine invertebrate fossils compiled from Rosales et al. (2001, 2004), Jenkyns et al. (2002),  
883 Bailey et al. (2003), van de Schootbrugge et al. (2005), Gómez et al. (2008), Metodiev and Koleva-Rekalova (2008), Suan et al.  
884 (2008), Korte et al. (2009), Dera et al. (2011), Gómez et al. (2015). c), red dot line  $\delta^{13}\text{C}$  of marine carbonates and organic matters in  
885 western Tethys, composed from Jenkyns and Clayton (1986, 1997), Hesselbo et al. (2000), Dera et al. (2011), Arabas et al., 2017;  
886 black dot and solid line  $\delta^{13}\text{C}$  of organic matters from Paris Basin, France (Peti et al., 2017). Smoothed  $\delta^{18}\text{O}$  and seawater  
887 temperature (red curves) in b) and c) are after Dera et al. (2011). d),  $\delta^{13}\text{C}$  of organic matters from North Atlantic. Composed from  
888 the Mochras borehole, Cardigan Bay Basin, UK (Xu et al., 2018; Storm et al., 2020), seven-point average smoothing against depth  
889 (mbs).

891 **Table**892 **Table 1 Stratigraphic framework of the Lower Jurassic Ziliujing Fm in Sichuan and adjacent area (GSB), Southwest China**

Epoch	Age	Formation	W Sichuan (Ya'an)	E Sichuan and Chongqing	S Sichuan and N Guizhou	N Sichuan
Middle Jurassic	Aalenian	Xintiangou Fm	Xintiangou Fm	Xintiangou Fm	Xintiangou Fm	Qianfuyan / Xintiangou Fm
Early Jurassic	Toarcian	Ziliujing Fm	Da'anzhai Mem (Bed 20-34)	Da'anzhai Mem	Da'anzhai Mem	Baitianba Fm
	Pliensbachian		Ma'anshan Mem (Bed 9-18)	Ma'anshan Mem	Ma'anshan Mem	
	Sinemurian		Dongyuemiao Mem (Bed 8)	Dongyuemiao Mem	Dongyuemiao Mem	
			Zhenzhuchong Mem (Bed 1-7)	Zhenzhuchong Mem	Zhenzhuchong Mem	
	Hettangian		<b>Hiatus</b>	Qijiang Mem	Qijiang Mem	
Late Triassic	Rhaetian	Xujiahe Fm	Xujiahe Fm	Xujiahe Fm	Xujiahe Fm	

Notes: Straigraphic classification and correlation were composed from Dong (1984); SBGM (1997), Wang et al. (2010), Wen and Zhao (2010), Xu et al (2017). Re-Os isotope age of the lower Da'anzhai Member is  $180.3 \pm 3.2$  Ma in western Sichuan (Xu et al., 2017). Fm, Formation; Mem, Member.

893

894 **Supplementary data**895 **Captions of supplementary figures**

896 **Figure S1 Lithological log of the Lower Jurassic Ziliujing Fm with depositional environment interpretations and sample**  
897 **positions at the Shaping section, Ya'an of Sichuan. Bed number and thickness are partly referred to Wen and Zhao (2010).**

898

899 **Figure S2 Lithological log of the Lower Jurassic Ziliujing Fm at the Tanba-Maliuping section, Hechuan of Chongqing with**  
900 **depositional environment interpretations and sample positions. Bed number and thickness are partly referred to Wang et al**  
901 **(2010).**

902

903 **Figure S3 Field photographs of the Lower Jurassic Ziliujing Fm lithofacies in the GSB. a, Well roundness and sorting gravels in**  
904 **the alluvial fan conglomerate. Basal and lower Baitianba Fm. Puji, Wangcang. Hammer 30 cm long. b, Large trough**  
905 **cross-bedding with scours in the point bar and channel sandstones. Upper Baitianba Fm; Puji, Wangcang. c, Calcisol developed**  
906 **within strong leaching overbank mudrocks on channelized sandstones. Middle of Bed B2, the Zhenzhuchong Member, Shaping**  
907 **section, Ya'an. d, Purple red mudrocks intercalated with thin siltstones in flood plain facies. Bed H7 of the Ma'anshan Member,**  
908 **Tanba section, Hechuan. e, Whitish medium-thick micritic dolomites in lacustrine facies. Bed H12 of the Da'anzhai Member,**  
909 **Maliuping section, Hechuan. Hammer 34 cm long. f, Greeinsh gray lacustrine muddy dolomites and dolomitic mudrocks**  
910 **associated with brownish / reddish purple mudrocks. Bed B21 of the Da'anzhai Member, Shaping section, Ya'an.**

911

912 **Figure S4 Microscopic photos showing lithological microfacies of the Lower Jurassic Ziliujing Fm. a, Fine lithic (quartz)**  
913 **sandstone. Lithic-dominant fragments are mudrock. Sample J<sub>1z</sub>-02-01b, Zhenzhuchong Member, Shaping section, Ya'an.**  
914 **Plain-polarised light. b, Laminated muddy dolomite and dolomitic mudrocks. Sample J<sub>1z</sub>-21S2B, Da'anzhai Member, Shaping**

915 section, Ya'an. Plain-polarised light. *c*, Fine quartz arenite. Sample 18HC-02b3, Bed H2, Qijiang Member, Tanba section,  
916 Hechuan. Cross-polarised light. *d*, Micritic dolomite. Sample 18HC-06b, Bed H12, Da'anzhai Member, Maliuping section,  
917 Hechuan. Plain-polarised light. *e*, Coquina. Shell wall of bivalves were micritized. Mud and recrystalline calcites filled inter-shells  
918 and intra-shells. Sample 18HC-04b, Base of Bed H12, Da'anzhai Member, Maliuping section, Hechuan. Cross-polarised light. *f*,  
919 Relict of coquina. Shell wall of bivalves were partly micritized. Strongly recrystalline calcites replaced the fills and shells. Sample  
920 18HC-05b, Bed H12, Da'anzhai Member, Maliuping section, Hechuan. Cross-polarised light.

921

922 **Figure S5** Field photographs of the Lower Jurassic Ziliujing Fm lithofacies in the GSB. *a*, Lithofacies and stratigraphic sequence.  
923 Beds B8 to B10 of the lower Ma'anshan and Dongyuemiao members at Shaping, Ya'an. *b*, Karstified gravels within the limestone.  
924 The horizon and location is same as *a*. Pen 15 cm long. *c*, Layered dolomites with Karstified cave gravels. Bed H12 of the  
925 Da'anzhai Member at Maliuping, Hechuan. *d*, Karstified cave gravels. The horizon and location is same as *c*. Hammer 34 cm long.

926

927 **Figure S6** Stratigraphic correlation of the Lower Jurassic Baitianba Fm in northern GSB. Locations and sources refer to Figure  
928 1. Plant fossils and stratal thickness in the Shiguansi section, Wanyuan are cited from SBG (1980b).

929

### 930 Captions of supplementary tables

931 **Table S1** Occurrence list of the Early Jurassic climate-sensitive sediments in the GSB

932

933 **Table S2** Early Jurassic paleosols in Ya'an of Sichuan and Hechuan of Chongqing, Southwest China

934

935 **Table S3** Carbon-oxygen isotope composition of lacustrine carbonates from the Lower Jurassic Ziliujing Fm (Da'anzhai Mem) in  
936 the GSB

937

938 **Table S4**  $p\text{CO}_2$  estimate by carbon isotope of pedogenic carbonates from the Lower Jurassic Ziliujing Fm at Shapington, Ya'an  
939 of Sichuan

940

941 **Table S5** Calculation of Gaussian error propagation for the Early Jurassic  $p\text{CO}_2$  estimate in the Sichuan paleobasin

942

943 **Table S6** Global  $p\text{CO}_2$  data of the Latest Triassic - Early Jurassic by stomatal method

944

945 **Table S7** Global  $p\text{CO}_2$  data of the Latest Triassic - Early Jurassic estimated by carbon isotope of pedogenic carbonates

946

### 947 Captions of supplementary notes

948 **Note S1**, Description and interpretation of sedimentary facies and its evolution

949

950

1 **Early Jurassic climate and atmospheric CO<sub>2</sub> concentration in the**  
2 **Sichuan paleobasin, Southwest China**

3  
4 Xianghui Li<sup>1</sup>, Jingyu Wang<sup>1</sup>, Troy Rasbury<sup>2</sup>, Min Zhou<sup>1</sup>, Zhen Wei<sup>1</sup>, Chaokai Zhang<sup>1</sup>

5 <sup>1</sup>State Key Laboratory for Mineral Deposits Research, School of Earth Sciences and Engineering, Nanjing University,  
6 Nanjing 210023 China.

7 <sup>2</sup>Department of Geosciences, Stony Brook University, Stony Brook, NY 11794-2100, USA

8 *Correpondence to:* Xiangui Li ([leeschhui@126.com](mailto:leeschhui@126.com))

9

10 **Abstract:**

11 ~~Climatic oscillations had been developed through the (Early) Jurassic from marine sedimentary archives, but remain unclear~~  
12 ~~from terrestrial records. Climatic oscillations took place through the (Early) Jurassic from marine sedimentary archives, but~~  
13 ~~were not clear from terrestrial records. Unlike marine archives, terrestrial sediments show more complicated and dynamic~~  
14 ~~environment and climate. This work presents investigation of climate-sensitive sediments and new results of~~  
15 ~~climate sensitive sediment observation and carbon and -oxygen isotope analyses of lacustrine and pedogenic carbonates for~~  
16 ~~the Early Jurassic Ziliujing Formation from the grand Sichuan paleobasin (GSB), Southwest China. Lithofacies analysis~~  
17 ~~indicates calcisols were widespread in riverine and flood plain facies. Climate sensitive sSedimentary and~~  
18 ~~carbon-oxygen stable isotope proxies with and palynofloral assemblages manifest that an overall secular (semi-) arid climate~~  
19 ~~dominated the GSB during the Early Jurassic; and that it became drier through the time except for the Hettangian,~~  
20 ~~accompanied by occasional evaporites in the Toarcian. This climate pattern is similar with to the arid climate in the Colorado~~  
21 ~~Plateau region, western North America, but distinct from the relatively warm-humid climate in North China and northern~~  
22 ~~Gondwanaland high latitude in Southern Hemisphere. The estimated Early Jurassic atmospheric CO<sub>2</sub> concentration (*p*CO<sub>2</sub>)~~  
23 ~~from carbon isotopes of pedogenic carbonates shows a range of 980-2610 ppmV (~ 3.5-10 times the pre-industrial value)~~  
24 ~~with a mean of 1660 ppmV. Three phases of *p*CO<sub>2</sub> (the Sinemurian 1500-2000 ppmV, the Pliensbachian 1000-1500 ppmV,~~  
25 ~~and the early Toarcian 1094-2610 ppmV) and two events of rapid falling *p*CO<sub>2</sub> by ~1000-1300 ppmV are observed,~~  
26 ~~illustrating the *p*CO<sub>2</sub> perturbation in the Early Jurassic. The pattern perturbation and associated rapid falling events of *p*CO<sub>2</sub>~~  
27 ~~are is compatible with the excursions of stable isotopes and seawater temperature and carbon cycle from the coeval marine~~  
28 ~~sediments, suggesteonsisteingnt with a positive feedback of climate to *p*CO<sub>2</sub> in a total tendency and eventful change through~~  
29 ~~the Early Jurassic; but the. However, a lack of synchronicity.~~

## 31 1. Introduction

32 ~~The Jurassic was a typical greenhouse period with g~~Global paleotemperatures were possibly 5-10-°C higher than present  
33 during the Jurassic greenhouse period based on climate modelling results (e.g., ~~Chandler et al., 1992;~~ Rees et al., 1999;  
34 Sellwood and Valdes, 2008), ~~but the~~. However, seawater temperature fluctuatedion of by-5 °C to +5 °C, or even much  
35 higher magnitude (e.g., Suan et al., 2008; Littler et al., 2010),could have taken place during the period relying on based on  
36 esitmates from the oxygen isotopes of the belemnite and bivalve fossils (details see Dera et al., 2011, and references therein).  
37 Corresponding climatic oscillations had experienced through Tthe Early Jurassic epoch (e.g., van de Schootbrugge et al.,  
38 2005; Dera et al., 2011; Gómez et al., 2016; Arabas et al., 2017) was an interval of extreme environmental change., For  
39 instance, inIn the Sinemurian–Pliensbachian age, the mean sea surface temperatures of the North Atlantic were in excess of  
40 28°C (TEX<sub>86</sub>), comparable with similar palaeolatitudes during the Cretaceous and Early Cenozoic (Robinson et al., 2017);  
41 whereas in the late Pliensbachian age, the northern West Tethys Ocean (e.g., Paris basin, northern Spain basin) was ~12.7°C  
42 (e.g., Gómez et al., 2008; Gómez and Goy, 2011; Arabas et al., 2017), leading to a polar icesheet hypothesis (e.g., Sellwood  
43 and Valdes, 2008; Suan et al., 2010; Dera et al., 2011; Gómez et al., 2015). At ~183 Ma of the early Toarcian oceanic anoxia  
44 event (T-OAE)Other more, tTre is a climate events were recorded byrecord of highly enhanced organic carbon burial., the  
45 surface seawater temperature was high to ~35°C (e.g., Bailey et al., 2003; Korte et al., 2015), and a high temperature  
46 (plateau) even continued in the whole Toarcian (Dera et al., 2011)including multiple isotopic anomalies, clay mineral  
47 composition and evidence for, oceanic anoxic regimeocean anoxia associated with, global sea level change, \_ vegetation  
48 turnover, and mass extinction (e.g. Price, 1999; Hesselbo et al., 2000; Dera et al., 2009; Jenkyns, 2010; Korte and Hesselbo,  
49 2011; Riding et al., 2013; Arabas et al., 2017; Robinson et al., 2017). Recently, examplesExamples of seawater temperature  
50 rapid transitions betweenfrom \_ cold, or even glacial, climates t ando super greenhouse eventshot are documentedshow in  
51 some inthe climate oscillation through ervals of the Early Jurassic (e.g., van de Schootbrugge et al., 2005; Suan et al., 2010;  
52 Gómez et al., 2016; Arabas et al., 2017). The study of these deep time climate events may serve as analogues for present day  
53 and future environmental transitions (Hesselbo et al., 2013). \_  
54 Though the climate eventchanges in the Early Jurassic epoch are largely based on the marine sedimentary and geochemical  
55 recorded son land remain relatively poor understanding., \_ dataData from the terrestrial realm eanalso provide important  
56 details of environmental and climatic change (e.g., Hesselbo et al., 2000; Suan et al., 2010; Jenkyns, 2010; Philippe et al.,  
57 2017), from which the oscillated climate could be observed and revealed too. Terrestrial proxies, such as flora (e.g., Riding  
58 et al., 2013; Deng et al., 2017; Philippe et al., 2017; ~~Ros Franch et al., 2019~~), vegetation (Pole, 2009), and geochemistry (e.g.,  
59 Riding et al., 2013; Kenny, 2015; Tramoy et al., 2016) as well as the pCO<sub>2</sub> perturbation record (e.g., Retallack, 2001a;  
60 Beerling and Royer, 2002; McElwain et al., 2005; Berner, 2006; Retallack, 2001a, 2009; Steinthorsdottir and Vajda, 2015)  
61 havewere recently begun to provide used to recover important information of the Mesozoic Cenozoicprovide an emerging



62 ~~record of the~~ Early Jurassic terrestrial climate and environmental changes ~~on continents~~. ~~Particularly, a negative feedback~~  
63 ~~in the global exogenic carbon cycle, from carbon isotopes of lacustrine organic matter, has been hypothesized to account for~~  
64 ~~the Toarcian oceanic anoxic event (Xu et al., 2017), opening a new avenue to link marine and terrestrial climate in the Early~~  
65 ~~Jurassic. Correspondingly, the proxy application of terrestrial sedimentary archives could play a key role in the global Early~~  
66 ~~Jurassic correlation of the marine and terrestrial climate.~~

67 ~~Obviously, of the pProxies for ,pCO<sub>2</sub> is the most probable~~ provide ~~are the important linkage between the marine and~~  
68 ~~terrestrial climatic condition. Up to date, the reconstruction of~~ Studies of the terrestrial pCO<sub>2</sub> record was have focused at on  
69 ~~the Triassic-Jurassic boundary (e.g., Tanner et al., 2001; Cleveland et al., 2008; Schaller et al., 2011; Steinthorsdottir and~~  
70 ~~Vajda, 2015) and at the Toarcian oceanic anoxic event (McElwain et al., 2005), where~~ and pCO<sub>2</sub> estimates range 1000 ppm to  
71 ~~4000 ppmV (e.g., Tanner et al., 2001; Cleveland et al., 2008; Schaller et al., 2011). Inconsistent pCO<sub>2</sub> results occur in~~  
72 ~~different proxies, however, and~~ However, few ~~relatively continuous pCO<sub>2</sub>terrestrial climate records records~~ and coupled  
73 ~~terrestrial climate environmental~~ changes have been documented for the Early Jurassic.

74  
75 There are several large Triassic-Jurassic terrestrial basins in West China, ~~providing a great opportunity to recover the coeval~~  
76 ~~terrestrial environment and climate, in which~~ in which ~~T~~ the Sichuan Basin has a relatively complete and continuous  
77 continental sedimentary sequence of the Upper Triassic-Paleogene (e.g., SBGM, 1991, 1997; Wang et al., 2010). During the  
78 Early Jurassic, it had been laid ~~the Sichuan Basin was in a Boreotropical climate zone by~~ based on climate-sensitive sediments  
79 (Fig. 1a. Boucot et al., 2013), or ~~or~~ and a warm temperate climate is suggested based ~~y~~ on clay mineralogys and  
80 phytogeography (e.g., Dera et al., 2009). Correspondingly, the sedimentary archive could play a key role in the global Early  
81 ~~Jurassic correlation of the marine and terrestrial climate.~~ In this work, we present new results of a field investigation,  
82 including lithofacies and paleosol recognitioninterpretation, and carbon-oxygen ~~carbon and oxygen~~ isotope analyses of both  
83 lacustrine and pedogenic carbonates, ~~and pCO<sub>2</sub> estimates in the Early Juassic terrestrial Sichuan paleob~~ Basin. TheseNew  
84 results allow us to, reconstruct the paleoclimate and relatively consecutiove pCO<sub>2</sub> change ~~record through the Early Juassic,~~  
85 for ~~and we discuss the relationship of pCO<sub>2</sub>terrestrial climatic change to~~ which we compare to stable isotopes of marine  
86 sediments and that of the estimated sea water temperature ~~marine counterpart.~~

## 87 2. Geological setting and stratigraphy

88 Southwest China, including the provinces of Yunnan, Sichuan, Chongqing, and Guizhou, had been the main part of the  
89 upper Yangtze Plate since the Proterozoic, possibly since the Neoproterozoic. With the amalgamation of the Cathaysia and  
90 Yangtze plates, it became the western South China plate or cratonic basin since ~~in~~ the Neoproterozoic (Sinian), ~~and marine~~  
91 ~~Neoproterozoic through~~ continued to the late Middle Triassic ~~strata is well preserved.~~ With ~~By~~ the Indosinian orogeny, new

92 foreland basins were formed since the Late Triassic (e.g., He and Liao, 1985; Li et al., 2003), ~~which recording~~ the Mesozoic  
93 and Cenozoic evolution of tectonics, environment, and climate in Southwest China.

94 The Mesozoic Sichuan paleobasin was confined by the Longmenshan thrust belt in the northwest, the Micangshan-Dabashan  
95 arcuate thrust belt in the northeast (Fig. 1b), and the northern hilly topography boundary of the Yunnan-Guizhou plateau in  
96 the south and east. It was mainly developed during the Late Triassic-Jurassic and includes provincial areas of eastern  
97 Sichuan, entire Chongqing, northern Guizhou, western Hubei, and northwestern Hunan. This Triassic-Jurassic Sichuan  
98 foreland basin was much larger than the present Sichuan Basin in the eastern Sichuan province. We estimate the size of  
99 Sichuan paleobasin is roughly 480,000 km<sup>2</sup> ~~by the based on~~ lithofacies paleogeography (Fig. 1b. Ma et al., 2009; Li and He,  
100 2014), and suggest naming this the grand Sichuan paleobasin (GSB).

101 The Mesozoic terrestrial sediments accumulated up to ~9 km (Guo et al., 1996) in the GSB; and the Jurassic part can be as  
102 much as 3-3.5 km thick (SBGM, 1991). Two types of Lower Jurassic deposits have been distinguished (Table 1): the  
103 Baitianba Formation (Fm) in the north (~10%) and the Ziliujing Fm (e.g., SBGM, 1991; Wang et al., 2010) in the south  
104 (over 90% of the basin).

105 The Baitianba Fm was deposited unconformably on the Upper Triassic Xujiahe Fm and is overlain conformably by the  
106 Middle Jurassic Xintiangou Fm / Qianfuyan Fm (Table 1). It is mainly composed of grayish shales and sandstones with coal  
107 layers and massive conglomerates. Abundant plant fossils, sporopollens, conchostracans, bivalves, and gastropods indicate it  
108 is ~~of~~ the Early Jurassic (SBGM, 1991, 1997). Sporopollen assemblages of the Hettangian-Sinemurian age were found in the  
109 lower part (Zhang and Meng, 1987) and the Pliensbachian-Toarcian assemblages were reported in the upper part (Wang et  
110 al., 2010).

111 The Ziliujing Fm is composed of variegated and reddish mudrocks (some shales) intercalated with sandstones, siltstones, and  
112 bioclastic limestones as well as ~~dolomitic~~ marlstones / ~~limy dolomites~~, conformably or unconformably overlying the Xujiahe  
113 Fm or Luqiao Fm and conformably underlying the Xintiangou Fm (SBGM, 1997. Table 1). It has been dated as the Early  
114 Jurassic by fossil assemblages of ~~dinosaurs~~, bivalves, ostracods, conchostracans, and plants, ~~within which the~~ ~~dinosaur~~  
115 ~~Dinosaur~~ fauna can be well correlated to the Lufeng Fauna in central Yunnan (e.g., Dong, 1984; SBGM, 1991, 1997; Peng,  
116 2009). This formation is subdivided ~~as into~~ five parts in an ascending order: the Qijiang, Zhenzhuchong, Dongyuemiao,  
117 Ma'anshan, and Da'anzhai members (SBGM, 1997. Table 1). Of ~~them these~~, the former two are sometimes combined ~~as~~ the  
118 Zhenzhuchong Fm (e.g., SBGM, 1991; Wang et al., 2010).

119 The Da'anzhai Member is characterized by dark gray to black shales and bioclastic limestones with a southward increase of  
120 reddish mudrocks (SBGM, 1991, 1997; Wang et al., 2010), ~~which has been mainly and is~~ regarded the sediment in a grand  
121 Sichuan paleolake (e.g., Ma et al., 2009; Li and He, 2014). Ostracod ~~assemblage~~ ~~assemblages~~ indicate it is the late Early  
122 Jurassic (e.g., Wei, 1982; Wang et al., 2010). A Re-Os isochron age ~~of~~ 180.3 ± 3.2 Ma ~~associated combined~~ with ~~the an~~

123 organic carbon isotope excursion indicates that the lower Da'anzhai Member corresponds to the [Toarcian Oceanic Anoxic](#)  
124 [event](#) (T-OAE) (Xu et al., 2017), [consistent with the assigned Toarcian age](#).

125 The Ma'anshan Member is comprised of violet-red mudrocks with a few greyish, greenish thin-bedded fine sandstones and  
126 siltstones, in which floral fossils are common (Li and Meng, 2003). The Dongyuemiao Member consists of greenish and  
127 reddish mudrocks and siltstones with greyish bioclastic limestone and marlstone, of which abundant bivalve and plant fossils  
128 were reported from eastern Sichuan and Chongqing (Li and Meng, 2003; Meng et al., 2003; Wang et al., 2010). The  
129 Zhenzhuchong Member is dominated by violet red mudrocks/shales intercalated with thin-~~bedded~~ sandstones and / or  
130 siltstones and numerous plant fossils of the Early Jurassic affinity (e.g., Duan and Chen, 1982; Ye et al., 1986). Taken  
131 together, fossil associations suggest that the three members were deposited in the middle-late Early Jurassic. The age  
132 limitation of the overlying Da'anzhai Member and the correlation to the Lufeng dinosaur fauna places these members in the  
133 Sinemurian – Pliensbachian, and the Zhenzhuchong and Dongyuemiao Fms are ~~temporally~~ [suggested to be the](#)  
134 [Sinemurian age](#) (Table 1).

135 The Qijiang Member is composed of quartz arenite interbedded/intercalated with dark shales. Coal seams ~~can be~~ [are](#) often  
136 seen in the middle of the Qijiang Member. This member mainly occurs in the central part of the GSB. It is likely the earliest  
137 Jurassic, possibly Hettangian age, but plant fossils cannot precisely indicate the age (Wang et al., 2010).

138

### 139 3. Materials and methods

140 ~~We have measured sections and made detailed~~ [Observations](#) and descriptions [of sedimentary characteristics](#) for  
141 ~~sedimentary litho~~facies analysis ~~were executed on~~ at six outcrop sections (Locations A1 to A4, A6 and A7, Fig. 1). Published  
142 descriptions for other sections (Locations A5, A8, and A9, Fig. 1) ~~is~~ [are](#) integrated into our observations. Details of  
143 microscopic examination of sedimentary rocks and [analysis of](#) sedimentary facies ~~analysis which are the~~ underpinning ~~the of~~  
144 climate analysis are attached as the supplementary data Note S1. Below ~~are chiefly introduced materials and~~ [we discuss](#) ~~state~~  
145 ~~methods of~~ climate-sensitive sediment observation, ~~carbon oxygen~~ [carbon and oxygen](#) isotope analyses, and estimate of  
146  $p\text{CO}_2$ .

#### 147 3.1. Observation of climate-sensitive sediments

148 Climate-sensitive sediments are mainly ~~the~~ dolomites, ~~gypsum~~ [gypsum](#), and paleosols, which are used to analyze the climate  
149 in this work [\(Table S1\)](#).

150 Dolomites and ~~gy~~ [ypsum](#) are relatively easy to recognize in both field and under microscope. We distinguish dolomites from  
151 limestones following Tucker (2003) and Flügel (2004). As Flügel (2004) stated, field distinctions of limestone and  
152 dolomite can also be made although detailed differentiation of carbonate rocks is best performed in the laboratory. ~~The basic~~

153 ~~method that we use to examine dolomites is: limestone will fizz strongly and dolomite will show little or no reaction when~~  
154 ~~add dilute 10 % hydrochloric acid on carbonate (Flügel, 2004); and limestone will stain pink to mauve but dolomite will be~~  
155 ~~unstained (e.g., Tucker, 2003; Flügel, 2004) when Alizarin red S in weak HCl is added on fresh outcrop or coverslip free~~  
156 ~~thin section. Gypsum is recognizable by properties of low Mohs hardness (2) and transparency to translucence.~~ In field, we  
157 ~~also~~ recognize gypsum by particular structures such as chicken-wire cage, gypsum pseudomorph, and cluster of (0.5-1 cm)  
158 pore.

159 There are multiple classifications of paleosols (e.g., Wright, 1992; Mack et al., 1993; Retallack, 2001b; Imbellone, 2011),  
160 mostly based on the US Soil Taxonomy. We recognized paleosols in the field based on color, structures, horizonation, root  
161 traces, and textures, and followed the general classification paleosols by Mack et al. (1993) and Retallack (2001b). In this  
162 paper, paleosols ~~were~~ are described following the procedures of the Soil Survey Manual and classified according to Soil  
163 Survey Staff (1998).

164 Within the measured and observed sections, paleosol profiles were mainly identified from the two main locations/sections  
165 A4 and A6 (Figs. S1 and S2, and Table ~~S1~~S2). Horizonation, BK horizon thickness, boundary ~~condition~~ condition, structures, trace  
166 fossils, rootlets, carbonate accumulations (calcretes), etc. were ~~observed and described~~ recorded (Table ~~S1~~S2). Paleosols  
167 interpreted in other cited sections (Fig. 1) rely on the ~~description~~ description of lithology, structure, and calcrete in the  
168 original references.

169 Based upon a modification of the Retallack (1998) categorization of paleosol maturity, the relative paleosol development  
170 (maturity) was assigned.

### 171 **3.2. Analyses of carbon and-oxygen isotopes**

172 Ten lacustrine carbonate samples were ~~collected to analyse~~ d for carbon oxygen carbon and oxygen isotopes from the  
173 Da'anzhai Member ~~of the Ziliujing Fm~~ at the Shaping section, Ya'an (Location A4, Fig. S1 and Table S3). ~~Twenty six~~ 26  
174 pedogenic carbonate samples were ~~selected to measure~~ analyzed for carbon oxygen carbon and oxygen isotopes from  
175 ~~thirty one~~ 32 paleosol ~~horizon~~ horizons of the Ziliujing Fm at the same section (Fig. S1 and Table S4). Two or three microdrilling  
176 powder samples (columns 7 and 8 in Table S4) were taken from the same individual calcrete for stable isotope analysis, and  
177 then a mean value for each calcrete sample was calculated (columns 9 and 10 in Table S4).

178 At the field scale, calcretes are ginger-like and sporadically spaced within the soil horizon. We observed no linear and planar  
179 calcretes that would indicate precipitation at or below the water table. Before drilling, ~~the diagenetic fabrics of thin sections~~  
180 ~~of the samples~~ were petrographically studied ~~under a microscope~~ petrographically. Each sample was cut and prepared as thin  
181 ~~sections for diagenetic diagnosis,~~ using polarized light microscopy and cathodoluminescence (CL) ~~images~~ imaging.  
182 Micritic calcite is predominant in both lacustrine and pedogenic carbonate samples, with no evidence for carbonate detritus  
183 in calcretes (Fig. 2a and 2b). The micritic calcites used for stable isotope analyses are chiefly null- to non-luminescent, with

184 <10% light orange and brownish luminescence, indicating genesis primarily in the vadose zone. While luminescent calcretes  
185 indicate a high possibility of hydrological influence (e.g., Mintz, et al., 2016), we sampled to avoid this. Based on  
186 petrography and CL imaging together with the field observations, the dense micritic zones sampled for the stable isotope  
187 composition should give pristine  $\delta^{13}\text{C}$  values that can be used to estimate  $p\text{CO}_2$ .

188 (Fig. 2) were used to examine if the calcites were evenly precipitated. Only the areas that were a uniform (often orange)  
189 luminescence (Fig. 2) were microsampled for isotope analyses. Diagenetic s from Cracks, veins, and vug spaces in concretion  
190 samples were found to be filled by multidirectional growth of spar crystals. These crack spar fills were was avoided when  
191 microsampling as they were interpreted as recrystallization and replacement diagenetic phases. Microsampling of lacustrine  
192 and pedogenic carbonate samples focused on avoiding spar and sampling only micrites, and avoiding spar diagenetic spar  
193 from cracks, veins, and vug spaces. Powder samples were obtained by dentist drilling machine using a dental drill (aiguille  
194 diameter  $\phi=1-2$  mm).

195 Isotopic analyses were conducted on 0.3 ~ 0.5 mg powder samples. Powder samples were dried in an oven at 60°C for 10  
196 hours before being moved to the instrument. Carbon dioxide for isotopic analysis was released using orthophosphoric acid at  
197 70°C and analysed on-line in a DELTA-Plus xp (CF-IRMS) mass spectrometer at the State Key Laboratory for Mineral  
198 Deposits Research, Nanjing University. The precision of the measurements was regularly checked with a Chinese national  
199 carbonate standard (GBW04405) and the international standard (NBS19) and the standard deviation of  $\delta^{13}\text{C}$  was  $\pm 0.1\%$  over  
200 the period of analysis. Calibration to the international Pee Dee Belemnite (PDB) scale was performed using NBS19 and  
201 NBS18 standards.

### 202 3.3. Calculation of atmospheric $\text{CO}_2$ concentration

203 There are multiple methods to reconstruct the concentration of atmospheric carbon dioxide (i.e.,  $p\text{CO}_2$ ) in deep time. It can  
204 be determined from the  $\delta^{13}\text{C}$  values of pedogenic carbonate using a paleobarometer model (Cerling, 1999), and the  
205 reconstruction of  $p\text{CO}_2$  has been applied in the climate case study of the Mesozoic climate time (e.g., Ekart et al., 1999;  
206 Nordt et al., 2003; Myers et al., 2012; Li et al., 2014; Zhang et al., 2018).

207 The Cerling (1991, 1999) equation was used to calculate the  $p\text{CO}_2$  using the carbon isotope of pedogenic carbonates as  
208 below:

$$209 C_a = S_{(z)}(\delta^{13}\text{C}_s - 1.0044\delta^{13}\text{C}_r - 4.4)/(\delta^{13}\text{C}_a - \delta^{13}\text{C}_s)$$

210 where  $C_a$  is  $p\text{CO}_2$ ;  $\delta^{13}\text{C}_s$ ,  $\delta^{13}\text{C}_r$ ,  $\delta^{13}\text{C}_a$  are the isotopic compositions (‰) of soil  $\text{CO}_2$ , soil-respired  $\text{CO}_2$ , and atmospheric  $\text{CO}_2$ ,  
211 respectively; and  $S_{(z)}$  is the  $\text{CO}_2$  contributed by soil respiration (ppmV). Details of parameter usage and selection for the  
212  $p\text{CO}_2$  calculation are in the supplementary data Note S2.

213  $-\delta^{13}\text{C}_s$  is often calibrated by fractionation factor  $-8.98\%$  with the formula  $-8.98\% + \delta^{13}\text{C}_c$  (Ekart et al., 1999), with which  
214  $\delta^{13}\text{C}_c$  is the measured result of pedogenic calcrete. Or Alternatively,  $\delta^{13}\text{C}_s$  can be replaced by  $\delta^{13}\text{C}_{sc}$ , which is calibrated by

215 carbon isotope ratio of pedogenic carbonate at 25°C based on latitude–temperature correlations (Besse and Courtillot, 1988;  
216 Ekart et al., 1999) following the equation  $\delta^{13}C_{sc} = (\delta^{13}C_c + 1000) / ((11.98 - 0.12 * T) / 1000 + 1) - 1000$  (Romanek et al., 1992). We  
217 used both  $\delta^{13}C_s$  and  $\delta^{13}C_{sc}$  to calculate the  $pCO_2$ , respectively (Table S4).  
218  $\delta^{13}C_r$  represents carbon isotope ratio of average bulk C3 vascular tissue (Arens et al., 2000), reflecting atmospheric  $\delta^{13}C$   
219 (Jahren et al., 2008). ~~So, the~~ The  $\delta^{13}C_{om}$  of organic matter within paleosols based on the range of modern C3 ecosystem  
220 fractionations (Buchmann, et al., 1998; Ekart et al., 1999), is commonly ~~the representative of~~ used for  $\delta^{13}C_r$  ~~in the above~~  
221 ~~model equation~~. However, the  $\delta^{13}C_r$  could be ~~not almost applied in the measurement of~~ could be compromised in the fossil  
222 soils due to oxidation and metabolism of organic matter after burial (Nadelhofer and Fry, 1988). In this paper, we used the  
223  $\delta^{13}C_{om}$  from the Paris Basin (Bougeault et al., 2017; Peti et al., 2017) for the Sinemurian-Pliensbachian  $\delta^{13}C_r$  and from  
224 Cardigan Bay, UK (Xu et al., 2018) for the Toarcian ~~one which was not oxidated, metabolized and well dated~~.  
225  $\delta^{13}C_a$ , the carbon isotopic composition of the atmosphere, was about -8‰ in the 1980s, being depleted relative to the  
226 pre-industrial atmosphere which was around -6.5‰ (Friedli et al., 1986). The average value of -6.5‰ has been chosen as the  
227  $\delta^{13}C_a$  for acquiring  $\delta^{13}C_r$  and  $S_{(z)}$  (e.g., Ekart et al., 1999; Robinson et al., 2002), and the  $\delta^{13}C_a$  was generally calibrated as  
228  $\delta^{13}C_{ac}$  from  $\delta^{13}C_r$  using the formula  $(\delta^{13}C_r + 18.67) / 1.1$  (Arens et al., 2000). Herein we used both calibrations to calculate the  
229  $\delta^{13}C_a$  (Table S4).  
230  $S_{(z)}$  is the largest source of uncertainty in  $pCO_2$  estimates (Breecker, 2013) and the uncertainty arises primarily from their  
231 sensitivity to soil-respired  $CO_2$  ( $S_{(z)}$ ) (Montañez, 2013). It is a function of depth and effectively constant below 50 cm (e.g.,  
232 Cerling, 1991). ~~In earlier publications,  $S_{(z)}$  = 5000 ppmV was often adopted. Large discrepancy of  $S_{(z)}$  was interpreted and~~  
233  $S_{(z)}$  = 2500 ppmV is suggested for the sub-humid temperate and tropical climates (Breecker et al., 2010), 2500-5000 ppmV for  
234 higher moisture and productivity soil (Montañez, 2013), 2000 ppmV for semi-arid areas (Breecker et al., 2009), 1500-2000  
235 ppmV for aridisols and alfisols (calcisol-argillisol) and 2000±1000 for paleo-vertisol (Montañez, 2013), and 1000 ppmV in  
236 desert areas (Breecker et al., 2010) or 400 ± 200 ppmV for immature soil (Montañez, 2013). In this context, we chose the  
237  $S_{(z)}$  = 2000 ppmV for calculating  $pCO_2$  at 25°C as the calcisols are reddish-brownish aridisols, and we also compared the  
238 results with that by  $S_{(z)}$  = 2500 ppmV (Table S4). Additionally, we took samples at the middle and lower Bk horizon (often >  
239 ~20-30 cm to the BK top). That means the depth of calcrete samples in the examined palaeosols was generally deeper than  
240 50 cm below the paleosol surface, meeting the requirement for a constant value of  $S_{(z)}$ .  
241

#### 242 4. Results

243 Based on the investigation of cross-sections (locations A1-A4, and A6-A7. Fig. 1), we have classified six sedimentary facies  
244 units in the Ziliujing Fm. They are alluvial fan, fluvial river, flood plain, lake, lake-delta, and swamp facies. Details of

245 description and interpretation are in the supplementary data Note S1. Below are results of climate-sensitive sediment  
246 observation, stable isotope analyses, and  $p\text{CO}_2$  calculation.

#### 247 **4.1. Climate-sensitive sediments**

248 Field observation combined with published calcrete materials shows that paleosols widely occur in the Lower Jurassic  
249 Ziliujing Fm of the GSB (Figs. 1, 3, and 4). A total of 32 paleosols were observed and described at the Shaping section,  
250 Ya'an, and five paleosols were found at the Tanba section, Hechuan (Table [S1S2](#)).

251 Most of paleosols are reddish (GSA Munsell Rock-Color 5R 2/2, 5R 3/4, 5R 4/2) and brownish (10R 3/4, 10R 5/4) (Fig. 3  
252 and Table [S1S2](#)). Peds of paleosols are mainly angular and subangular, and a few are prismatic and platy. Slickensides are  
253 common. Mottles (Fig. 3a), rootlets /rhizoliths (Fig. 3c), and burrows sometimes occur with strong leaching structures (Fig.  
254 3a). Occasionally mudcracks are associated with the aforementioned structures (Fig. 3d).

255 All paleosols are calcic with more or less calcretes in Bk horizons. The thickness of Bk horizons ~~mainly changes is~~  
256 ~~mainly from~~ -30-50 cm and 50-100 cm, and partly ~~up to~~ 100-170 cm (Table [S12](#)). Calcretes are generally ginger-like,  
257 ellipsoid, subglobular, and irregular in shape (Fig. 3b and 3e) and nodules are 1-3 cm even up to 8-15 cm (paleosols  
258 J1z-10-01 and J1z-12-01) in size (Fig. 3e). Calcrete is often less than 0.5-1% in an individual paleosol ~~horizon~~, but a few can  
259 be up to 3-5% (paleosol J1z-3-01. Fig. 3b) even 10% (paleosols J1z-5-02 and 18HC-10).

260 ~~Based on the description of the paleosols described above, a~~ All ~~above paleosols~~ are defined as relatively mature calcisols  
261 (Mack et al., 1993), a kind of aridisol (Soil Survey Staff, 1998; Retallack, 2001b). The original lithofacies were chiefly  
262 argillaceous and silty (split-fan) overbank, interchannel, and flood plain deposits (Figs. S1 and S2). Some formed  
263 land~~shareward~~ of the paleo-lakeshore.

264 Dolomites were found at seven loactions in central and southern GSB (Figs. 1, 4, and Table [S2S1](#)), ~~which are to some~~  
265 ~~degree an indicative of arid/evapoatre climate~~. The dolomites chiefly occur in the Toracian Da'anzhai Member and a few in  
266 the Sinemurian-Plienbachian Dongyuemiao and Ma'anshan members (Fig. 4). They are often massive whitish (Figs. 3f and  
267 S3e) and micritic (Figs. S4b and S4d), likely indicating an ~~authigenic-syndeositional~~ ~~\_~~origin.

268 Gypsum is ~~only~~ recorded in two loactions (Figs. 1, 4, and Table [S2S1](#)). One is located at Zigong (Location A5. SBG, 1980a).  
269 The other lies at Hechuan (Location A6), which can be identified by chicken-wire cage structure and is associated with  
270 micriditic dolomites (Fig. 3f).

#### 271 **4.2. ~~Carbon-oxygen~~Carbon and oxygen isotope values**

272  $\delta^{13}\text{C}$  values of lacustrine carbonate samples range from -2.02‰ to -4.07‰ and  $\delta^{18}\text{O}$  values ~~derangerange~~ from -9.91‰ to  
273 -12.28‰ (Table S3 and Fig. 5). An ~~distinct~~ increasing trend of both carbon and oxygen isotope ratios ~~can be detected is~~  
274 ~~observed~~ from lower to upper horizons across a ~~405~~ m stratal interval of the lower Da'anzhai Member (Fig. 6).

275 Pedogenic carbonate samples have  $\delta^{13}\text{C}$  values from -3.52‰ to -8.10‰, which fall in the typical stable isotope range for  
276 pedogenic carbonates. Values of -6‰ to -8.0‰ characterize the sequence of the Zhenzhuchong Member and main  
277 Ma'anshan Member, with an abrupt increase to -5.5‰ to -3.5‰ at the top of Ma'anshan Member (samples J1z-16-01 and  
278 J1z-18-01, Fig. 6).  $\delta^{18}\text{O}$  values are mainly from -11.3‰ to -13.10‰ in the interval of the Zhenzhuchong Member and  
279 Ma'anshan Member.  $\delta^{18}\text{O}$  follows  $\delta^{13}\text{C}$  with a sudden increase to -5.5‰ at the top of the Ma'anshan Member (Fig. 6). Large  
280 and frequent variations of both carbon and oxygen isotope ratios can be observed in the lower Da'anzhai Member (Fig. 6 and  
281 Table S4).

### 282 4.3. CO<sub>2</sub> concentrations

283  $p\text{CO}_2$  values based on paleobarometer modelling of paleosol calcite (Cerling, 1999) of the Early Jurassic paleosols vary in the  
284 Early Jurassic when different depending on the parameters are selected used for the calculation.

285 If  $S_{(z)}=2500$  ppmV and  $\delta^{13}\text{C}_a=-6.5$ ‰ (constant pre-industrial atmosphere),  $p\text{CO}_2$  values range between ~1140 ppmV and  
286 ~3460 ppmV with a mean of 1870 ppmV (column 15 in Table S4); and when  $S_{(z)}=2500$  ppmV and  $\delta^{13}\text{C}_a=(\delta^{13}\text{C}_r+18.67)/1.1$ ,  
287  $p\text{CO}_2$  values change between ~1230 ppmV and ~3260 ppmV with a mean of 2070 ppmV (column 16 in Table S4).

288 ~~If~~When  $S_{(z)}=2000$  ppmV and  $\delta^{13}\text{C}_s=-8.98+\delta^{13}\text{C}_c$  are used,  $p\text{CO}_2$  values are ~ 940-2530 ppmV with the mean 1600 ppmV  
289 (column 17 in Table S4); and if  $S_{(z)}=2000$  ppmV and  $\delta^{13}\text{C}_s = (\delta^{13}\text{C}_c+1000) / ((11.98-0.12*25) / 1000+1) -1000$  are adopted,  
290  $p\text{CO}_2$  values become ~980 ppmV to ~2610 ppmV with the mean 1660 ppmV (column 18 in Table S4). Details of the  
291 different parameters and  $p\text{CO}_2$  results can be seen in Table S4.

292 Results further show that  $p\text{CO}_2$  values at  $S_{(z)}=2500$  ppmV are larger than at  $S_{(z)}=2000$  ppmV, and the discrepancy of  
293 the difference between the The highest difference calculated  $p\text{CO}_2$  is ~ 1000 (3640-2610) ppmV, but while that the difference  
294 of the lowest value is ~300 (1230-930) ppmV and that of the mean value is ~ 370 (2070-1600) ppmV. In addition, when  $S_{(z)}$   
295 is the same, the  $p\text{CO}_2$  values are close even if other parameters are different (comp. between columns 15 and 16, 17 and 18  
296 in Table S4, and Fig. 6).

297 However, ~~Which~~ whatever parameters used, the trend of  $p\text{CO}_2$  over the epoch is quite similar using different values of  $S_{(z)}$  and  
298 other parameters (Fig. 6). We chose  $S_{(z)}=2000$  ppmV (column 18 in Table S4) to illustrate the nature of the Early Jurassic  
299  $p\text{CO}_2$  estimated from calcisols in the GSB.

300  $p\text{CO}_2$  values mostly range between 980 ppmV and 2610 ppmV, and the mean 1660 ppmV is ~6 times the pre-industrial 275  
301 ppmV. Most of the  $p\text{CO}_2$  values are 1000-2000 ppmV with the mean 1580 ppmV in the Zhenzhuchong and Ma'anshan  
302 members, ~3.5-7.5 times the pre-industrial  $p\text{CO}_2$  value.

303 It is noted that the errors of  $p\text{CO}_2$  range from 384 ppmV to 1017 ppmV with a mean 647 ppmV (Table S5), leading to a large  
304 uncertainty of the mean ~39%. The largest source of the uncertainty is the standard error (766 ppmV) of modern soil carbonate  
305 (Breecker and Retallack, 2014). The  $p\text{CO}_2$  uncertainty decreases by ~ 20% if half (383 ppmv) of the standard error of soil



306 carbonate is selected, and decreases to ~12% if 1/4 (~191 ppmV) standard error is used. The second largest source of error in  
307 the  $p\text{CO}_2$  is the  $S_{(z)}$  estimate. The uncertainty of  $p\text{CO}_2$  becomes much smaller when the  $S_{(z)}$  is larger, e.g., it will fall from ~39%  
308 to ~17% if  $S_{(z)}$ =5000 ppmV instead of 2000 ppmV. Other parameters such as temperature,  $\delta^{13}\text{C}_p$ ,  $\delta^{13}\text{C}_a$ ,  $\delta^{13}\text{C}_s$ , contribute very  
309 little to the calculated  $p\text{CO}_2$  uncertainty.

## 311 5. Discussion

312 ~~Similar with the entire Jurassic period, the Early Jurassic epoch had experienced~~The Jurassic marine record shows climatic  
313 and environmental oscillations (e.g., van de Schootbrugge et al., 2005; Dera et al., 2011; Gómez et al., 2015; Arabas et al.,  
314 2017), ~~expressing the~~including sea water temperature fluctuation and carbon cycle reorganization recorded in ~~s~~ both  
315 carbonate and organic matters. The climate ~~ie~~ changes and events ~~of~~ recorded in the the marine realm have been mainly  
316 attributed to ~~the~~Karoo-Ferrar volcanism (e.g., Hesselbo et al., 2000; Caruthers et a., 2013), ~~and alternatively~~ sea-level  
317 change (e.g., Hesselbo and Jenkyns, 1998; Hallam and Wignall, 1999), orbital forcing (e.g., Kemp et al., 2005; Huang and  
318 Hesselbo, 2014, Storm et al., 2020), and / or the opening of the Hispanic corridor (e.g., van de Schootbrugge et al., 2005;  
319 Arias, 2009). ~~The volcanic forcing hypothesis is that the volcanism had triggered the degassing, increasing~~Eruption of the  
320 Karoo-Ferrar and Central Atlantic ~~basalts~~ magma is thought to have released large amounts of  $\text{CO}_2$  ~~concentration in~~ into the  
321 atmosphere in a short amount of time, ~~and~~ resulting in rising temperatures of both marine and continental realms. The  
322 nearly continuous record of Jurassic strata in the GSB provides an excellent test of this hypothesis in the terrestrial realm. ~~Te~~  
323 ~~test this hypothesis, we analyzed~~We compare the climate and  $p\text{CO}_2$  record ~~of~~ from the GSB and ~~discussed the~~  $p\text{CO}_2$  change  
324 ~~with~~ in relationship to the marine temperature records.

### 325 5.1. Paleoclimate variation

326 ~~Results show that the depositional environment and paleoclimate in the Early Jurassic were distinctly different from those in~~  
327 ~~the Late Triassic in Southwest China. As a whole, the climate became dry and  $p\text{CO}_2$  varied in three phases through the Early~~  
328 ~~Jurassic.~~

329 Sedimentary facies analysis indicates two lithofacies cycles were developed and calcisols were largely spread in the Lower  
330 Jurassic Ziliujing Fm in the GSB, Southwest China. The first cycle is the riverine and flood plain lithofacies of the Qijiang  
331 Membe and Zhenzhuchong Member which is succeeded by the lacustrine facies of the Dongyuemiao Member, and the  
332 second is the flood plain and river facies with swamp lithofacies of the Ma'anshan Member followed by the lacustrine facies  
333 of the Da'anzhai Member. We interpret the two packages to reflect two major lake stages (for details refer to supplementary  
334 data Note S1).

335 ~~Results of climate sensitive sediment analyses show that the depositional environment and climate in the Early Jurassic were~~

336 ~~distinctly different from those in the Late Triassic in Southwest China. With the change of depositional environments,~~  
337 ~~paleoclimate and pCO<sub>2</sub> changed, as reflected by climate-sensitive facies and stable isotope analyses.~~

### 338 ~~5.1. Paleoclimate variation~~

339 During the Late Triassic, Southwest China was warm-hot and humid ~~in and occupied~~ a tropical and /or subtropical zone, as  
340 demonstrated by palynoflora, coals, and perennial riverine and lacustrine lithofacies in the Xujiahe Fm (e.g., Huang, 1995; ~~Xu~~  
341 ~~et al., 2015; Li et al., 2016; Yang et al., 2019).~~). ~~However, the whereas and a distinct transfer of climate took place in~~  
342 ~~the~~ Climate became dry through the Early Jurassic manifested by climate-sensitive sediments and stable isotopes ~~of the~~  
343 ~~Ziliujing Fm in GSB~~ albeit there are two lithofacies packages reflecting two major lake stages (for details refer to  
344 supplementary data Note S1) in the GSB. As a whole, the climate became dry through the Early Jurassic. Below are  
345 illustrations of climate by age.

#### 346 ~~4)~~ 5.1.1 The Hettangian Age

347 ~~By~~ In the Hettangian ~~time (the Qijiang Member), the climate was a~~ warm-humid ~~climate followed~~ like the Late Triassic in the  
348 GSB. The ~~limited sedimentary records~~ Qijiang Member is comprised of ~~are~~ mainly mature quartz ~~sandstone~~ arenites and  
349 siltstones with coals ~~(Fig. 7) and as well as~~ siderite concretions ~~(Fig. 7)~~, indicating a stable tectonic setting and  
350 warm-humid climate in the eastern and southern GSB. ~~In the northern margin, the~~ Climate was similar across the whole  
351 region, because multiple coal layers occur in the lower Baitianba Fm. ~~and the hosted a~~ The alluvial fan system of the lower  
352 Baitianba Fm. (Figs. 7 and S6) is characterized by moderate-good roundness and sorting of gravels with sandy fillings matrix  
353 (Fig. S3a. e.g., Liu et al., 2016; Qian et al., 2016; and this work). In the Newark basin of eastern North America,  
354 climate-sensitive sediments such as nodules of carbonate and gypsum (pseudomorph) as well as mudcrack in mudflat facies  
355 indicate an arid climate in the fifth cycle of the Hettangian (>199 Ma). ~~Kent et al., 2017~~ Passaic Fm (Kent et al., 2017)  
356 (Smoot and Olsen, 1994). More widespread, the eolian Navajo Sandstone, dated as Hettangian-Sinemurian (200-195 Ma.  
357 Parrish et al., 2019), indicates an arid climate in Colorado Plateau (Fig. 1a. Boucot et al., 2013). ~~Obviously, the arid climate~~  
358 ~~in western America was different from that in the GSB at the time.~~

#### 359 5.1.2) The Sinemurian Age

360 The early Sinemurian Zhenzhuchong Member is a combination of riverine ~~and~~ flood plain ~~facies with~~ and lacustrine facies  
361 (supplementary Note S1). ~~in which the~~ The lithology is dominated by violet-red mudrocks with few thin greyish, greenish  
362 fine sandstones and siltstones. The reddish color of rocks may indicate a change of climate ~~even if there is a little bit~~  
363 ~~difference in the color appearance of reddish color sediments in the western and central basin. The difference~~ Differences in  
364 the red-color appearance. That show that is, the reddish color the reddish rocks started in the middle member in the central  
365 basin (Location A6. Fig. S2) but almost developed through the whole member in the western margin basin (Location A4.

Fig. 6), but it started in the middle member in the central basin (Location A6. Fig. S2).

Within the red colorish mudrocks of, a kind of climate sensitive pedogenesis is recognized from the flood plain facies demonstrates an arid climate. Multiple calcisols horizons were observed at the Shaping section, Ya'an (Location A4. Figs. 1, 4, and 7), within which including a strongly leaching calcisol horizon can be found (Fig. S3c). Calcisols were also interpreted the reddish muddy sediments with the description of abundant calcretes as the calcisol at sections of Dafang (Location A8. Zhang et al., 2016), Tianzhu (Location A9. Li and Chen, 2010), and Weiyuan (Location A10. SBG, 1980a), respectively. The Calcisols indicate a transition from the humid climate of the Late Triassic and Hettangian to that a (semi-) arid climate at least began to replace the previous humid climate in western and southern margins of the basin in the Sinemurian (Figs. 1, 4, and 7 and Table S2).

This climate change, indicated interpreted from reddish mudrocks and paleosols, is consistent with the climatic signal from floral fossils (e.g., Huang, 2001; Wang et al., 2010), that, suggesting the a decrease in decreasing humidity and an increase in increasing temperature across the interval, compared to that in from the Late Triassic epoch and the Hettangian age into the Sinemurian Qijiang Member and Late Triassic Xujiahe Fm into the Sinemurian age in the southern GSB.

However, the climate was not distinct in humidity and temperature in the northern GSB without there are few proxies for of sediments and flora climate change, even though and alluvial fan and lacustrine delta facies are common in the middle of the Baitianba Fm (Fig. S6. e.g., Qian et al., 2016) do not give us information on climate.

No climate sensitive sediments are documented in the late Sinemurian Dongyuemiao Member from previous studies, in which it is characterized by lacustrine limestones. However, The late Sinemurian Dongyuemiao Member also has similar to the Zhenzhuchong Member, reddish mudrocks and calcisols, with similar to the Zhenzhuchong Member. Pedogenic newly interpreted calcisols indicate drier climate (Figs. 4 and 7 and Table S2). Calcretes within reddish mudrocks were reported at Dafang (Location A8. Zhang et al., 2016), Tianzhu (Location A9. Li and Chen, 2010), and Yunyang (Location A15. Meng et al., 2005) and in the central and southern GSB (Figs 4 and 7 and Table S2), newly interpreted calcisols indicated displaying indicating a drier continued arid climate conditions (Figs. 4 and 7 and Table S2) at the time.

The probable calcisols indicate the (semi-) arid climate may have interrupted the long term warm and (semi-) humid climate interpreted based on flora in the Early Jurassic (e.g., Meng et al., 1997; Li and Meng, 2003). This interpretation of (semi-) arid. The interpreted Sinemurian (semi-) arid climate from reddish mudrocks and calcisols and it punctuation is also supported by the floral changes (Meng et al., 1997; Li and Meng, 2003) and as well as and the mudrock geochemistry of mudrocks (Guo et al., 2017).

Few records of coeval terrestrial climate are known from other continents or regions in the literature. A report occurs in eastern England, where the co-occurrence of the acmes of thermophilic pollens *Classopollis classoides* and *Liasidium variabile* indicates the warm humid climate in the late Sinemurian (Riding et al., 2013). The Whitmore Point Member of the Moenave Fm deposited in dryland lakes (Tanner and Lucas, 2008) and the upper part of eolian Navajo Sandstone

398 (Blakey et al., 1988) could represent the coevally similar climate in Colorado Plateau although relatively cool (~9 to 18 °C)  
399 continental climate was inferred from oxygen and hydrogen isotope composition of chert precipitated in interdune,  
400 freshwater lakes in the Navajo Sandstone (Kenny, 2015). ~~With a difference, in eastern England, the co-occurrence of the~~  
401 ~~acmes of thermophilic pollens *Classopollis classoides* and *Liasidium variabile* indicates the warm-humid climate in the late~~  
402 ~~Sinemurian (Riding et al., 2013).~~

### 403 **5.1.3) The Pliensbachian Age**

404 ~~The Ma'an-shan Member is likely the Pliensbachian, though age information is lacking. In comparison to the previous~~  
405 ~~member, the Ma'an-shan Member of the Pliensbachian age, displays displays a prominent change in the distribution and~~  
406 extent of red color sediment and pedogenesis. The reddish sediments extend through the entire member (comp. Figs. 6 and  
407 S2) and can be observed across most of the GSB. Calcisols are documented in both the western and central GSB (Figs. 6, 7,  
408 S1, and S2). Ten calcisol horizons were recognized at the Shaping section, Ya'an (Figs. 6 and S1); ~~and strongly leaching~~  
409 ~~pedogenic structures~~ and mudcracks are seen in Bed H8 of the Tanba section, Hechuan (Fig. 3a and 3d). ~~Other more~~  
410 ~~abundant calcretes within terrestrial red mudrocks were are~~ widely described at ~~the Gaoxian section~~ of Dafang (Location  
411 A8. Zhang et al., 2016), ~~the Hulukou section~~ of Weiyuan (Location A10. SBG, 1980a), ~~the Geyaoguan section~~ of Gulin  
412 (Location A13. SBG, 1976), ~~the Taiyuan section~~ of Fengdu (Location A16. SBG, 1975), and ~~the Yaxi section~~ of Zunyi  
413 (Location A17. Yang, 2015). ~~We interpret these calcretes were formed by the pedogenesis calcisol origin.~~ The widespread  
414 distribution of redbeds and calcisols (Figs. 4 and 7) ~~denotes implies an a intensification of the~~ (semi-) arid climate ~~had been~~  
415 ~~intensified in the GSB during the Pliensbachian age.~~

416 Plant and sporopollen fossils also ~~show indicate~~ a change to drier climate in the Pliensbachian. ~~With comparison Compared~~  
417 to the ~~Zhenzhuchong and Dongyuemiao Members~~ Sinemurian members, ~~much many fewer more~~ plant fossils ~~were are~~  
418 reported in this member (e.g., Meng and Chen, 1997; Wang et al, 2010), ~~likely implying a rapid climatic change.~~ The  
419 Pliensbachian-Toarcian sporopollen assemblages are dominated by ~~classical~~ sporomorph genera assemblage  
420 ~~(*Dictyophyllidites*–*Cyathidites*–*Classopollis*)~~, in which the dry-type gymnosperm spore *Classopollis* is more prevalent than  
421 in the Hettangian-Sinemurian (Zhang and Meng, 1987), ~~also indicating consistent with the interpretation of the intensification~~  
422 ~~of arid climate.~~

423 Similar dry temperate / subtropical climate ~~was verified by~~ is interpreted for the upland coniferous forest in Qaidam Basin,  
424 Northwest China (Wang et al., 2005). ~~In other hand and, by interdune playa mudstones of the Kayenta Fm (e.g., Bromley,~~  
425 ~~1992) indicate similar arid climate in Colorado Plateau, western America (e.g., Bromley, 1992). However, at the same time~~  
426 ~~albeit,~~ it was at the probably cool est / most humid climate in South Kazakhstan, central Asia (Tramoy et al., 2016). ~~These~~  
427 ~~discrepancies might corroborate the unstable and heterogeneous climate in the mid-latitude area of North Hemisphere in the~~  
428 ~~Pliensbachian. In other hand, interdune playa mudstones of the Kayenta Fm (e.g., Bromley, 1992) indicate similar arid~~

429 ~~climate in Colorado Plateau, western America.~~

#### 430 **5.1.4) The Toarcian Age**

431 In spite the fact that the Da'anzhai Member was deposited in the largest lacustrine transgression period (Fig. 7. details see  
432 ~~Appendix supplementary data Note S1~~), abundant evidence for arid conditions, including backshore reddish mudrocks with  
433 calcsols, lacustrine ~~climate sensitive facies~~ micritic dolomites and / or gypsum, and stable isotopic geochemistry of  
434 lacustrine carbonate, together indicate that the Toarcian the aridification could be the most intensive ~~in~~ of the late Early  
435 Jurassic in the GSB.

436 Redbeds with abundant calcretes are well developed in the ~~Da'anzhai~~ Member member (Figs. 4 and 7). Four calcsols  
437 horizons in the Shaping section, Ya'an (Figs. 6 and S1) and the leaching illuvial structure (Bed H13) in the Tanba section,  
438 Hechuan (Fig. 3c); were observed. Calcsols with calcretes also occur at sections of Dafang (Location A8. Zhang et al.,  
439 2016), Nanxi (Location A11. SBG 1980a), Gongxian (Location A12. Liang et al., 2006), and Yunyang (Location A15. Meng  
440 et al., 2005), ~~also record the occurrence of~~ calcsols. The widespread occurrence of calcsols within this lacustrine  
441 facies reveals that subaerial exposure of sediments often interrupted the lake environment, illustrating dynamic lake level  
442 fluctuations and aridification and an arid climate.

443 ~~In addition to redbeds and calcsols,~~ Gypsum and micritic dolomites (SBG, 1980a; Mo and Yu, 1987; Peng, 2009; and this  
444 work) were are reported in the western and southern GSB (SBG, 1980a; Mo and Yu, 1987; Peng, 2009; and this work) (Figs.  
445 1, 4, and 7). ~~It is plausible that gypsum and dolomites indicate arid climate type. Though there are a number of hypotheses~~  
446 on the dolomite formation in deep time,s ~~have been in dispute for the significance of climate due to great dealsuch as~~  
447 authigenic origin, diagenetic replacement, of diagenetic dolomites microbial mediation (e.g., Vasconcelos et al., 1995;  
448 Mckenzie et al., 2009; Petrash et al., 2017), in deep time, a high abundance of dolomite was interpreted to form during  
449 greenhouse periods, characterized by warm climates, probably reflecting favourable conditions for evaporite deposition and  
450 dolomitization via hypersaline reflux (Warren, 2000). Dolomites are aslo thought the results of interplay of climate and  
451 sea-level / base-level change (e.g., Newport et al., 2017) or are interacted with climatic regimes (Vandeginste et al., 2012).

452 ~~Therefore, It is plausible that micritic gypsum and dolomites may indicate represent deposits of arid/evaporate climate~~  
453 ~~when are associated with other climate sensitive sediments type. That is So, the~~ The widespread micritic dolomites in the  
454 Da'anzhai ~~Fm~~ Member, which are associated with gypsum (Fig. 3f), ~~probably likely indicate can serve the determination of~~  
455 ~~climate and suggest~~ an arid climate in the central and western GSB (Fig. 1b). Gypsum occasionally occurs at Maliuping of  
456 Hechuan (Fig. 3f) and Wujiaba of Zigong (SBG, 1980a), ~~implying showing a short-term possible~~ evaporitic climate in the  
457 early Toarcian in the central GSB.

458 Carbon and oxygen isotopes of lacustrine carbonates further support the interpretation of an arid climate in the Toarcian age  
459 in the GSB. ~~In general, -9.0‰ to -3.0‰ of  $\delta^{13}\text{C}$  and  $\delta^{18}\text{O}$  values represent a range of normal river lake and groundwater~~

460 carbonates (Alonso Zarza, 2003). Therefore, ~~the~~ The mainly positive  $\delta^{13}\text{C}$  values 0 to 2 ‰ (Fig. 5) from Hechuan (Wang et  
461 al., 2006) indicate the lakes were brackish or even saline, ~~and the~~ The relatively heavy negative  $\delta^{13}\text{C}$  values -1‰ to -3.5 ‰  
462 (Fig. 5) from Zigong (Wang et al. 2006) and Ya'an (this work) denote low depletions of  $^{13}\text{C}$  during calcite/argonite  
463 precipitation and mean that the lakes were possibly brackish. ~~In other hand,~~ Lightly negative  $\delta^{18}\text{O}$  values -5‰ to -12 ‰ (Fig.  
464 5) ~~dominate of~~ the lacustrine carbonates, suggesting ~~that~~ closed lacustrine, palustrine and pond systems formed in a regional  
465 arid-semiarid climate with ~~significant~~ evaporation ~~relative to~~ exceeding precipitation.

466 The covariance of  $\delta^{13}\text{C}$  and  $\delta^{18}\text{O}$  is ~~also~~ a criterion to distinguish closed or open lakes (e.g., Talbot, 1990; Li and Ku, 1997).  
467 ~~That is, high  $\delta^{18}\text{O}$  and low  $\delta^{13}\text{C}$  values will be produced in relatively low temperature lake water when the covariation is~~  
468 ~~negative; high values of both  $\delta^{18}\text{O}$  and  $\delta^{13}\text{C}$  will be produced in high temperature meteoric water and indicate increased~~  
469 ~~evaporation when the covariation is positive.~~ Pronounced positive covariances ( $R^2=0.44-0.96$ ) between carbon and oxygen  
470 isotopes (Fig. 5) indicate a typical arid-semiarid pattern of lakes in the central and western GSB.

471 The Da'anzhai Member has the same palynofloral assemblage with the Ma'anshan Member, in which the dry-type  
472 gymnosperm spore *Classopollis* is ~~much more~~ more abundant than in ~~previous~~ underlying strata (e.g., Zhang and Meng, 1987;  
473 Wang et al., 2010), supporting the aridification indicated by climate-sensitive sediments and stable isotope ratios of  
474 lacustrine carbonates aforementioned.

475 Coastal Cheirolepidiacean (gymnosperm) forests indicate (temperate to subtropical) warm-humid climate punctuated by  
476 locally dry and/or arid events in the Toarcian in Qaidam Basin, Northwest China (Wang et al., 2005). In Inner Mongolia of  
477 North China, the thermophilous plants such as the dipteridaceous fern *Hausmannia*, bennettitales *Ptilophyllum*, display  
478 similar warm and humid climate interrupted by hot and even arid conditions in a short intervals of the Toarcian (Deng et al.,  
479 2017). The warm-wet climate was also indicated by assemblages of sporomorph and vegetation in the late Early Jurassic in  
480 Jurong of Jiangsu, Lower Yangtze area (Huang et al., 2000). In South Kazakhstan, central Asia, paleoflora and  $\delta^2\text{H}$  values  
481 suggest slightly less humid and warmer conditions starting from the early Toarcian (Tramoy et al., 2016).

482 ~~In summary,~~ climate-sensitive sediments, ~~carbon oxygen~~ carbon and oxygen isotope values and covariance, and  
483 palynoflora, together indicate that an overall (semi-) arid climate dominated the GSB during the Early Jurassic, possibly  
484 accompanied by occasional evaporitic climate. Relatively abundant calcisols suggest that the GSB was in a subtropical arid  
485 zone based on the paleoclimatic zonation model of paleosols (Mack and James, 1994) during the middle-late Early Jurassic.  
486 Through the Early Jurassic, this (semi-) arid climate in GSB is thoroughly comparable with the simultaneous arid climate  
487 recorded in dryland lacustrine and eolian facies in Colorado Plateau, ~~western America~~ (e.g., Blakey et al., 1988; Bromley,  
488 1992; Tanner and Lucas, 2008; Parrish et al., 2017), but distinct from the relatively warm-humid climate indicated by  
489 sedimentological and floral characteristics in North China (e.g., Wang et al., 2005, Deng et al., 2017) and in the northern  
490 margin of Gondwanaland, relatively high latitudes of Southern Hemisphere (Jansson et al., 2008; Pole, 2009).

491 In summary, the increasing aridity and warming in the GSB and arid climate in the Corlorado Plateau could have been

492 consecutive through the Early Jurassic, and seems not harmonized with the global fluctuating climate that could be  
493 imprinted by two large volcanic eruptions of the Central Atlantic magmatic province and Karro-Ferrar Large Igneous  
494 Province. The secular arid climate in the two areas might be more possibly constrained by paleotopography, where both were  
495 laid in the relatively low latitudes 15-30°N (Fig. 1a).

## 496 **5.2. $p\text{CO}_2$ perturbations and events**

497 Pedogenic carbonates found in various continental settings precipitate in direct contact with soil atmosphere and bed rock  
498 and hold a meaningful signature of past climate (Alonso-Zarza and Tanner, 2006). ~~Ancient  $p\text{CO}_2$  has been estimated by~~  
499 ~~carbon isotope of pedogenic carbonates using the empirical (Cerling, 1991) and optimized (Ekart et al., 1999) formula. This~~  
500 ~~paleosol method has roughly been applying in the Phanerozoic  $p\text{CO}_2$  estimate (e.g., Cerling, 1991; Ekart et al., 1999;~~  
501 ~~Retallack, 2001a) with >10 Myr interval of age resolution.~~ There are few high age resolution  $p\text{CO}_2$  reconstructions for the  
502 Early Jurassic. The focus on  $p\text{CO}_2$  estimates has on the event horizons, such as the transition of the Triassic to Jurassic (e.g.,  
503 Tanner et al., 2001; Schaller et al., 2011). Herein we present ~~the a~~  $p\text{CO}_2$  estimate based on data from the GSB in at ~1.0 Myr  
504 age resolution for a ~120 Myr (199-179 Ma) interval of the Early Jurassic (Figs. 6 and ~~8e~~8a).

### 505 **5.2.1. $p\text{CO}_2$ perturbation**

506 Results of model estimates show that the  $p\text{CO}_2$  values range 980-2610 ppmV with a mean 1660 ppmV in the Early Jurassic  
507 ~~except for the post the~~ Hettangian and can be divided into three intervals (Figs. 6 and ~~8e~~8a): phase I, stable 1500-2000 (mean  
508 ~1700) ppmV in the Zhenzhuchong and Dongyuemiao ~~m~~Members (Sinemurian age); phase II, main 1000-1500 (mean ~  
509 1300) ppmV in the Ma'anshan Members (Pliensbachian age); and phase III, great fluctuation 1094-2610 (mean ~1980)  
510 ppmV in the lower Da'anzhai Member (early Toarcian age).

511 The evolution and level of  $p\text{CO}_2$  estimated by carbon isotope ratios of the pedogenic carbonates from the GSB ~~are roughly~~  
512 ~~comparable~~compare favorably with the global composite based on the plant stomata method (data of the composite curve see  
513 Table S66), but ~~difficult to compare~~show significant differences relative to the global composite  $p\text{CO}_2$  based on paleosols  
514 (Fig. ~~8a~~8e. Suchecki et al., 1988; Cerling, 1991; Ekart et al., 1999), which may be attributed to the shortage (<4 samples) of  
515 global data and large age uncertainties (Fig. ~~8a~~8a and Table S55 and S66).

516 ~~On the other hand, the swing of~~The changes the in  $p\text{CO}_2$  from the GSB, has a similar pattern to coeval seawater temperature  
517 estimates through the Early Jurassic although there are some discrepancies in pace and at a high time resolution and in detail  
518 (comp. Fig. ~~8a~~8ab and ~~8e~~8eb). That is, the relatively high  $p\text{CO}_2$  1500-2000 ppmV approximately corresponds to the relatively  
519 high seawater mean temperature -2°C to +2°C in the Sinemurian ~~age~~ (Fig. ~~8b~~8b), low  $p\text{CO}_2$  1000-1500 ppmV corresponds to  
520 low seawater mean temperature -5°C to -2°C in the Pliensbachian ~~age~~ (Fig. ~~8b~~8b), and quick rising  $p\text{CO}_2$  of 1200 ppmV to  
521 ~2500 ppmV corresponds to the rapidly increased seawater temperature of -4°C to +4°C in the late Pliensbachian-early

522 Toarcian (Fig. 8b).

523 The  $p\text{CO}_2$  record ~~and the carbon isotope of the marine carbonates are also somewhat roughly comparable trends with the~~  
524 ~~carbon isotope records of marine carbonates and organic matter s—in tendency—~~ (comp. Fig. 8aa to 8d and 8e),  
525 ~~implying~~ suggesting a possible linkage of the  $p\text{CO}_2$  record in the GSB to the global carbon cycle ~~in total trend and rapid~~  
526 ~~change—~~ (see section 5.2.2). Nevertheless, it is difficult for the proxies to compare ~~—in a higher time resolution detail, making it~~  
527 ~~difficult to relate the record to even if it could be attributed to the low resolution of paleosol sample intervals and to the~~  
528 ~~orbital forcing of the global carbon cycle in the Sinemurian-Pliensbachian (Storm et al., 2020).~~  
529 ~~It has been disputed whether climate change was resulted from  $p\text{CO}_2$  perturbation in the Phanerozoic (e.g., Veizer et al.,~~  
530 ~~2000; Crowley and Berner, 2001; Royer, 2006).~~ For instance, ~~the~~ As a greenhouse gas, atmospheric  $\text{CO}_2$  has a strong  
531 control over global temperatures for much of the Phanerozoic (e.g., Crowley and Berner, 2001; Royer, 2006; Price et al.,  
532 2013; Mills et al., 2019), but a decoupling of  $\text{CO}_2$  and temperature has also been suggested (e.g., Veizer et al., 2000; Dera et  
533 al., 2011; Schaller et al., 2011; Kashiwagi, 2016). The pattern of the Early Jurassic  $p\text{CO}_2$  reconstructed from the carbon  
534 isotope of pedogenic carbonates in GSB, Southwest China, supports the ~~coupling—coupled~~ relationship of  $\text{CO}_2$ -temperature ~~at~~  
535 ~~a—1.0 Myr resolution scale. Even so, m~~ Models of the coupling and decoupling of  $\text{CO}_2$ -temperature ~~and  $\text{CO}_2$ -carbon cycle~~  
536 have to consider: 1), age order of  $\text{CO}_2$ -temperature/~~carbon cycle~~ relevance, i.e. they should be related in the same age (long  
537 term or short term) hierarchy; 2) precise age constraints of individual  $\text{CO}_2$  and temperature data; 3) methods of  $\text{CO}_2$  and  
538 temperature estimates, depending on precondition, presumptions, parameters, uncertainty, sample diagenesis, etc.; 4)  
539 controls or influences of key factors such ice sheet, tectonic, paleogeography, cosmic ray flux, biota, volcanic eruption, and  
540 so on.

### 541 5.2.2. Rapid $p\text{CO}_2$ falling events

542 The ~~recovered—GSB~~ Early Jurassic  $p\text{CO}_2$  curve reveals two rapid falling events (Fig. 6 and 8a). The first event ( $1E_{\text{CO}_2}$ )  
543 shows a quick drop from ~2370 ppmV (sample J1z-08-01 at depth 84.7 m) to 1350 ppmV (sample J1z-10-02 at depth 94.4 m)  
544 near the boundary of the Dongyuemiao and Ma'anshan Members (Fig. 6), or to 1075 ppmV (sample J1z-11-02 at depth  
545 111.7 m), which took place in the early Pliensbachian (~190.4-189.9/189.1 Ma. Fig. 8c). The extent of the rapid falling  
546  $p\text{CO}_2$  is ~1000-1300 ppmV in 9.7-17.0 m. In other words, ~1000 ppmV drop could be accomplished within ~0.5-1.0 Myr  
547 based on the estimate of ~~the rate of sedimentation rate deposition~~ (Table S4).

548 While the corresponding early Pliensbachian climatic and isotopic-shifting events ~~cannot be are not~~ observed in the smoothed  
549 curves of the Early Jurassic seawater temperature and carbon cycle (Dera et al. 2011), the rapid falling event  $1E_{\text{CO}_2}$  is well  
550 correlated to the nearly coeval excursion events of ~~carbon—oxygen~~ carbon and oxygen isotopes recorded in western Tethys  
551 ~~and North Atlantic~~ (Fig. 8). The  $1E_{\text{CO}_2}$  compares well to: 1) the rapid carbon isotope negative excursion ~~—of~~ (oysters,  
552 belemnites, and brachiopods) shells from the Cleveland Basin, UK (Korte and Hesselbo, 2011) and northwest Algeria



553 (Baghli et al., 2020), 2) that of organic matter and marine carbonates from southern Pairs Basin (Bougeault et al., 2017; Peti,  
554 et al., 2017) and Cardigan Bay Basin, UK (Storm et al., 2020), and 3) rapid oxygen isotope negative excursion (seawater  
555 warming) of belemnites from northern Spain (van de Schootbrugge et al., 2005). The rapid change of the stable isotope  
556 record had been called the Sinemurian-Pliensbachian boundary event (SPBE) and dated in the ammonite of the upper  
557 *Raricostatum* - lower *Jamesoni* zones (Bougeault et al., 2017).

558 The second event 2E<sub>CO2</sub> displays a large drop of 2574 ppmV (sample J1z-18-01 at depth 252.7 m) to 1094 ppmV (sample  
559 J1z-19-01 at depth 272.3 m), ~1500 ppmV decrease within 19.6 m (estimated age interval ~0.8 Myr. Table S4 and Fig. 8ea).  
560 Following the second drop, *p*CO<sub>2</sub> rises rapidly by ~1300 ppmV of 1094 ppmV to 2386 ppmV (sample J1Z-20-01 at depth  
561 294.3 m) although only a few samples support the this cycle of *p*CO<sub>2</sub> falling-rising.

562 Strata in western Sichuan (Xu et al., 2017), may correlate to the time interval of the T-OAE, during which *p*CO<sub>2</sub> doubled  
563 over background values, from ~1000 ppmV to ~2000 ppmV (e.g., Beerling and Royer, 2002; McElwain et al., 2005; Berner,  
564 2006). Given ~~the~~that chronostratigraphical correlation is challenging, the *p*CO<sub>2</sub> falling-rising cycle might correspond to the  
565 quick shifting cycle of stable isotopes during the T-OAE (Fig. ~~8b-8a~~ and 8c-8d). In detail, the rapid falling-rising of *p*CO<sub>2</sub>  
566 is consistent with: 1) the quick negative-positive carbon isotope excursion of marine carbonates from Italy (Jenkyns and  
567 Clayton, 1986; Sabatino et al., 2009), England and Wales (Jenkyns and Clayton, 1997), north Spain (van de Schootbrugge et  
568 al., 2005), the Lusitanian Basin of Portugal (Hesselbo et al., 2007), Paris Basin (Hermoso et al., 2009), and Morocco (Bodin  
569 et al., 2016); 2) that of invertebrate calcareous shells from the Cleveland Basin of UK (Korte and Hesselbo, 2011) and  
570 northwest Algeria (Baghli et al., 2020); 3) that of marine organic matter from Morocco (Bodin et al., 2016), Yorkshire of  
571 England (Cohen et al., 2004; Kemp et al, 2005), Cardigan Bay Basin of UK (Xu et al., 2018), northern Germany (van de  
572 Schootbrugge et al., 2013), Alberta and British Columbia of Canada (Them II et al., 2017), northern Tibet of China (Fu et al.,  
573 2016), and Japan (Izumi et al., 2018); 4) that of terrestrial organic matter from Sichuan Basin, China (Xu et al., 2017); and 5)  
574 quick oxygen isotope negative-positive shifting (seawater warming) of brachiopods (Suan et al., 2008) and fossil wood  
575 (Hesselbo et al., 2007) from the Lusitanian Basin, Portugal.

576 Multiple hypotheses have been proposed to interpret the 5°–6 °C decrease of sea surface temperatures in the late  
577 Pliensbachian (Bailey et al., 2003; van de Schootbrugge et al., 2005; Suan et al., 2010) and warming ~8 °C in the early  
578 Toarcian (Bailey et al., 2003; Suan et al., 2010), such as the sea level falling and rising (~~Hallam, 1978; Hesselbo and Jenkyns,~~  
579 ~~1998~~), methane release (~~e.g., Hesselbo et al., 2000; Kemp et al, 2005; Hermoso et al., 2009; Them II et al., 2017~~), and the  
580 Karoo–Ferrar eruptions (e.g., Hesselbo et al., 2000; Beerling and Brentnall, 2007; Bodin et al., 2016)., Hispanic corridor  
581 opening, etc. Perhaps, these hypotheses somewhat explain the rapid change of sea surface temperatures, but ~~it remains~~  
582 ~~unclear how~~might not link ~~the hypotheses~~ to drastic falling of *p*CO<sub>2</sub> in a high age resolution. As we know, atmospheric CO<sub>2</sub>  
583 is controlled by volcanism, weathering, vegetation on land and phytoplankton in ocean, and orbiting forcing. The Sr isotope  
584 curve shows a rapid change in the early Toarcian but does not in the early Pliensachian (e.g., Jones et al., 1999), indicating a

585 ~~distinct transfer of weathering took place on the land only at the T-OAE time. No robust evidence shows the rapid changes~~  
586 ~~of terrestrial vegetation and marine primary productivity for the two intervals except for the floral change in western Tethys~~  
587 ~~during the T-OAE (Slater et al. 2019). The Karoo–Ferrar eruption could be responsible for the rapid rising of  $p\text{CO}_2$  but not~~  
588 ~~for the falling. Then the orbital forcing might be an alternative.~~

589 To sum up, the ~~perturbation and~~ rapid falling events of the Early Jurassic  $p\text{CO}_2$  values ~~estimated from the carbon isotope of~~  
590 ~~pedogenic carbonates~~ in the GSB, are compatible with the response of stable isotopes (carbon cycle) and seawater  
591 temperature from coeval marine sediments in a total tendency and eventful change, but not harmonized at a high-resolution  
592 time scale. Whatever caused the rapid variations of sea surface temperatures, stable isotopes, and  $p\text{CO}_2$ , their near  
593 concordance ~~implies~~ suggests that it is a positive feedback of the sea surface temperature and carbon cycle to the  $p\text{CO}_2$  in  
594 trend and event through the Early Jurassic; ~~accordingly, positive linkage could have taken place between the Early Jurassic~~  
595 ~~climate and  $p\text{CO}_2$ , whereas the uncomparability at a high resolution time scale~~ higher frequency changes in the  
596 Sinemurian-Pliensbachian might may support other causal driving of the climate, such as orbital forcing (Storm et al.,  
597 2020) in the Sinemurian-Pliensbachian of the Early Jurassic. Other more, as concluded in section 5.1, the Thein North from  
598 suggested by

## 599 6. Conclusions

600 Based on analyses of climate-sensitive sediments and stable isotopes ~~of the GSB, leading to a~~ and the reconstruction of  
601 paleoclimate and  $p\text{CO}_2$ , we conclude:

- 602 1) ~~Climate sensitive sediments and carbon oxygen isotope values and covariances with palynofloral reference indicate that~~  
603 An overall warm-hot and (semi-) arid climate dominated the GSB during the Early Jurassic, possibly accompanied by  
604 occasional evaporitic climate in the Toarcian. This (semi-) arid climate in GSB is comparable with that in Colorado Plateau,  
605 western America, but distinct from the relatively warm-humid terrestrial climate recognized in other places of Chinese  
606 mainland (e.g., Qaidam, Inner Mongolia, and Lower Yangtze) and the ~~northern Gondwanaland, relatively~~ high latitudes of  
607 Southern Hemisphere; \_
- 608 2) The Early Jurassic  $p\text{CO}_2$  values ~~estimated from the carbon isotope of pedogenic carbonates in GSB~~ show that a range  
609 between 980 ppmV and 2610 ppmV is ~3.5-10 times the pre-industrial value 275 ppmV and the mean 1720 ppmV is ~6  
610 times the pre-industrial value.
- 611 ~~3) Three phases of  $p\text{CO}_2$  values were distinguished: 1500-2000 (mean ~1700) ppmV in the Sinemurian age, 1000-1500~~  
612 ~~(mean ~ 1300) ppmV in the Pliensbachian age, and 1094-2610 (mean ~1980) ppmV in the early Toarcian. The phases~~  
613 ~~manifest the perturbation of  $p\text{CO}_2$  in the Early Jurassic.~~
- 614 ~~4) Two events of rapidly falling  $p\text{CO}_2$  were also recognized: ~1000-1300 ppmV drop at the Sinemurian-Pliensbachian~~

615 boundary and quick falling (-rising) by ~1500 ppmV in the early Toarcian. The phases and events manifest the perturbation  
616 of  $p\text{CO}_2$  in the Early Jurassic.  
617 3) The rapid falling events of  $p\text{CO}_2$  are compatible with the response of stable isotopes and seawater temperature from the  
618 coeval marine sediments, implying a positive feedback of climate to  $p\text{CO}_2$  during the Early Jurassic. The perturbation and  
619 rapid falling events of the Early Jurassic  $p\text{CO}_2$  from the GSB are compatible with the carbon cycle and seawater temperature  
620 from coeval marine sediments in the North Atlantic and western Tethys in a total tendency and eventful change, but not  
621 consistent in between at a high time resolution. The compatibility suggests that it is a positive linkage of the sea surface  
622 temperature and carbon cycle to the  $p\text{CO}_2$  in whole trend and event through the Early Jurassic. On the contrary, the  
623 uncomparability differences at a high-resolution time scale implies the different additional climate drivers, such as orbital  
624 forcing are important in the Sinemurian-Pliensbachian record.  
625

## 626 Acknowledgements

627 We thank ~~reviewer~~ Professors Helmut Weisserts and Dan Breecker ~~xxx xxx~~ for careful scrutiny, constructive comments  
628 and suggestions. It is acknowledged this research was supported by Natural Science Foundation of China (NSFC) project  
629 41672097.  
630

## 631 References

- 632 Alonso-Zarza, A. M. and Tanner, L. H.: Preface. Geol. Soc. Am. Spe. Pap., 416, v-vii, doi, 10.1130/0-8137-2416-3.v, 2006.
- 633 ~~Alonso Zarza, A. M.: Palaeoenvironmental significance of palustrine carbonates and calcretes in the geological record. Earth~~  
634 ~~Sci. Rev., 60, 261-298, 2003.~~
- 635 Arabas, A., Schlogl, J., and Meiste C.: Early Jurassic carbon and oxygen isotope records and seawater temperature variations:  
636 Insights from marine carbonate and belemnite rostra (Pieniny Klippen Belt, Carpathians), Palaeogeogr. Palaeoclimatol.  
637 Palaeoecol., 485, 119–135, 2017
- 638 Arens, N. C., Jahren, A. H., and Amundson, R.: Can C3 plants faithfully record the carbon isotopic composition of  
639 atmospheric carbon dioxide, Paleobiology, 26, 137–164, 2000.
- 640 Arias, C.: Extinction pattern of marine Ostracoda across the Pliensbachian-Toarcian boundary in the Cordillera Ibérica, NE  
641 Spain: Causes and consequences, Geobios. 42, 1-15, 2009.
- 642 Baghli, H., Mattioli, E., Spangenberg, J. E., Bensalah, M., Arnaud-Godet, F., Pittet, B., and Suan, G.: Early Jurassic climatic  
643 trends in the south-Tethyan margin. Gondwana. Res., 77, 67-81, doi, 10.1016/j.gr.2019.06.016, 201920.

644 Bailey, T. R., Rosenthal, Y., McArthur, J. M., van de Schootbrugge, B., and Thirlwall, M. F.: Paleocyanographic changes of  
645 the Late Pliensbachian-Early Toarcian interval: a possible link to the genesis of an Oceanic Anoxic Event, *Earth Planet.*  
646 *Sci. Lett.*, 212, 307-320, 2003.

647 ~~Beerling, D. J. and Brentnall, S. J.: Numerical evaluation of mechanisms driving Early Jurassic changes in global carbon~~  
648 ~~cycling, *Geology*, 5, 247–250, 2007.~~

649 Beerling, D. J. and Royer, D. L.: Reading a CO<sub>2</sub> signal from fossil stomata, *The New Phytologist*, 153, 387-397, doi:0.  
650 1046/j.0028-646X.2001.00335.x, 2002.

651 Berner, R. A.: GEOCARBSULF: A combined model for Phanerozoic atmospheric O<sub>2</sub> and CO<sub>2</sub>, *Geochi. Cosmochi. Ac.*,  
652 70(23 Spec. Iss. ), 5653-5664, 2006.

653 Beše, J. and Courtillot, V.: Paleogeographic maps of the continents bordering the Indian Ocean since the Early Jurassic: *J.*  
654 *Geophys. Res.*, 93, 11791–808, 1988.

655 Blakey, R. C., Peterson, F., and Kocurek, G.: Synthesis of late Paleozoic and Mesozoic eolian deposits of the Western  
656 Interior of the United States, *Sediment. Geol.*, 56, 3-125, doi, [https://doi.org/10.1016/0037-0738\(88\)90050-4](https://doi.org/10.1016/0037-0738(88)90050-4), 1988.

657 Bodin, S., Krencker, F. N., Kothe, T., Hoffmann, R., Mattioli, E., Heimhofer, U., and Kabiri, L.: Perturbation of the carbon  
658 cycle during the late Pliensbachian – early Toarcian: New insight from high-resolution carbon isotope records in  
659 Morocco, *J Afri. Earth Sci.*, 116, 89–104, doi, 10.1016/j.jafrearsci.2015.12.018, 2016.

660 Boucot, A. J., Chen, X., Scotese, C. R., and Morley, R. J.: Phanerozoic Paleoclimate: An Atlas of Lithologic Indicators of  
661 *Climate, SEPM Concepts in Sedimentology and Paleontology 11. SEPM, Tulsa, 1-478, 2013.*

662 Bougeault, C., Pellenard, P., Deconninck, J. F., Hesselbo, S. P., Dommergues, J. L., Bruenau, L., Cocquerez, T., Laffont, R.,  
663 Huret, E., and Thibault, N.: Climatic and palaeocyanographic changes during the Pliensbachian (Early Jurassic) inferred  
664 from clay mineralogy and stable isotope (C-O) geochemistry (NW Europe), *Global Planet. Change*, 149, 139-152,  
665 2017.

666 Breecker, D. O. and Retallack, G. J.: Refining the pedogenic carbonate atmospheric CO<sub>2</sub> proxy and application to Miocene  
667 CO<sub>2</sub>, *Palaeogeogr. Palaeoclimatol. Palaeoecol.*, 406, 1-8, 2014.

668 Breecker, D. O., Sharp, Z. D., and McFadden, L. D.: Atmospheric CO<sub>2</sub> concentrations during ancient greenhouse climates  
669 were similar to those predicted for A. D. 2100, *PNAS*, 107, 2, 576-580, 2009.

670 Breecker, D. O., Sharp, Z. D., and McFadden, L. D.: Seasonal bias in the formation and stable isotope composition of  
671 pedogenic carbonate in modern soil from central New Mexico, USA, *Geol. Soc. Am. Bull.*, 12, 630-640, 2010.

672 Breecker, D. O.: Quantifying and understanding the uncertainty of atmospheric CO<sub>2</sub> concentrations determined from calcic  
673 paleosols. *Geochem. Geophys. Geosyst.*, 14, 3210–3220, 2013.

674 Bromley, M.: Topographic inversion of early interdune deposits, Navajo Sandstone (Lower Jurassic), Colorado Plateau,  
675 USA, *Sediment. Geol.*, 80, 1-25, 1992.

676 [Buchmann, N., Brooks, R. J., Flanagan, L. B., and Ehleringer, J. R.: Carbon isotope discrimination of terrestrial ecosystems.](#)  
677 [In Griffiths, H., ed. Stable Isotopes: Integration of Biological, Ecological and Geochemical Processes, BIOS Scientific](#)  
678 [Publications, Oxford, United Kingdom, 203–21, 1998.](#)

679 [Caruthers, A. H., Smith, P. L., Gröcke, D. R.: The Pliensbachian-Toarcian \(Early Jurassic\) extinction, a global multi-phased](#)  
680 [event, \*Palaeogeogr. Palaeoclimatol. Palaeoecol.\*, 386, 104-118, 2013.](#)

681 Cerling, T. E.: Carbon dioxide in the atmosphere: evidence from Cenozoic and Mesozoic paleosols: *Am. J. Sci.*, 291,  
682 377-400, 1991.

683 Cerling, T. E.: Stable carbon isotopes in palaeosol carbonates, in: *Palaeoweathering, palaeosurfaces and related continental*  
684 *deposits*, edited by: Thiry, M. and Simm-Coinçon, R., *Spec. P Intl. Asso. Sedi.*, 27, 43-60, 1999.

685 ~~[Chandler, M. A., Rind, D., and Ruedy, R.: Pangaeon climate during the Early Jurassic: GCM simulations and the](#)~~  
686 ~~[sedimentary record of paleoclimate, \*Geol. Soc. Am. Bull.\*, 104, 543–559, 1992.](#)~~

687 ~~[Cheng, L. X., Chen, H. D., and Guo, Y.: Fan delta sedimentary facies and reservoir characteristics of Lower Jurassic](#)~~  
688 ~~[Zhenzhuchong segment in Yuanba area, Northeast Sichuan, China, \*J Chengdu Uni. Technol. \(Sci. Technol. Ed\)\*, 41\(3\),](#)~~  
689 ~~[283-292, 2014 \(in Chinese with English abstract\).](#)~~

690 [Cleveland, D. M., Nordt, L. C., Dworkin, S. I., and Atchley, S. C.: Pedogenic carbonate isotopes as evidence for extreme](#)  
691 [climatic events preceding the Triassic-Jurassic boundary: implications for the biotic crisis? \*GSA Bull.\*, 120, 1408-1415,](#)  
692 [2008.](#)

693 [Cohen, K. M., Finney, S. C., Gibbard, P. L., and Fan, J. X. The ICS International Chronostratigraphic Chart \(2013 updated\).](#)  
694 [\*Episodes\*, 36, 199-204, 2013.](#)

695 Cohen, A. S., Coe, A. L., Harding, S. M., and Schwark, L.: Osmium isotope evidence for the regulation of atmospheric CO<sub>2</sub>  
696 by continental weathering, *Geology*, 32, 157–160, 2004.

697 Crowley, T. J. and Berner, R. A.: CO<sub>2</sub> and climate change, *Science*, 292, 870–872, 2001.

698 Deng, S. H., Zhao, Y., Lu, Y. Z., Shang, P., Fan, R., Li, X., Dong, S. X., and Liu, L.: Plant fossils from the Lower Jurassic  
699 coal-bearing formation of central InnerMongolia of China and their implications for palaeoclimate, *Palaeoworld*, 26:  
700 279-316, 2017.

701

702 Dera, G., Brigaud, B., Monna, F., Laffont, R., Pucéat, E., Deconinck, J. F., Pellenard P., Joachimski, M. M., and Durlet, C.:  
703 Climatic ups and downs in a disturbed Jurassic world, *Geology*, 39(3), 215-218, 2011.

704 [Dera, G., Pellenard, P., Neige, P., Deconinck, J. F., Pucéat, E., and Dommergues, J. L.: Distribution of clay minerals in Early](#)  
705 [Jurassic Peritethyan seas: Palaeoclimatic significance inferred from multiproxy comparisons, \*Palaeogeogr.\*](#)  
706 [\*Palaeoclimatol. Palaeoecol.\*, 271\(1-2\), 39–51, doi, 10.1016/j.palaeo.2008.09.010, 2009.](#)

707 Dong, Z. M.: A new prosauropod from Ziliujing Formation of Sichuan Basin, *Verte. Palasiatica*, 22(4), 310-313, 1984 (in

708 Chinese with English abstract).

709 Duan, S. Y. and Chen, Y.: Mesozoic fossil plants and coal formation of eastern Sichuan Basin, in: Continental Mesozoic  
710 Stratigraphy and Paleontology in Sichuan Basin of China: Part II, Paleontological Professional Papers, People's Publ.  
711 House Sichuan, Chengdu, 491-519, 1982 (in Chinese).

712 Ekart, D. D., Cerling, T. E., Montñez, I. P., and Tabor, N. J.: A 400 million year carbon isotope record of pedogenic  
713 carbonate: implications for paleoatmospheric carbon dioxide, *Am. J. Sci.*, 299, 805-827, 1999.

714 Flügel, E.: *Microfacies of Carbonate Rocks: Analysis, Interpretation and Application*, Springer-Verlag, Berlin, Heidelberg,  
715 New York, 976 pp. 2004.

716 [Friedli, H., Lotscher, H., Oeschger, H., Siegenthale, U., and Stauffer, B.: Ice core record of the  \$^{13}\text{C}/^{12}\text{C}\$  ratio of atmospheric](#)  
717  [\$\text{CO}\_2\$  in the past two centuries, \*Nature\*, 324, 237–238, 1986.](#)

718 Fu, X. G., Wang, J., Feng, X. L., Wang, D., Chen, W. B., Song, C. Y., and Zeng, S. Q.: Early Jurassic carbon-isotope  
719 excursion in the Qiangtang Basin (Tibet), the eastern Tethys: implications for the Toarcian Oceanic anoxic event, *Chem.*  
720 *Geol.*, 442, 67–72, 2016.

721 [Gómez, J. J., and Goy, A.: Warming-driven mass extinction in the Early Toarcian \(Early Jurassic\) of northern Spain.](#)  
722 [Correlation with other time-equivalent European sections. \*Palaeogeogr. Palaeoclimatol. Palaeoecol.\*, 306, 176-195,  
723 \[2011.\]\(#\)](#)

724 Gómez, J. J., Comas-Rengifo, M. J., and Goy, A.: Palaeoclimatic oscillations in the Pliensbachian (Early Jurassic) of the  
725 Asturian Basin (Northern Spain), *Clim. Past*, 12, 1199-1214, 2015.

726 Gómez, J. J., Goy, A., and Canales, M. L.: Seawater temperature and carbon isotope variations 15 in belemnites linked to  
727 mass extinction during the Toarcian (Early Jurassic) in Central and Northern Spain. Comparison with other European  
728 sections, *Palaeogeogr. Palaeoclimatol. Palaeoecol.*, 258, 28-58, 2008.

729 Guo, L. Y., Zhang, S. W., Xie, X. N., Li, Z. S., Huang, C. Y., and Chen, B. C.: Geochemical characteristics and organic  
730 matter enrichment of the Dongyuemiao Member mudstone of Lower Jurassic in the Western Hubei-Eastern Chongqing,  
731 *Ear. Sci.*, 42(7): 1235-1246, 2017 (in Chinese with English abstract).

732 ~~[Guo, X. S., Hu, D. F., Li, Y. P., Wei, X. F., Liu, R. B., Liu, Z. J., Yan, J. H., and Wan, Q. B.: Analyses and thoughts on](#)~~  
733 ~~[accumulation mechanisms of marine and lacustrine shale gas: A case study in shales of Longmaxi Formation and](#)~~  
734 ~~[Da'anzhai Section of Ziliujing Formation in Sichuan Basin, \*Ear. Sci. Front.\*, 23\(2\), 18-28, 2016, \(in Chinese with](#)~~  
735 ~~[English abstract\).](#)~~

736 Guo, Z. W., Deng, K. L., and Han, Y. H.: *Formation and Evolution of the Sichuan Basin*, Geo. Publ. House, Beijing, 200,  
737 1996.

738 [Hallam, A., and Wignall, P. B.: Mass extinctions and sea-level changes, \*Earth Sci. Rev.\*, 48, 217-250, 1999.](#)

739 ~~[Hallam, A.: Eustatic cycles in the Jurassic, \*Palaeogeogr. Palaeoclimatol. Palaeoecol.\*, 23, 1-32, 1978.](#)~~

- 740 He, T. H. and Liao, C. F.: Control of Upper Triassic division and correlation and Indosinian Movement on oil and gas  
741 accumulation in Sichuan Basin, *Acta Geol. Sichuan*, 00, 40–55, 1985 (in Chinese).
- 742 Hermoso, M., Le Callonnec, L., Minoletti, F., Renard, M., and Hesselbo, S. P.: Expression of the Early Toarcian negative  
743 carbon-isotope excursion in separated carbonate microfactions (Jurassic, Paris Basin), *Earth Planet. Sci. Lett.*, 277,  
744 194-203, 2009.
- 745 Hesselbo, S. P. and Jenkyns, H. C.: British Lower Jurassic sequence stratigraphy, in: *Mesozoic-Cenozoic Sequence*  
746 *Stratigraphy of European Basins*, edited by: de Graciansky, P. C., Hardenbol, J., Jacquin, Th., and Vail, P. R., SEPM  
747 Spec. Pap., 60, 562-581, 1998.
- 748 ~~Hesselbo, S. P., Bjerrum, C. J., Hinnov, L. A., MacNiocail, C., Miller, K. G., Riding, J. B., van de Schootbrugge, B., and the~~  
749 ~~Mochras Revisited Science Team: Mochras borehole revisited: a new global standard for Early Jurassic earth history,~~  
750 ~~*Sci. Dril.*, 16, 81–91. doi:10.5194/sd-16-81-2013, 2013.~~
- 751 Hesselbo, S. P., Gröcke, D. R., Jenkyns, H. C., Bjerrum, C. J., Farrimond, P., Morgans Bell, H. S., Green, O. R.: Massive  
752 dissociation of gas hydrate during a Jurassic oceanic anoxic event, *Nature*, 406, 392-395, doi:10. 1038/35019044.,  
753 2000.
- 754 Hesselbo, S. P., Jenkyns, H. C., Duarte, L. V., and Oliveira, L. C. V.: Carbon-isotope record of the Early Jurassic (Toarcian)  
755 Oceanic Anoxic Event from fossil wood and marine carbonate Lusitanian Basin, Portugal, *Earth Planet. Sci. Lett.*, 253,  
756 455-470, 2007.
- 757 Huang, P., Guan, Y. M., and Yang, X. Q.: Early Jurassic palynoflora from a drilling section of Jurong, Jiangsu, *Acta*  
758 *Micropalaeontol. Sin.*, 17(1), 85- 98, 2000.
- 759 ~~Huang, C. J., and Hesselbo, S. P.: Pacing of the Toarcian Oceanic Anoxic Event (Early Jurassic) from astronomical~~  
760 ~~correlation of marine sections. *Gondwana Res.*, 25, 1348-1356, doi. org/10.1016/j.gr.2013.06.023, 2014.~~
- 761 Huang, Q. S.: Paleoclimate and coal-forming characteristics of the Late Triassic Xujiahe stage in northern Sichuan, *Geol.*  
762 *Rev.*, 41(1): 92–99, 1995, (in Chinese with English abstract).
- 763 Huang, Q. S.: The flora and paleoenvironment of the Early Jurassic Zhenzhuchong Formation in Daxian-Kaixian region,  
764 northern margin of the Sichuan Basin, *Ear. Sci.*——— *J. China Uni. Geosci.*, 3, 221-229, 2001 (in Chinese with  
765 English abstract).
- 766 Imbellone, P. A.: Classification of Paleosols. São Paulo, UNESP, *Geociências*, 30(1), 5-13, 2011,
- 767 Izumi, K., Kemp, D., Itamiya, S., and Inui, M.: Sedimentary evidence for enhanced hydrological cycling in response to rapid  
768 carbon release during the early Toarcian oceanic anoxic event, *Earth Planet. Sci. Lett.*, 481, 162–170, 2018.
- 769 ~~Jahren, A. H., Arens, N. C., and Harbeson, S. A.: Prediction of atmospheric  $\delta^{13}\text{C}_{\text{CO}_2}$  using fossil plant tissues, *Rev. Geophy.*,~~  
770 ~~46, RG1002, doi: 10. 1029/2006RG000219, 2008.~~
- 771 ~~Jansson, I. M., McLoughlin, S., Vajda, V., and Pole, M.: An Early Jurassic flora from the Clarence Moreton Basin, Australia,~~

772 [Rev. Palaeobot. Palyno., 150, 5–21, http://dx.doi.org/10.1016/j.revpalbo.2008.01.002, 2008.](http://dx.doi.org/10.1016/j.revpalbo.2008.01.002)

773 Jenkyns, H. C. and Clayton, C. J.: Black shales and carbon isotopes in pelagic sediments from the Tethyan Lower Jurassic,  
774 *Sedimentology*, 33, 87-106, 1986.

775 Jenkyns, H. C., and Clayton, C. J., Lower Jurassic epicontinental carbonates and mudstones from England and Wales:  
776 chemostratigraphic signals and the early Toarcian anoxic event, *Sedimentology*, 44, 687-706, 1997.

777 Jenkyns, H. C., Jones, C. E., Gröcke, D. R., Hesselbo, S. P., and Parkinson, D. N.: Chemostratigraphy of the Jurassic System:  
778 Applications, limitations and implications for palaeoceanography, *J. Geol. Soc. London*, 159, 351-378, 2002.

779 Jenkyns, H. C.: Geochemistry of oceanic anoxic events, *Geochem. Geophys. Geosyst.*, 11, Q03004. doi:10.  
780 1029/2009GC002788, 2010.

781 [Jones, C. E., Jenkyns, H. C., and Hesselbo, S. P.: Strontium isotopes in Early Jurassic seawater: \*Geoch. Cosmoch. Acta\*, 58,](#)  
782 [1285–1301, 1994.](#)

783 [Kashiwagi, H.: Atmospheric carbon dioxide and climate change since the Late Jurassic \(150 Ma\) derived from a global](#)  
784 [carbon cycle model, \*Palaeogeogr. Palaeoclimatol. Palaeoecol.\*, 454, 82–90, 2016.](#)

785 Kemp, D. B., Coe, A. L., Cohen, A. S., and Schwark, L.: Astronomical pacing of methane release in the Early Jurassic  
786 period, *Nature*, 437, 396-399, doi, org/10. 1038/nature04037, 2005.

787 Kenny, R.: A cool time in the Early Jurassic: first continental palaeoclimate estimates from oxygen and hydrogen isotope  
788 ratios in chert from Navajo Sandstone carbonate lenses, Utah (USA), *Carbonate Evaporite*, doi,  
789 10.1007/s13146-015-0276-z, 2015.

790 Kent, D. V., Olsen, P. E., and Muttoni, G.: Astrochronostratigraphic polarity time scale (APTS) for the Late Triassic and  
791 Early Jurassic from continental sediments and correlation with standard marine stages, *Earth-Sci. Rev.*, 166, 153-180,  
792 2017.

793 Korte, C., and Hesselbo, S. P.: Shallow marine carbon and oxygen isotope and elemental records indicate  
794 icehouse-greenhouse cycles during the Early Jurassic, *Paleoceanography*, 26, 1–18, 2011.

795 Korte, C., Hesselbo, S. P., Jenkyns, H. C., Rickaby, R. E. M., and Spötl, C.: Palaeoenvironmental significance of carbon-  
796 and oxygen-isotope stratigraphy of marine Triassic-Jurassic boundary sections in SW Britain, *J. Geol. Soc. London*,  
797 166(3), 431-445, 2009.

798 [Korte, K., Hesselbo, S. P., Ullmann, C.V., Dietl, G., Ruhl, M., Schweigert, G., Thibault, N.: Jurassic climate mode governed](#)  
799 [by ocean gateway, \*Nat. Commun.\*, 6, 10015, doi, 10.1038/ncomms10015, 2015.](#)

800 Li, H. C. and Ku, T. L.:  $\delta^{13}\text{C}$ - $\delta^{18}\text{O}$  covariance as a paleohydrological indicator for closed basin lakes, *Palaeogeogr.*  
801 *Palaeoclimatol. Palaeoecol.*, 133, 69-80, 1997.

802 Li, L. Q., Wang, Y. D., Liu, Z. S., Zhou, N., and Wang, Y.: Late Triassic palaeoclimate and palaeoecosystem variations  
803 inferred by palynological record in the northeastern Sichuan Basin, China, *Paläontol. Zeits.*, 309-324, DOI 10.



- 1007/s12542-016-0309-5, 2016.
- Li, W. M. and Chen, J. S.: Discovery and significances of the Jurassic Ziliujing Formation in Tianzhu, Guizhou, China New Techn. Prod., 13, 134-135, 2010 (in Chinese).
- Li, X. B. and Meng, F. S.: Discovery of fossil plants from the Ziliujing Formation in Hechuan of Chongqing. Geol. Min. Resour. South China, 3: 60-65, 2003 (in Chinese with English abstract).
- ~~Li, X. H., Jenkyns, H. C., Zhang, C. K., Wang, Y., Liu, L., and Cao, K.: Carbon isotope signatures of pedogenic carbonates from SE China: Rapid atmospheric pCO<sub>2</sub> changes in the mid-late Early Cretaceous, Geol. Mag., 151 (5), 830-849, doi:10.1017/S0016756813000897, 2014.~~
- Li, Y. Q. and He, D. F.: Evolution of tectonic-depositional environment and prototype basins of the Early Jurassic in Sichuan Basin and adjacent areas, Acta Petrol. Sin., 35(2), 219-232, 2014 (in Chinese with English abstract).
- Li, Y., Allen, P. A., Densmore, A. L., and Xu, Q.: Evolution of the Longmen Shan Foreland Basin (Western Sichuan, China) during the Late Triassic Indosinian Orogeny. Basin Res., 15, 117-138, 2003.
- Liang, B., Wang, Q. W., and Kan, Z. Z.: Geochemistry of Early Jurassic mudrocks from Ziliujing Formation and implications for source-area and weathering in dinosaur fossils site in Gongxian, Sichuan province, J. Min. Petr., 26(3), 94-99, 2006 (in Chinese with English abstract).
- ~~Littler, K., Hesselbo, S. P., and Jenkyns, H. C.: A carbon-isotope perturbation at the Pliensbachian-Toarcian boundary: evidence from the Lias Group, NE England. Geol. Mag., 147, 181-192, 2010.~~
- ~~Liu, B. J. and Zeng, Y. F., eds.: Foundation and methodology of lithofacies and paleogeography, Geo. Publ. House, Beijing, 442, 1986 (in Chinese).~~
- Liu, J. L., Ji, Y. L., Zhang, K. Y., Li, L. D., Wang, T. Y., Yang, Y., and Zhang, J.: Jurassic sedimentary system transition and evolution model in western Sichuan Foreland Basin, Acta Petrol. Sin., 37(6), 743-756, 2016 (in Chinese with English abstract).
- Ma, Y. S., Chen, H. D., Wang, G. L., Guo, T. L., Tian, J. C., Liu, W. J., Xu, X. S., Zheng, R. C., Mou, C. L., and Hou, M. C.: Atlas of Lithofacies Paleogeography on the Sinian-Neogene Tectonic-Sequence in South China, Science Press, Beijing, 162-165, 2009 (in Chinese).
- Mack, G. H. and James, W. C.: Paleoclimate and the Global Distribution of Paleosols, J. Geol., 102, 360-366, 1994.
- Mack, G. H., James, W. C., and Monger, H. C.: 1 Classification of paleosols, Geol. Soc. Am. Bull., 105, 129-136, 1993.
- ~~McArthur, J. M., Donovan, D. T., Thirlwall, M. F., Fouke, B. W., and Matthey, D.: Strontium isotope profile of the early Toarcian (Jurassic) oceanic anoxic event, the duration of ammonite biozones, and belemnite palaeotemperatures, Earth Planet. Sci. Lett., 179, 269-285, 2000.~~
- McElwain, J. C., Wade-Murphy, J., and Hesselbo, S. P.: Changes in carbon dioxide during an oceanic anoxic event linked to intrusion into Gondwana coals, Nature, 435, 479-482, doi:org/10.1038/nature03618, 2005.

836 [Mckenzie, J. A., and Vasconcelos C.: Dolomite Mountains and the origin of the dolomite rock of which they mainly consist:](#)  
837 [historical developments and new perspectives, \*Sedimentology\*, 56, 205 – 219, doi, 10.1111/j.1365-3091.2008.01027.x,](#)  
838 [2009.](#)

839 ~~[Meng, F. S. and Chen, D. Y.: Fossil plants and palaeoclimatic environment from the Ziliujing Formation in the western](#)  
840 [Yangtze Gorges area, China, \*Geol. Min. Resour. S. China\*, 1, 51–59, 1997 \(in Chinese with English abstract\).](#)~~

841 Meng, F. S., Chen, H. M., and Li, X. B.: Study on Lower Middle Jurassic boundary in Chongqing region, *Geol. Min. Resour.*  
842 *S China*, 3, 64-71, 2005 (in Chinese with English abstract).

843 Meng, F. S., Li, X. B., and Chen, H. M.: Fossil plants from Dongyuemiao Member of the Ziliujing Formation and  
844 Lower-Middle Jurassic boundary in Sichuan basin, China, *Acta Palaeontol. Sin.*, 42(4), 525-536, 2003. (in Chinese with  
845 English abstract).

846 Metodiev, L. and Koleva-Rekalova, E.: Stable isotope records ( $\delta^{18}\text{O}$  and  $\delta^{13}\text{C}$ ) of Lower - Middle Jurassic belemnites from  
847 the Western Balkan mountains (Bulgaria), *Palaeoenvironmental application, Appl. Geochem.*, 23, 2845–2856, 2008.

848 [Mintz, J. S., Driese, S. G., Breecker, D. O., and Ludvigson, G. A.: Influence of changing hydrology on pedogenic calcite](#)  
849 [precipitation in Vertisols, Dance Bayou, Brazoria County, Texas, USA: implications for estimating paleoatmospheric](#)  
850 [pCO<sub>2</sub>, \*J. Sedi. Res.\*, 81\(6\), 394-400, 2011.](#)

851 ~~[Mills B. J. W., Krause A. J., Scotese C. R., Hill D. J., Shields G. A., and Lenton T. M.: Modelling the long-term carbon cycle,](#)  
852 [atmospheric CO<sub>2</sub>, and Earth surface temperature from late Neoproterozoic to present-day, \*Gondwana Res.\*, 67, 172–186,](#)  
853 [2019.](#)~~

854 Mo, Y. Z. and Yu, H. Y.: The discovery and its geological significance of dolomite in Ziliujing Groups of Middle and Lower  
855 Jurassic Series in Ma'anshan Member, *Geol Guizhou*, 10(1), 110-113, 1987 (in Chinese with English abstract).

856 [Montañez, I. P.: Modern soil system constraints on reconstructing deep-timeatmospheric CO<sub>2</sub>, \*Geochim. Cosmochim. Acta\*,](#)  
857 [101, 57–75, 2013.](#)

858 ~~[Myers, T. S., Tabor, N. J., Jacobs, L. L., and Mateus, O.: Estimating soil pCO<sub>2</sub> using paleosol carbonates: implications for](#)  
859 [the relationship between primary productivity and faunal richness in ancient terrestrial ecosystems, \*Paleobiology\*, 38\(4\),](#)  
860 [585–604, 2012.](#)~~

861 [Nadelhofer K. J., and Fry B.: Controls on natural nitrogen-15 and carbon-13 abundances in forest soil organic matter, \*Soil\*](#)  
862 [Sci. Soc. Am. J.](#), 52, 1633-1640, 1988.

863 Newport, R., Hollis, C., Bodin, S., and Redfern, J.: Examining the interplay of climate and low amplitude sea-level change  
864 on the distribution and volume of massive dolomitization: Zebbag Formation, Cretaceous, Southern Tunisia, *Deposit.*  
865 *Rec.*, 3(1), 38–59, doi,10.1002/dep2.25, 2017.

866 ~~[Nordt, L., Atehley, S., and Dworkin, S.: Terrestrial evidence for two greenhouse events in the latest Cretaceous, \*Geol. Soc.\*](#)  
867 [Am. Today](#), 13, 12, 4–9, doi, 10.1130/1052-5173(2003)013<4>, 2003.~~

- 868 Parrish, J. T., Hasiotis, S. T., and Chan, M. A.: Carbonate deposits in the Lower Jurassic Navajo Sandstone, southern Utah  
869 and northern Arizona, *J. Sedi. Res.*, 87, 740-762, doi, <https://doi.org/10.2110/jsr.2017.42>, 2017.
- 870 Parrish, J. T., Rasbury, E. T., Chan, M. A., and Hasiotis, S. T.: Earliest Jurassic U-Pb ages from carbonate deposits in the  
871 Navajo Sandstone, southeastern Utah, USA, *Geology*, 47(11), 1015–1019, doi, 10.1130/g46338.1, 2019.
- 872 Peng, G. Z.: Assemblage characters of Jurassic dinosaurian fauna in Zigong of Sichuan, *J. Geosci.*, 33(2), 113-123, 2009 (in  
873 Chinese with English abstract).
- 874 Peti, L., Thibault, N., Clémence, M. E., Korte, C., Dommergues, J. L., Bougeault, C., Pellenard, P., Jelby, M. E., and  
875 Ullmann, C. V.: Sinemurian-Pliensbachian Calcareous Nannofossil Biostratigraphy and Organic Carbon Isotope  
876 Stratigraphy in the Paris Basin: Calibration to the Ammonite Biozonation of NW Europe, *Palaeogeogr. Palaeoclimatol.*  
877 *Palaeoecol.*, 468, 142–161, 2017.
- 878 [Petrash, D. A., Bialik, O. M., Bontognali, T. R. R., Vasconcelos, C., Roberts, J. A., McKenzie, J. A., and Konhauser, K. O.:](#)  
879 [Microbially catalyzed dolomite formation: From near-surface to burial, \*Earth Sci. Rev.\*, 171, 558–582, doi,](#)  
880 [10.1016/j.earscirev.2017.06.015, 2017.](#)
- 881 Philippe M., Puijalon S., Suan G., Mousset S., Thévenard F., and Mattioli E.: The palaeolatitudinal distribution of fossil  
882 wood genera as a proxy for European Jurassic terrestrial climate, *Palaeogeogr. Palaeoclimatol. Palaeoecol.*, 466, 373–  
883 381, 2017.
- 884 Pole, M.: Vegetation and climate of the New Zealand Jurassic, *GFF*, 131:1-2, 105-111, DOI: 10. 1080/11035890902808948,  
885 2009.
- 886 Price, G. D., Twitchett, R. J., Wheeley, J. R., and Buono, G.: Isotopic evidence for long term warmth in the Mesozoic, *Sci.*  
887 *Rep.*, 3, 1438, doi, 10.1038/srep01438, 2013.
- 888 [Price, G. D.: The evidence and implications of polar ice during the Mesozoic, \*Earth Sci. Rev.\*, 48, 183–210, 1999.](#)
- 889 Qian, T., Liu, S. F., Wang, Z. X., Li, W. P., and Chen, X. L.: Characteristics of the Baitianba Formation conglomerate of  
890 Lower Jurassic in the northern Sichuan basin and its constraint to the uplift of the south Dabashan, *China Sci. Paper*,  
891 11(21), 2402-2408, 2016 (in Chinese with English abstract).
- 892 Rees, P. A., Zeigler, A. M., and Valdes, P. J.: Jurassic phytogeography and climates: new data and model comparisons, in:  
893 *Warm Climates in Earth History*, edited by: Huber, B., MacLeod, K., and Wing, S., Cambridge University Press, 297–  
894 318, 1999.
- 895 Retallack, G. J.: A 300-million-year record of atmospheric carbon dioxide from fossil plant cuticles, *Nature*, 411, 287-290,  
896 2001a.
- 897 Retallack, G. J.: Adapting soil taxonomy for use with paleosols. *Quatern. Int.*, 51/52: 55-57, doi,  
898 10.1016/S1040-6182(98)00039-1, 1998.
- 899 Retallack, G. J.: *Soils of the Past--An Introduction to Paleopedology*, Blackwell Science Ltd, Oxford, 333, 2001b.

- 900 Riding, J. B., Leng, M. J., Kender, S., Hesselbo, S. P., and Feist-Burkhardt, S.: Isotopic and palynological evidence for a new  
901 Early Jurassic environmental perturbation, *Palaeogeogr. Palaeoclimatol. Palaeoecol.*, 374;: 16–27, 2013.
- 902
- 903 [Robinson, S. A., Andrews, J. E., Hesselbo, S. P., Radley, J. D., Dennis, P. F., Harding, I. C., and Allen, P.: Atmospheric](#)  
904 [pCO<sub>2</sub> and depositional environment from stable-isotope geochemistry of calcrete nodules \(Barremian, Lower](#)  
905 [Cretaceous, Wealden Beds, England\), \*J. Geol. Soc., London\*, 159, 215–24, 2002.](#)
- 906 [Robinson, S. A., Ruhl, M., Astley, D. L., Naafs, B. D. A., Farnsworth, A. J., Bown, P. R., Jenkyns, H. C., Lunt D. J.,](#)  
907 [O'Brien, C., Pancost, R. D., and Markwick, P. J.: Early Jurassic North Atlantic sea-surface temperatures from TEX86](#)  
908 [palaeothermometry. \*Sedimentology\*, 64\(1\), 215–230, doi, 10.1111/sed.12321, 2017.](#)
- 909 [Romanek, C., Grossman, E. and Morse, J.: Carbon isotopic fractionation in synthetic aragonite and calcite: effects of](#)  
910 [temperature and precipitation rate, \*Geochim. Cosmochim. Ac.\*, 56, 419-430, 1992.](#)
- 911 Rosales, I., Quesada, S., and Robles, S.: Primary and diagenetic isotopic signals in fossils and hemipelagic carbonates: the  
912 Lower Jurassic of northern Spain, *Sedimentology*, 48, 1149–1169, 2001.
- 913 ~~[Ros Franch, S., Echevarría, J., Damborenea, S. E., Manceñido, M. O., Jenkyns, H. C., Al-Suwaidi, A., Hesselbo, S. P., and](#)~~  
914 ~~[Riccardi A. C.: Population response during an Oceanic Anoxic Event: The case of Posidonotis \(Bivalvia\) from the](#)~~  
915 ~~[Lower Jurassic of the Neuquén Basin, Argentina, \*Palaeogeogr. Palaeoclimatol. Palaeoecol.\*, 525, 57–67, 2019.](#)~~
- 916 Royer, D. L.: CO<sub>2</sub>-forced climate thresholds during the Phanerozoic: *Geochim. Cosmochim. Ac.*, 70, 56, 65–75, doi: 10.  
917 1016/j.gca.2005.11.031, 2006.
- 918 Sabatino, N., Neri, R., Bellanca, A., Jenkyns, H., Baudin, F., Parisi, G., and Maseti, D.: Carbon isotope records of the Early  
919 Jurassic (Toarcian) oceanic anoxic event from the Valdorbia (Umbria-Marche Apennines) and Monte Mangart (Julian  
920 Alps) sections: palaeogeographic and stratigraphic implications, *Sedimentology*, 56, 1307-1328, 2009.
- 921 SBG (Sichuan Bureau of Geology): Reports of 1:200,000 Regional Geology Investigations (Profile Qianjiang), 48, 1975 (in  
922 Chinese).
- 923 SBG (Sichuan Bureau of Geology): Reports of 1:200,000 Regional Geology Investigations (Profile Xuyong), 55, 1976 (in  
924 Chinese).
- 925 SBG (Sichuan Bureau of Geology): Reports of 1:200,000 Regional Geology Investigations (Profiles Suining, Zigong,  
926 Neijiang, Yibin, and Luzhou), 43-50, 1980a (in Chinese).
- 927 SBG (Sichuan Bureau of Geology): Reports of 1:200,000 Regional Geology Investigations (Profiles Yilong, Tongjiang,  
928 Nanchong, Guang'an, and Chongqing), 100-101, 1980b (in Chinese).
- 929 SBGM (Sichuan Bureau of Geology and Mineral Resources): Geology of Sichuan Province, Geol. Publ. House, Beijing, 730,  
930 1991 (in Chinese with English summary).
- 931 SBGM: Lithostratigraphy of Sichuan Province, China Uni. Geosci. Press, Wuhan, 388, 1997 (in Chinese).

932 Schaller, M. F., Wright, J. D., and Kent, D. V.: Atmospheric  $p\text{CO}_2$  perturbations associated with the Central Atlantic  
933 Magmatic Province, *Science*, 331, 1404-1409, doi, 10.1126/science.1199011, 2011.

934 ~~Selley, R. C.: *Ancient Sedimentary Environments and their sub-surface diagnosis* (fourth edition), Chapman & Hall, London,  
935 296, 1996.~~

936 Sellwood, B. W., and Valdes, P. J.: Jurassic climates, *P. Geologist Assoc.*, 119, 5-17, 2008.

937 ~~Scotese, C. R.: *Atlas of Jurassic Paleogeographic Maps, PALEOMAP Atlas for ArcGIS, volume 4, The Jurassic and Triassic,*  
938 Maps 32-42, Mollweide Projection, PALEOMAP Project, Evanston, IL, 2014.~~

939 ~~Slater, S. M., Twitchett, R. J., Danise, S., and Vajda, V.: *Substantial vegetation response to Early Jurassic global warming*  
940 with impacts on oceanic anoxia, *Nature Geo.*, doi, 10.1038/s41561-019-0349-z, 2019.~~

941 ~~Smoot, J. P. and Olsen, P. E.: *Climatic cycles as sedimentary controls of rift basin lacustrine deposits in the early Mesozoic*  
942 Newark basin based on continuous core, edited by Lomando, A. J. and Harris, M., *Lacustrine Depositional Systems,*  
943 SEPM Core Workshop Notes, 19, 201-237, 1994.~~

944 Soil survey Staff: *Keys to Soil Taxonomy*, Pocahontas Press, Blacksburg, VA, 1998.

945 Steinhorsdottir, M. and Vajda, V.: Early Jurassic (late Pliensbachian)  $\text{CO}_2$  concentrations based 5 on stomatal analysis of  
946 fossil conifer leaves from eastern Australia, *Gondwana Res.* 27, 829-897, 2015.

947 ~~Storm, M. S., Hesselbo, S. P., Jenkyns, H. C., Ruhl, M., Ullmann, C. V., Xu, W., Leng, M. J., Riding, J. B., Gorbanenko, O.:  
948 Orbital pacing and secular evolution of the Early Jurassic carbon cycle. *PNAS*, 117(8), 3974-3982, doi,  
949 10.1073/pnas.1912094117, 2020.~~

950 Suan, G., Mattioli, E., Pittet, B., Lécuyer, C., Suchéras-Marx, B., Duarte, L. V., Philippe, M., Reggiani, L., and Martineau, F.:  
951 Secular environmental precursors to Early Toarcian (Jurassic) extreme climate changes, *Earth Planet. Sci. Letts.*, 290,  
952 448-458, doi, org/10. 016/j.epsl.2009.12.047, 2010.

953 Suan, G., Mattioli, E., Pittet, B., Mailliot, S., and Lécuyer, C.: Evidence for major environmental perturbation prior to and  
954 during the Toarcian (Early Jurassic) oceanic anoxic event from the Lusitanian Basin, Portugal, *Paleoceanography*, 23,  
955 PA1202, doi, org/10. 1029/2007PA001459, 2008.

956 ~~Succechi, R. K., Hubert, F. F., and Birney de Wet, C. C.: *Isotopic imprint of climate and hydrogeochemistry on terrestrial*  
957 strata of the Triassic-Jurassic Hartford and Fundy rift basins, *J. Sediment. Petr.*, 58, 801-811, 1988.~~

958 Talbot, M. R.: A review of the palaeohydrological interpretation of carbon and oxygen isotopic ratios in primary lacustrine  
959 carbonates. *Chem. Geol. (Isotope Geoscience Section)*, 80, 261-2791, 1990.

960 Tanner, L. H., and Lucas, S. The Whitmore Point Member of the Moenave Formation: Early Jurassic Dryland Lakes on the  
961 Colorado Plateau, Southwestern USA, *Volum. Jur.*, 6(6), 11-21, 2008.

962 Tanner, L. H., Hubert, J. F., Coffey, B. P., and McInerney, D. P.: Stability of atmospheric  $\text{CO}_2$  levels across the  
963 Triassic/Jurassic boundary, *Nature*, 411, 675-677, 2001.

- 964 Them, TR, II, Gill, B. C., Caruthers, A. H., Gröcke, D. R., Tulskey, E. T., Martindale, R. C., Poulton, T. P., and Smit, P. L.:  
965 High-resolution carbon isotope records of the Toarcian oceanic anoxic event (Early Jurassic) from North America and  
966 implications for the global drivers of the Toarcian carbon cycle, *Earth Planet. Sci. Lett.*, 459, 118–126, 2017.
- 967 Tramoy, R., Schnyder, J., Nguyen, Tu T. T., Yans, J., Jacob, J., Sebilho, M., Derenne, S., Philippe, M., Huguet, A., Pons, D.,  
968 and Baudin, F.: The Pliensbachian-Toarcian paleoclimate transition: New insights from organic geochemistry and C, H,  
969 N isotopes in a continental section from Central Asia, *Palaeogeogr. Palaeoclimatol. Palaeoecol.*, 461, 310–327, 2016.
- 970 Tucker, M. E.: *Sedimentary rocks in the field - a practical guide* (4th ed.), Wiley-Blackwell, Chichester, England, 276 pp,  
971 2011.
- 972 Vandeginste, V., and John, C. M.: Influence of climate and dolomite composition on dedolomitization: insights from a  
973 multi-proxy study in the central Oman Mountains, *J. Sediment. Res.*, 82(3), 177-195, doi, 10.2110/jsr.2012.19, 2012.
- 974 [van de Schootbrugge, B., Bachan, A., Suan, G., Richez, S., Payne, J. L.: Microbes, mud, and methane: Cause and  
975 consequence of recurrent Early Jurassic anoxia following the end-Triassic mass-extinction, \*Palaeont.\*, 56, 685-709,  
976 2013.](#)
- 977 van de Schootbrugge, B., Bailey, T. R., Katz, M. E., Wright, J. D., Rosenthal, Y., Feist-Burkhardt, S., and Falkowski, P. G.:  
978 Early Jurassic climate change and the radiation of organic walled phytoplankton in the Tethys Sea, *Paleobiology*, 31,  
979 73–97, 2005.
- 980 [Vasconcelos, C., McKenzie, J. A., Bernasconi, S., Grujic, D., and Tien, A. J.: Microbial mediation as a possible mechanism  
981 for natural dolomite formation at low temperatures, \*Nature\*, 377, 220–222, 1995.](#)
- 982 Veizer, J., Godderis, Y., and François, L. M.: Evidence for decoupling of atmospheric CO<sub>2</sub> and global climate during the  
983 Phanerozoic eon, *Nature*, 408, 698-701, 2000.
- 984 Wang, Q. W., Liang, B., Kan, Z. Z.: Carbon and oxygen isotopic compositions of lacustrine carbonates of the Early Jurassic  
985 Ziliujing Formation in the Sichuan Basin and their paleolimnological significance, *J. Min. Petr.*, 26(2), 87-91, 2006 (in  
986 Chinese with English abstract).
- 987 Wang, Y. D., Fu, B. H., Xie, X. P., Huang, Q. S., Li, K., Liu, Z. S., Yu, J. X., Pan, Y. H., Tian, N., and Jiang, Z. K.: The  
988 Terrestrial Triassic and Jurassic Systems in the Sichuan Basin, China, in: *Contributions to the 8<sup>th</sup> International Congress  
989 odd the Jurassic System*, edited by: Sha, J. G., Shi, X. Y., Zhou, Z. H., Wang, Y. D., Uni. Sci. Techn., China Press,  
990 Hefei, Anhui, 1-136, 2010 (in Chinese).
- 991 Wang, Y. D., Mosbrugger, V., and Zhang, H.: Early to Middle Jurassic vegetation and climatic events in the Qaidam Basin,  
992 Northwest China, *Palaeogeogr. Palaeoclimatol. Palaeoecol.*, 224, 200–216,  
993 <http://dx.doi.org/10.1016/j.palaeo.2005.03.035>, 2005.
- 994 Warren, J.: Dolomite: occurrence, evolution and economically important associations, *Earth Sci. Rev.*, 52, 1–81, 2000.
- 995 Wei, M.: *Continental Mesozoic Stratigraphy and Paleontology in the Sichuan Basin*, People's Publ. House of Sichuan,

996 Chengdu, 346-363, 1982 (in Chinese with English summary).

997 Wen, W. and Zhao, B.: Stratigraphic character and sedimentary facies of the Ziliujing Formation in the Pujiang-Ya'An area,  
998 Sichuan province, *J. Stratigr.*, 34(2), 219-224, 2010 (in Chinese with English abstract).

999 Wright, V. P.: Paleosol Recognition: A guide to early diagenesis in terrestrial settings (Chapter 12), in: *Developments in*  
1000 *Sedimentology*, edited by: Wolf K, H. and Chilingarian, G. V., 47, 591-619, 1992.

1001 ~~Xu, C. M., Gehenn, J. M., Zhao, D. H., Xie, G. Y., and Teng, M. K.: The fluvial and lacustrine sedimentary systems and~~  
1002 ~~stratigraphic correlation in the Upper Triassic Xujiahe Formation in Sichuan Basin, China, *AAPG Bull.*, 99(11),~~  
1003 ~~2023-2041, doi, 10.1306/07061514236, 2015.~~

1004 Xu, W. M., Ruhl, M., Jenkyns, H. C., Leng, M. J., Huggett, J. M., Minisini, D., Ullmann, C. V., Riding, J. B., Weijers, J. W.  
1005 H., Storm, M. S., Percival, L. M. E., Tosca, N. J., Idiz, E. F., Tegelaar, E. W., Hesselbo, S. P.: Evolution of the Toarcian  
1006 (Early Jurassic) carbon-cycle and global climatic controls on local sedimentary processes (Cardigan Bay Basin, UK),  
1007 *Earth Planet. Sci. Lett.*, 484, 396-411, 2018.

1008 Xu, W. M., Ruhl, M., Jenkyns, H. C., Hesselbo, S. P., Riding, J. B., Selby, D., Naafs, B. D. A., Weijers, J. W. H., Pancost, R.  
1009 D., Tegelaar, E. W., and Idiz, E. F.: Carbon sequestration in an expanded lake system during the Toarcian oceanic  
1010 anoxic event, *Nat. Geosci.*, 129-135, doi, 10.1038/NGEO2871, 2017.

1011 Yang, G. L.: Heavy mineral stratigraphy of Mesozoic continental clastic facies in Yaxi area, northern Guizhou, *J. Stratigr.*,  
1012 39(1), 89-96, 2015 (in Chinese with English abstract).

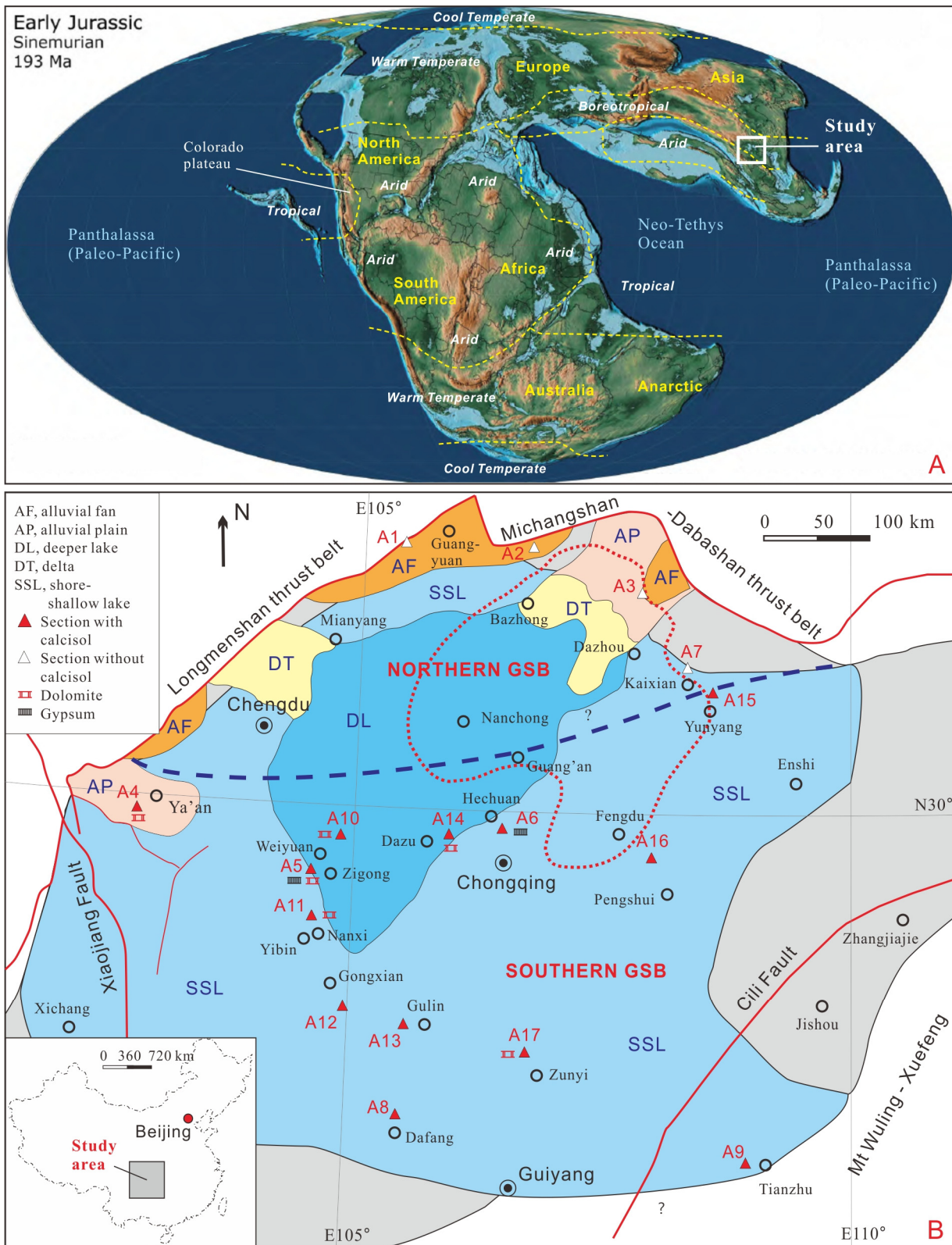
1013 ~~Yang, W., Zuo, R. S., Chen, D. X., Jiang, Z. X., Guo, L. S., Liu, Z. Y., Chen, R., Zhang, Y. P., Zhang, Z. Y., Song, Y., Luo,~~  
1014 ~~Q., Wang, Q. Y., Wang, J. B., Chen, L., Li, Y. H., Zhang, C.: Climate and tectonic driven deposition of sandwiched~~  
1015 ~~continental shale units: New insights from petrology, geochemistry, and integrated provenance analyses (the western~~  
1016 ~~Sichuan subsiding Basin, Southwest China), *Int. J. Coal Geol.*, 211, 103-227, 2019.~~

1017 Ye, M. N., Liu, X. Y., and Huang, G. Q.: Late Triassic and Early-Middle Jurassic fossil plants from northeastern Sichuan,  
1018 *Sci. Techn. Press. Hefei, Anhui*, 1986 (in Chinese with English summary).

1019 ~~Zhang, L. M., Wang, C. S., Wignall, P. B., Kluge, T., Wan, X. Q., Wang, Q., and Gao, Y.: Deccan volcanism caused~~  
1020 ~~coupled  $p\text{CO}_2$  and terrestrial temperature rises, and pre-impact extinctions in northern China, *Geology*, 46(3), 271-274,~~  
1021 ~~2018.~~

1022 Zhang, X. S., Zhao, B., Tan, M., Zhou, B. Y., Sun, J.: Stratigraphic Characteristics of Ziliujing Formation, Jurassic Series  
1023 and Discovery of Dinosaur Footprints in Dafang, Guizhou, *Geol. Guizhou*, 33(1), 50-70, 2016 (in Chinese with English  
1024 abstract).

1025 Zhang, Z. L. and Meng, F. S.: Chapter 2, the Jurassic. In Zhang Zhenlai and Meng Fansong eds. *The Triassic-Jurassic*  
1026 *Biostratigraphy in Yangtze Gorges* (4), Geol. Publ. House, Beijing, 408, 1987 (in Chinese with English summary).



1029

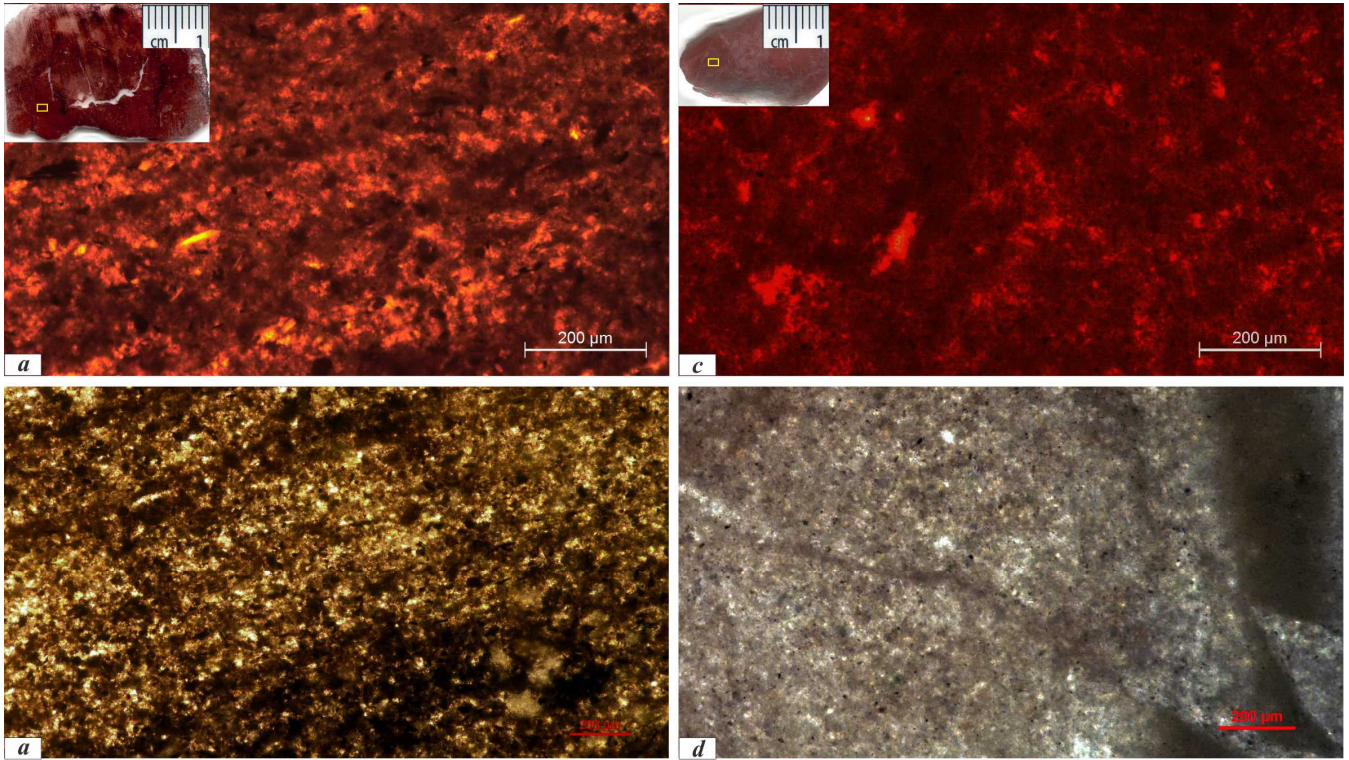
1030 **Figure 1** [A. Global Early-Middle Jurassic climate zones \(Boucot et al., 2013\) laid on the Early Jurassic \(~193 Ma, Sinemurian\)](#)  
 1031 [paleogeographic map \(Scotese, 2014\).](#) **B. Lithofacies paleogeographic sketch of the grand Sichuan paleobasin (GSB) in the early**  
 1032 **Early Jurassic (Zhenzhuchong and Dongyuemiao members) showing locations of the observed and analysed sections and**  
 1033 **climate-sensitive sediments. Lithofacies paleogeographic map was composed and modified from Ma et al. (2009) and Li and He**  
 1034 **(2014). Blue area is the extent of paleolake, estimated as ~380,000 km<sup>2</sup>; blue + gray region is the basin shape, estimated ~480,000**  
 1035 **km<sup>2</sup>. Dot red line confines the deeper lake area in the late Early Jurassic (Ma'anshan and Da'anzhai members). Bold dashed line is**



1036 the northern edge of calcisol occurrence, which may separate the climate of the GSB as the northern and southern types. Triangles  
 1037 with numbers are locations of observed and analysed sections: A1, Xiasi section, Jian'ge; A2, Puji section, Wangcang; A3,  
 1038 Shiguansi section, Wanyuan; A4, Shaping section, Ya'an (bed and thickness from Wen and Zhao, 2010); A6, Tanba and Maliping  
 1039 section, Hechuan (bed and thickness from Wang et al., 2010); A7, Wenquan section, Kaixian (thickness from Wang et al., 2010).  
 1040 Location and source data of sections A5 and A8-A17 (climate-sensitive sediments) refer to supplementary data Table S2S1.

1041

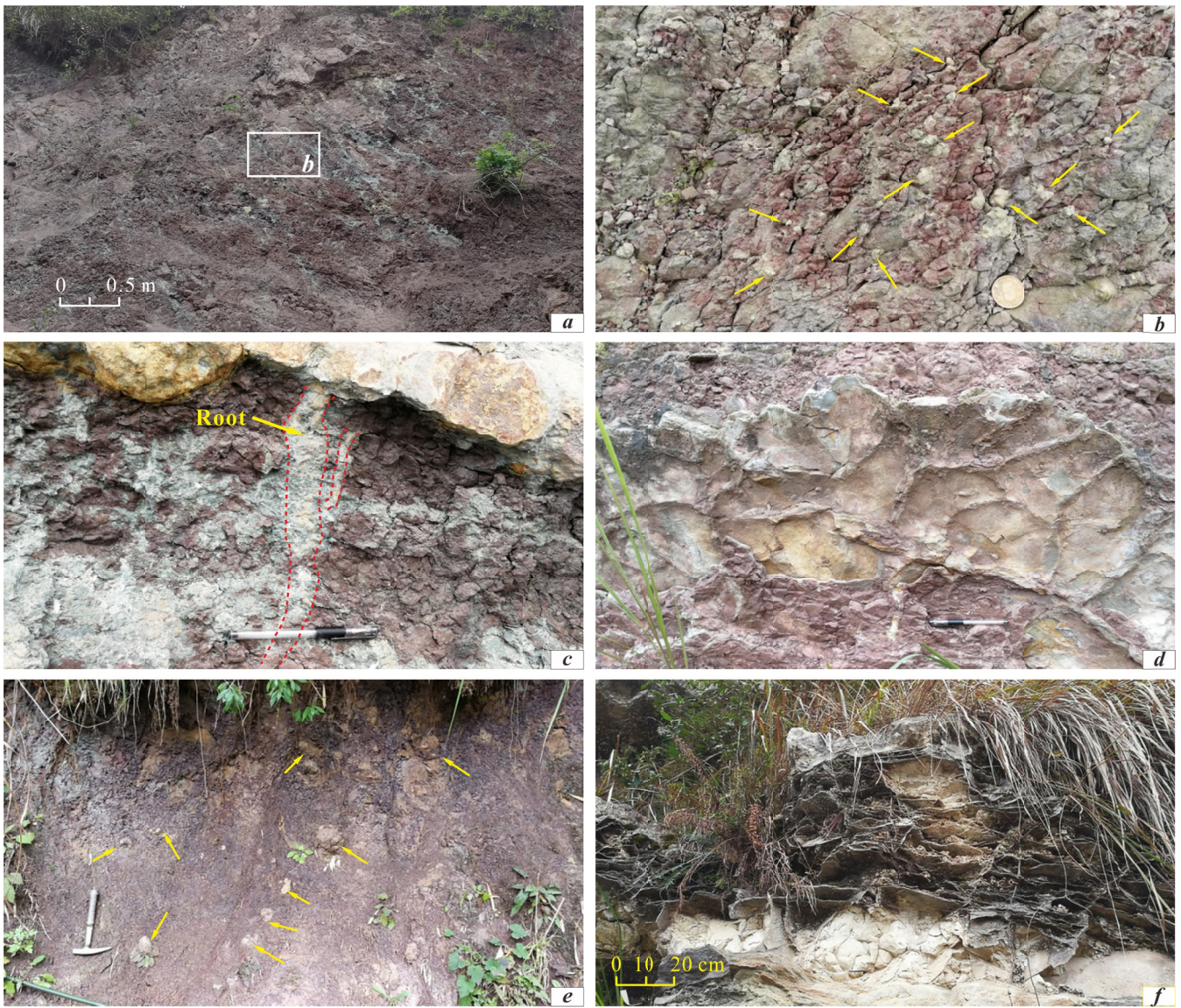
1042



1043

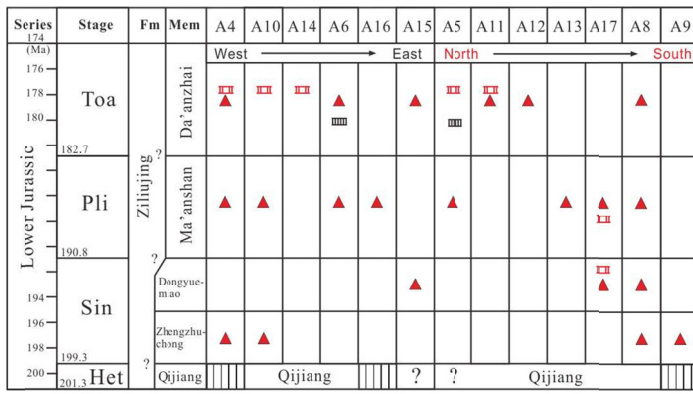
1044 Figure 2 Microscopic cathodoluminescence photos of representative calcrete samples from the Ziliujing Fm at the Shaping  
 1045 section, Ya'an. *a*, Sample J<sub>1z</sub>-12-01, Bed B12, Ma'anshan Member; *b*, Sample J<sub>1z</sub>-22-01, Bed B22, Da'anzhai Member. Pedogenic  
 1046 calcites are mainly null light orange and muds are not to non-luminescent, minor are orange/red luminescence. Pedogenic calcites  
 1047 of both samples are evenly luminescent light orange. Inserts are the scanned photos of thin-section, and rectangles are the area  
 1048 under cathodoluminescence and drilling.

1049



1050 **Figure 3** Field photographs of climate-sensitive sediments from the Lower Jurassic Ziliujing Fm in **the** GSB. *a*, Reddish purple  
 1051 calcisol with strong leaching structure. Lower Bed H8 of the upper Ma'anshan Member at Tanba-village, Hechuan. *b*, Reddish  
 1052 purple calcisol showing the density and size of calcretes. The horizon and location same as *a*. Arrows point to calcretes. Coin 2.0  
 1053 cm in diameter. *c*, Reddish purple calcisol with strong leaching structure and rhizoliths. Bed H13 of the top Ma'anshan Member at  
 1054 Maliuping, Hechuan. Pen 15 cm long. *d*, Mudcracks. Lower Bed H8 of the upper Ma'anshan Member at Maliuping, Hechuan. Pen  
 1055 15 cm long. *e*, Brownish red calcisol with big calcretes (calcareous concretions). Arrows point to big calcretes. Calcisol horizon  
 1056 J<sub>1z</sub>-10-01, Bed B10 of Ma'anshan Member at Shaping-village, Ya'an. Hammer 34 cm long. *f*, Chicken-wire structure. Bed H12 of  
 1057 the Da'anzhai Member at Maliuping-village, Hechuan.

1058  
 1059

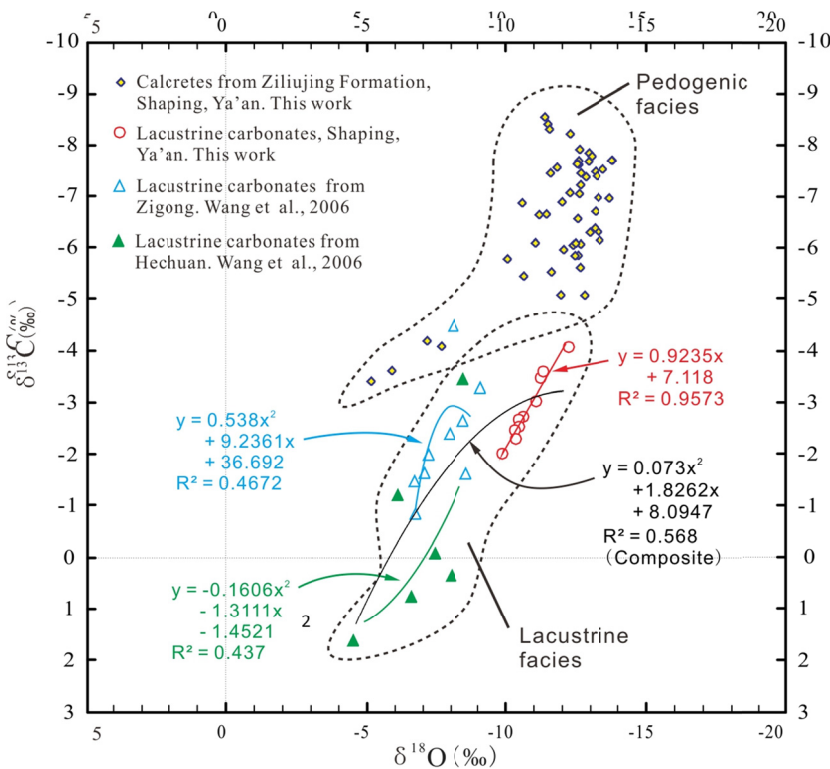


||||| Hiatus ▲ Calcisol ■ Dolomitic sediment ■ Gypsum?

1060 **Figure 4** Diagram showing the temporal and spatial variation of climate-sensitive sediments in GSB. Section loactions and data  
 1061 sources refer to Table [S2S1](#).

1062

1063

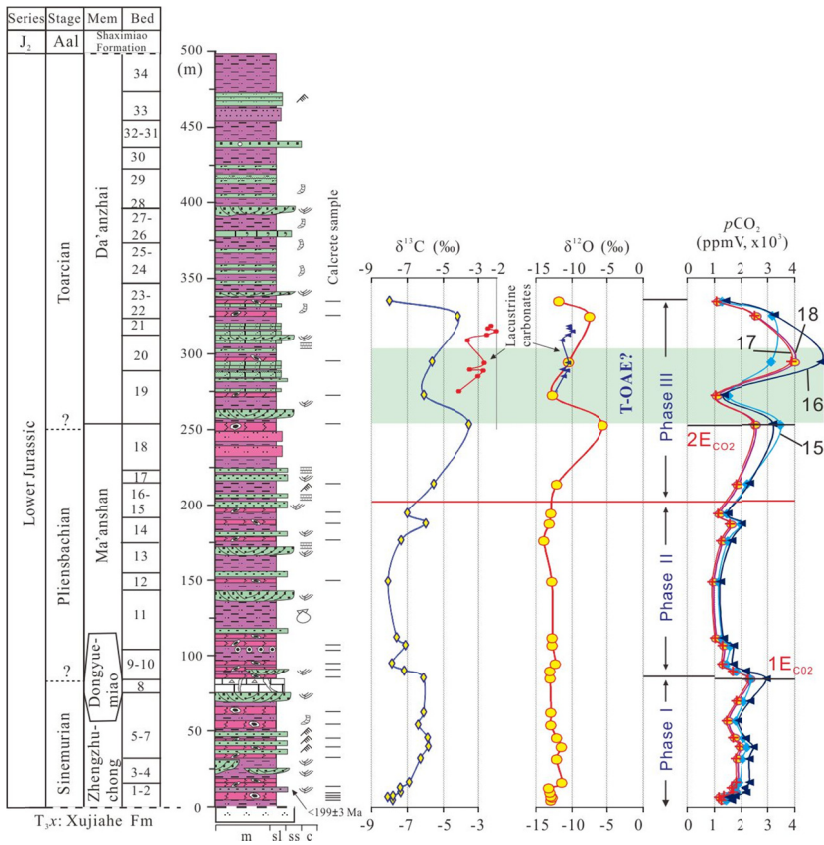


1064 **Figure 5** Cross-plot and covariance of carbon and oxygen isotopic values of the Lower Jurassic pedogenic and lacustrine  
 1065 carbonates from [the](#) GSB. Note, the pronounced covariance ( $R^2=0.957$ ) between  $\delta^{13}\text{C}$  and  $\delta^{18}\text{O}$  from Shaping section, Ya'an,  
 1066 indicating a compositional arid-evaporate and closed pattern lake; the moderate covariance ( $R^2=0.47$  and  $0.44$ ) between  $\delta^{13}\text{C}$  and  
 1067  $\delta^{18}\text{O}$  from Zigong and Hechuan, indicating a (semi-) arid and semi-closed pattern lake.

1068

1069

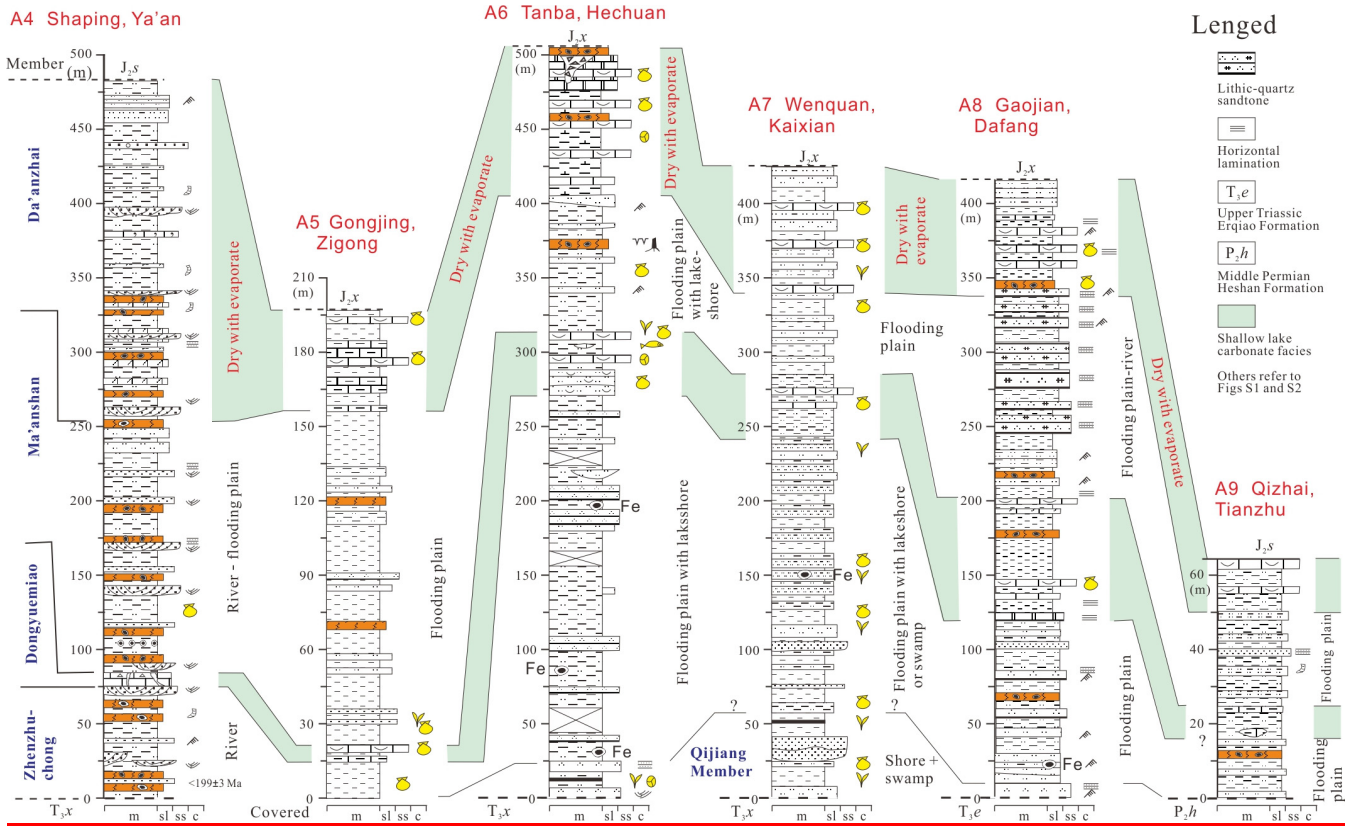
1070



1071

1072 **Figure 6** Diagram of the Lower Jurassic strata and lithological log at the Shaping section, Ya'an with **carbon-oxygen** **carbon and**  
 1073 **oxygen** isotope values of pedogenic and lacustrine carbonates and  $pCO_2$  curve. Three phases and two events can be observed for  
 1074 **both** stable isotope values of pedogenic carbonates and  $pCO_2$  estimate. **Legend of lithology in log refers to supplementary Figs. S1**  
 1075 **and S2.** T-OAE, Toarcian oceanic anoxic event.  $1E_{CO_2}$  and  $2E_{CO_2}$ , rapid falling event of  $pCO_2$ . Numbers 15 to 18 are the curves of  
 1076  $pCO_2$  in different parameters, and details refer to supplementary Table S4.

1077



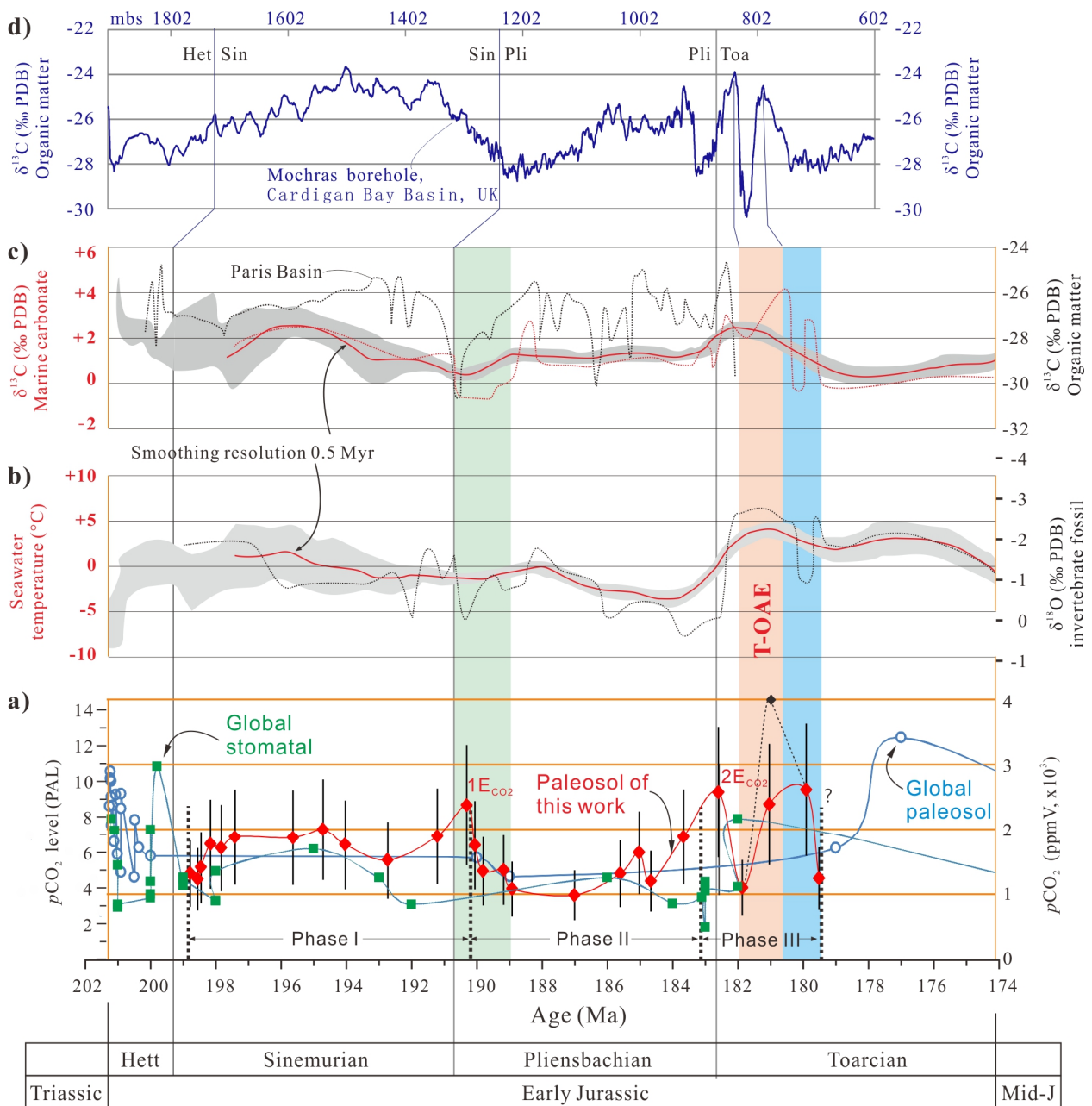
1078

1079

1080

1081

**Figure 7 Stratigraphic correlation and depositional environment interpretation of the Lower Jurassic in the GSB. Data of sections refer to [Figure 1](#) and [Table S2](#). Note, two lacustrine transgressive cycles are marked by correlative pale green areas.**



1082

1083 **Figure 8** Comparison among the Early Jurassic  $p\text{CO}_2$ ,  $\delta^{13}\text{C}$  of marine carbonates and organic matters,  $\delta^{18}\text{O}$  of invertebrate  
 1084 fossils, and seawater temperature. Age model is from Cohen et al. (2013). ea,  $p\text{CO}_2$  values of this work and, the composite  $p\text{CO}_2$   
 1085 by paleosol and stomatal index collected from the published literatures refer to supplementary Table S5-S6 and S6S7. Vertical  
 1086 bars are errors ( $1\sigma$ ) of  $p\text{CO}_2$  (Table S5). Errors are propagated using the Gaussian approach (Breecker and Retallack, 2014). Note:  
 1087 **1)**  $p\text{CO}_2 = 4027$  ppmV (black solid diamond, sample J1z-20-01) if the  $\delta^{13}\text{C}_r = -29.0$  ‰ at 181 Ma from Xu et al. (2018) in case of  
 1088 other constant parameters; **2)** the early published  $p\text{CO}_2$  values from both carbon isotope of pedogenic carbonates and stomatal  
 1089 index of fossil plants (data refer to Table S56 and S6S7) were awfully rough dated with the average age of a lithostratigraphic  
 1090 formation or group, with which the uncertainty can be upto 10 Myr, leading to the difficulty of precise and accurate  $p\text{CO}_2$   
 1091 correlation in pace, frequency, and event in deep time. b),  $\delta^{18}\text{O}$  and seawater temperature (black dot line) of marine invertebrate  
 1092 fossils compiled from McArthur et al. (2000), Rosales et al. (2001, 2004), Jenkyns et al. (2002), Bailey et al. (2003), van de  
 1093 Schootbrugge et al. (2005), Gómez et al. (2008), Metodiev and Koleva-Rekalova (2008), Suan et al. (2008), Korte et al. (2009), Dera  
 1094 et al. (2011), Gómez et al. (2015). Smoothed  $\delta^{18}\text{O}$  and seawater temperature (red curves) in b) and c) are after Dera et al. (2011). c).  
 1095 red dot line  $\delta^{13}\text{C}$  (red dot line) of marine carbonates and organic matters in western Tethys, composed from Jenkyns and Clayton  
 1096 (1986, 1997), Hesselbo et al. (2000), Dera et al. (2011), Arabas et al., 2017; black dot and solid line  $\delta^{13}\text{C}$  (black dot and solid line)  
 1097 of organic matters from Paris Basin, France (Peti et al., 2017) and Cardigan Bay Basin, UK (Xu et al., 2018). Smoothed  $\delta^{18}\text{O}$  and

seawater temperature (red curves) in b) and c) are after Dera et al. (2011). d),  $\delta^{13}\text{C}$  of organic matters from North Atlantic. Composed from the Mochras borehole, Cardigan Bay Basin, UK (Xu et al., 2018; Storm et al., 2020), seven-point average smoothing against depth (mbs).

## Table

**Table 1 Stratigraphic framework of the Lower Jurassic Ziliujing Fm in Sichuan and adjacent area (GSB), Southwest China**

Epoch	Age	Formation	W Sichuan (Ya'an)	E Sichuan and Chongqing	S Sichuan and N Guizhou	N Sichuan
Middle Jurassic	Aalenian	Xintiangou Fm	Xintiangou Fm	Xintiangou Fm	Xintiangou Fm	Qianfuyan / Xintiangou Fm
Early Jurassic	Toarcian	Ziliujing Fm	Da'anzhai Mem (Bed 20-34)	Da'anzhai Mem	Da'anzhai Mem	Baitianba Fm
	Pliensbachian		Ma'anshan Mem (Bed 9-18)	Ma'anshan Mem	Ma'anshan Mem	
	Sinemurian		Dongyuemiao Mem (Bed 8)	Dongyuemiao Mem	Dongyuemiao Mem	
			Zhengzhuchong Mem (Bed 1-7)	Zhengzhuchong Mem	Zhengzhuchong Mem	
	Hettangian		<b>Hiatus</b>	Qijiang Mem	Qijiang Mem	
Late Triassic	Rhaetian	Xujiahe Fm	Xujiahe Fm	Xujiahe Fm	Xujiahe Fm	

Notes: Straigraphic classification and correlation were composed from Dong (1984); SBGM (1997), Wang et al. (2010), Wen and Zhao (2010), Xu et al (2017). Re-Os isotope age of the lower Da'anzhai Member is  $180.3 \pm 3.2$  Ma in western Sichuan (Xu et al., 2017). Fm, Formation; Mem, Member.

## Supplementary data

### Captions of supplementary figures

**Figure S1 Lithological log of the Lower Jurassic Ziliujing Fm with depositional environment interpretations and sample positions at the Shaping section, Ya'an of Sichuan. Bed number and thickness are partly referred to Wen and Zhao (2010).**

**Figure S2 Lithological log of the Lower Jurassic Ziliujing Fm at the Tanba-Maliuping section, Hechuan of Chongqing with depositional environment interpretations and sample positions. Bed number and thickness are partly referred to Wang et al (2010).**

**Figure S3 Field photographs of the Lower Jurassic Ziliujing Fm lithofacies in the GSB. a, Well roundness and sorting gravels in the alluvial fan conglomerate. Basal and lower Baitianba Fm. Puji, Wangcang. Hammer 30 cm long. b, Large trough cross-bedding with scours in the point bar and channel sandstones. Upper Baitianba Fm; Puji, Wangcang. c, Calcisol developed within strong leaching overbank mudrocks on channelized sandstones. Middle of Bed B2, the Zhenzhuchong Member; Shaping section, Ya'an. d, Purple red mudrocks intercalated with thin siltstones in flood plain facies. Bed H7 of the Ma'anshan Member; Tanba section, Hechuan. e, Whitish medium-thick micritic dolomites in lacustrine facies. Bed H12 of the Da'anzhai Member; Maliuping section, Hechuan. Hammer 34 cm long. f, Greenish gray lacustrine muddy dolomites and dolomitic mudrocks**

1122 associated with brownish / reddish purple mudrocks. Bed B21 of the Da'anzhai Mem**ber**; Shaping section, Ya'an.

1123

1124 **Figure S4** Microscopic photos showing lithological microfacies of the Lower Jurassic Ziliujing Fm. *a*, Fine lithic (quartz)  
1125 sandstone. Lithic-dominant fragments are mudrock. Sample J<sub>1z</sub>-02-01b, Zhenzhuchong Mem**ber**; Shaping section, Ya'an.  
1126 Plain-polarised light. *b*, Laminated muddy dolomite and dolomitic mudrocks. Sample J<sub>1z</sub>-21S2B, Da'anzhai Mem**ber**; Shaping  
1127 section, Ya'an. Plain-polarised light. *c*, Fine quartz arenite. Sample 18HC-02b3, Bed H2, Qijiang Mem**ber**, Tanba section,  
1128 Hechuan. Cross-polarised light. *d*, Micritic dolomite. Sample 18HC-06b, Bed H12, Da'anzhai Mem**ber**; Maliuping section,  
1129 Hechuan. Plain-polarised light. *e*, Coquina. Shell wall of bivalves were micritized. Mud and recrystalline calcites filled inter-shells  
1130 and intra-shells. Sample 18HC-04b, Base of Bed H12, Da'anzhai Mem**ber**; Maliuping section, Hechuan. Cross-polarised light. *f*,  
1131 Relict of coquina. Shell wall of bivalves were partly micritized. Strongly recrystalline calcites replaced the fills and shells. Sample  
1132 18HC-05b, Bed H12, Da'anzhai Mem**ber**; Maliuping section, Hechuan. Cross-polarised light.

1133

1134 **Figure S5** Field photographs of the Lower Jurassic Ziliujing Fm lithofacies in the GSB. *a*, Lithofacies and stratigraphic sequence.  
1135 Beds B8 to B10 of the lower Ma'anshan Mem**ber** and Dongyuemiao mMem**bers** at Shaping village, Ya'an. *b*, Karstified gravels within  
1136 the limestone. The horizon and location is same as *a*. Pen 15 cm long. *c*, Layered dolomites with Karstified cave gravels. Bed H12  
1137 of the Da'anzhai Mem**ber** at Maliuping village, Hechuan. *d*, Karstified cave gravels. The horizon and location is same as *c*.  
1138 Hammer 34 cm long.

1139

1140 **Figure S6** Stratigraphic correlation of the Lower Jurassic Baitianba Fm in northern GSB. Locations and sources refer to Figure  
1141 1. Plant fossils and stratal thickness in the Shiguansi section, Wanyuan are cited from SBG (1980b).

1142

1143

#### 1144 Captions of supplementary tables

1145 [Table S41](#) Occurrence list of the Early Jurassic climate-sensitive sediments in the GSB

1146

1147 [Table S1—S2](#) Early Jurassic paleosols in Ya'an of Sichuan and Hechuan of Chongqing, Southwest China

1148

1149

1150 [Table S23](#) Carbon-oxygen isotope compositions of lacustrine carbonates from the Lower Jurassic Ziliujing Fm (Da'anzhai Mem)  
1151 in the GSB

1152

1153 [Table S34](#)  $p\text{CO}_2$  estimate by carbon isotope of pedogenic carbonates from the Lower Jurassic Ziliujing Fm at ~~the~~ Shaping ~~section~~,  
1154 Ya'an of Sichuan

1155

1156 ~~[Table S4](#) Occurrence list of the Early Jurassic climate sensitive sediments in the GSB~~

1157 [Table S5](#) Calculation of Gaussian error propagation for the Early Jurassic  $p\text{CO}_2$  estimate in the Sichuan paleobasin

1158

1159

1160 [Table S6](#) Global  $p\text{CO}_2$  data of the Latest Triassic - Early Jurassic by stomatal method

1161

1162 [Table S5—S7](#) Global  $p\text{CO}_2$  data of the Latest Triassic - Early Jurassic estimated by carbon isotope of pedogenic carbonates

1163

#### 1164 Captions of supplementary notes

1165 [Note S1](#), Description and interpretation of sedimentary facies and its evolution



1166

1167 | [Note S2, Notes of parameter usage and selection for the  \$p\text{CO}\_2\$  calculation](#)

1168